University of Alberta

NUMERICAL ANALYSIS OF MASONRY SHEAR WALLS STRENGTHENED WITH CFRP SHEETS

by

Xia Jin ©

A thesis submitted to the Faculty of Graduate Studies and Research in partial fulfillment of the requirements for the degree of Master of Science

in

Structural Engineering

Department of Civil and Environmental Engineering

Edmonton, Alberta

Spring 2005

ABSTRACT

This thesis forms a part of a research program which investigates the application of Carbon Fibre Reinforced Polymer (CFRP) sheets to strengthen masonry shear walls with openings.

Numerical models were prepared for four partially-grouted reinforced concrete masonry walls with window openings tested at the University of Alberta. The models were mainly established using two dimensional (2D) 4-node bilinear plane stress quadrilateral elements with reduced integration and hourglass control to simulate the behaviour of the specimens, which were subjected to the combination of constant axial loading and monotonically increasing lateral loading.

The results of the simulations were verified against the test results and relatively good agreement was found. Both the test results and numerical outputs indicated that lateral capacity and ductility of the masonry shear walls have been substantially increased because of CFRP strengthening. Conclusions were drawn based on the comparisons and discussions. Suggestions were proposed for future research.

ACKNOWLEDGEMENTS

Financial support for this research was provided by the Network of Intelligent Sensing for Innovative Structures (ISIS) of Canada.

There are a number of people who contribute to the completion of this thesis. First and foremost, the author would like to express her sincere gratitude and appreciation to her research supervisors, Professor A. E. Elwi and Professor J. J. Roger Cheng for their consistent guidance, support and encouragement throughout this study.

The author would like to acknowledge Honglan Miao for providing the test data derived from the experiment. Mohammad Behbahanifard, Erum Mohsin and Yue Wang gave the author great help during numerical modelling. Larry Burden and Richard Helfrich of the I. F. Morrison Structural Engineering Laboratory at the University of Alberta are also appreciated for their assistance in the experimental work.

Finally the author would like to appreciate the help and support from family members and all friends in assisting and encouraging her to successfully finish this thesis.

TABLE OF CONTENTS

1. INTRODUCTION 1

1.1 Background 1

1.2 Objectives 3

1.3 Thesis Outline 4

2. LITERATURE REVIEW 6

2.1 Introduction 6

2.2 Experimental Research 6

2.2.1 Masonry Shear Walls without Openings 6

2.2.2 Masonry Shear Walls with Openings 7

2.2.3 Masonry Shear Walls with FRP Composites 9

2.3 Finite Element Analysis 11

2.3.1 Models for Masonry 11

2.3.2 Material Behaviour 13

2.3.3 Masonry Shear Walls with FRP Composites 15

2.4 Summary 16

3. NUMERICAL MODEL 17

3.1 Introduction 17

3.2 Review of the Experimental Program 18

3.2.1 Test Specimens 18

3.2.2 Test Set-up 19

3.2.3 Test Method, Instrumentation and Procedure 20

3.2.4 Test Results 21

3.3 Numerical Simulation of Test Specimens 21

3.3.1 Geometric Modeling 23

3.3.2 Boundary Conditions and Loading 24

3.3.3 Material Properties 25

3.4 Constitutive Modeling of Masonry 29

3.4.1 Concrete Damaged Plasticity 29
3.4.2 Biaxial Yield Surface 30
3.4.3 Compression Hardening 30
3.4.4 Tension Stiffening 31
3.4.5 Crack Directions 33
3.5 Analysis Procedure 33
3.6 Summary 34

4. VERIFICATION AGAINST EXPERIMENTAL RESULTS 49
4.1 Introduction 49
4.2 Results of Numerical Analysis, Discussions and Verification 49
4.2.1 Specimen W1 50
4.2.2 Specimen W2 53
4.2.3 Specimen W3 57
4.2.4 Specimen W4 59
4.3 Summary 61

5. SUMMARY, CONCLUSIONS AND RECOMMENDATIONS 95
5.1 Summary 95
5.2 Conclusions from Numerical Analysis 96
5.3 Recommendations for Future Research 98

REFERENCES 100

LIST OF TABLES

Table Page

Table 3-1 Material Properties Used for Concrete Masonry 35
Table 3-2 Material Properties Used for CFRP Sheets 35
Table 3-3 Material Properties Used for Steel 36

LIST OF FIGURES

Figure Page

Figure 1-1 Shear Failure Patterns for Solid Walls (Lourenço et al.1997) 2
Figure 1-2 Shear Failure Patterns for Perforated Walls (Lourenço et al. 1997) 2

Figure 3-1 Reinforcement Details in the Specimens 37
Figure 3-2 CFRP Strengthening Schemes 38
Figure 3-3 Test Set-up and Loading System 39
Figure 3-4 Failure Mode for W1 40
Figure 3-5 Failure Mode for W2 40
Figure 3-6 Failure Mode for W3 41
Figure 3-7 Failure Mode for W4 41
Figure 3-8 Lateral Load - Displacement Curves from Test 42
Figure 3-9 Mesh, B.C. and Loading 42
Figure 3-10 CFRP Behaviour 43
Figure 3-11 Steel Behaviour 43
Figure 3-12 Distribution of Masonry Elements 44
Figure 3-13 Yield Surface in Plane Stress (ABAQUS 2002) 44
Figure 3-14 *CONCRETE COMPRESSION HARDENING Curves 45
Figure 3-15 Masonry Elements Affected by CFRP for W2 45
Figure 3-16 Masonry Elements Affected by CFRP for W3 46
Figure 3-17 Masonry Elements Affected by CFRP for W4 46
Figure 3-18 *CONCRETE TENSION STIFFENING Curves for W1 47
Figure 3-19 *CONCRETE TENSION STIFFENING Curves for W2 & W4 47
Figure 3-20 *CONCRETE TENSION STIFFENING Curves for W3 48

Figure 4-1 Cracking Patterns at Failure from Test 63
Figure 4-2 Distribution and Designation of CFRP Sheets 64
Figure 4-3 Lateral Load - Displacement Curves from Models 64
Figure 4-4 Deformed Mesh for Specimen W1 65

Figure 4-5 Lateral Load - Displacement Curves for W1 65
Figure 4-6 Strain Contour for W1 (at failure) 66
Figure 4-7 Stress Contour for W1 (at failure) 66
Figure 4-8 Deformed Mesh for Specimen W2 67
Figure 4-9 Lateral Load - Displacement Curves for W2 67
Figure 4-10 Deformation Comparison for W1 and W2 68
Figure 4-11 Strain Contour for W2 (at failure) 69
Figure 4-12 Stress Contour for W2 (at failure) 69
Figure 4-13 Strain Comparison for W1 and W2 70
Figure 4-14 H1 Strain Distribution of Horizontal CFRP for W2 71
Figure 4-15 H2 Strain Distribution of Horizontal CFRP for W2 71
Figure 4-16 H3 Strain Distribution of Horizontal CFRP for W2 72
Figure 4-17 H4 Strain Distribution of Horizontal CFRP for W2 72
Figure 4-18 H2 Strain Distribution of Masonry Elements for W1 73
Figure 4-19 H2 Strain Distribution of Horizontal CFRP for W2 73
Figure 4-20 V2 Strain Distribution of Vertical CFRP for W2 74
Figure 4-21 V3 Strain Distribution of Vertical CFRP for W2 74
Figure 4-22 V4 Strain Distribution of Vertical CFRP for W2 75
Figure 4-23 V5 Strain Distribution of Vertical CFRP for W2 75
Figure 4-24 V4 Strain Distribution of Masonry Elements for W1 76
Figure 4-25 V4 Strain Distribution of Vertical CFRP for W2 76
Figure 4-26 H1 Stress Distribution of Horizontal CFRP for W2 77
Figure 4-27 H2 Stress Distribution of Horizontal CFRP for W2 77
Figure 4-28 H3 Stress Distribution of Horizontal CFRP for W2 78
Figure 4-29 H4 Stress Distribution of Horizontal CFRP for W2 78
Figure 4-30 V2 Stress Distribution of Vertical CFRP for W2 79
Figure 4-31 V3 Stress Distribution of Vertical CFRP for W2 79
Figure 4-32 V4 Stress Distribution of Vertical CFRP for W2 80
Figure 4-33 V5 Stress Distribution of Vertical CFRP for W2 80
Figure 4-34 Deformed Mesh for Specimen W3 81
Figure 4-35 Lateral Load - Displacement Curves for W3 81

Figure 4-36 Strain Contour for W3 (at failure) 82
Figure 4-37 Stress Contour for W3 (at failure) 82
Figure 4-38 H2 Strain Distribution of Horizontal CFRP for W3 83
Figure 4-39 H3 Strain Distribution of Horizontal CFRP for W3 83
Figure 4-40 V3 Strain Distribution of Vertical CFRP for W3 84
Figure 4-41 V4 Strain Distribution of Vertical CFRP for W3 84
Figure 4-42 H2 Stress Distribution of Horizontal CFRP for W3 85
Figure 4-43 H3 Stress Distribution of Horizontal CFRP for W3 85
Figure 4-44 V3 Stress Distribution of Vertical CFRP for W3 86
Figure 4-45 V4 Stress Distribution of Vertical CFRP for W3 86
Figure 4-46 Deformed Mesh for Specimen W4 87
Figure 4-47 Lateral Load - Displacement Curves for W4 87
Figure 4-48 Strain Contour for W4 (at failure) 88
Figure 4-49 Stress Contour for W4 (at failure) 88
Figure 4-50 H2 Strain Distribution of Horizontal CFRP for W4 89
Figure 4-51 H3 Strain Distribution of Horizontal CFRP for W4 89
Figure 4-52 V1 Strain Distribution of Vertical CFRP for W4 90
Figure 4-53 V3 Strain Distribution of Vertical CFRP for W4 90
Figure 4-54 V4 Strain Distribution of Vertical CFRP for W4 91
Figure 4-55 V6 Strain Distribution of Vertical CFRP for W4 91
Figure 4-56 H2 Stress Distribution of Horizontal CFRP for W4 92
Figure 4-57 H3 Stress Distribution of Horizontal CFRP for W4 92
Figure 4-58 V1 Stress Distribution of Vertical CFRP for W4 93
Figure 4-59 V3 Stress Distribution of Vertical CFRP for W4 93
Figure 4-60 V4 Stress Distribution of Vertical CFRP for W4 94
Figure 4-61 V6 Stress Distribution of Vertical CFRP for W4 94

LIST OF ABBREVIATIONS AND SYMBOLS

Hereafter the abbreviations and symbols used in this thesis. Symbols are also defined where they first appear within the thesis.

Abbreviations

2D	Two-dimensional
3D	Three- dimensional
FRP	Fibre Reinforced Polymer
CFRP	Carbon Fibre Reinforced Polymer
GFRP	Glass Fibre Reinforced Polymer
DSF	Deformation Scale Factor
HSS	Hollow Structural Section
LVDT	Linear Variable Differential Transducer
MPC	Multi-Point Constraints
URM	Unreinforced Masonry
kN	Kilo Newton
mm	Milimetre
MPa	Mega Pascal
με	Micro Strain
Grouted	Grouted masonry elements
Ungrouted	Ungrouted masonry elements
Grouted 1	Grouted masonry elements unaffected by CFRP sheets
Grouted 2	Grouted masonry elements affected by CFRP sheets
Ungrouted1	Ungrouted masonry elements unaffected by CFRP sheets
Ungrouted2	Ungrouted masonry elements affected by CFRP sheets

Arabic Symbols

E_0	Modulus of elasticity corresponding to the initial undamaged material
E_m	Modulus of Elasticity of masonry, MPa

E_s	Modulus of Elasticity of steel, MPa
E_{p1}	Modulus of Elasticity of CFRP along fibre direction, MPa
E_{p2}	Modulus of Elasticity of CFRP in transverse direction, MPa
f'_m	Compressive strength of masonry, MPa
f_{mu}	Compressive strength of masonry units, MPa
f_{sy}	Yield strength of steel, MPa
f_{su}	Ultimate strength of steel, MPa
f_p	Ultimate tensile strength of CFRP, MPa
G_{12}	Shear modulus in 1-2 surface, MPa
G_f	Fracture energy, N.mm/mm^2
W1	Control wall without CFRP sheets
W2	Specimen with 8-156 mm CFRP sheets
W3	Specimen with 8-78 mm CFRP sheets
W4	Specimen with 12-78 mm CFRP sheets
SPRINGA	Axial spring between two nodes
B21	2-node linear beam in a plane
CPS4R	4-node bilinear plane stress quadrilateral, reduced integration, hourglass control
T2D2	2-node linear 2-D truss

Greek Symbols

ν	Poisson's ratio
ν_{12}	Poisson's ratio in 1-2 surface
ν_s	Poisson's ratio of steel
ε_{sp}	Plastic strain at ultimate strength of steel
ε_c	Total strain of concrete
$\tilde{\varepsilon}_t^{pl}$	Tensile equivalent plastic strain
$\tilde{\varepsilon}_c^{pl}$	Compressive equivalent plastic strain
σ_{cu}	Ultimate stress of concrete, MPa
σ_t	Remaining direct stress, MPa

$\tilde{\varepsilon}_c^{in}$	Inelastic or crushing strain of concrete
ε_{0c}^{el}	Elastic strain corresponding to the initial undamaged material
σ_c	Stress corresponding to the initial undamaged material
u_t^{ck}	Direct cracking displacement, mm

1. INTRODUCTION

1.1 Background

Partially-grouted masonry is defined as construction using hollow masonry units in which only those vertical and horizontal cells that contain reinforcement are grouted (Schultz 1994). Partially grouting in masonry structure is recognized as a more economical and attractive construction alternative preferred by the construction industry compared to full grouting in moderate seismic areas where full grouting may not be necessary. Thus it is essential to study the structural behaviour of partially-grouted masonry structure when the overall construction cost can be cut down in appropriate areas.

Openings are often provided to meet architecturally functional necessity. As a result, masonry shear walls with window and door openings are the most common type of walls used in buildings. However, only limited research work has been conducted to study the behaviour of such walls.

Depending on aspect ratio, loading conditions as well as the amount of vertical and horizontal reinforcement, two distinct inelastic load – deformation mechanisms are known for masonry shear walls under lateral loading. One is a flexural mechanism, which is characterized by tensile yielding of vertical reinforcement and/or compressive crushing of critical masonry sections. The other is a shear mechanism, which is featured by diagonal tensile cracking (Shing et al. 1989). This research program focuses on the latter mode because it is found that masonry shear walls with shear-dominant mode exhibit a more brittle behaviour than those dominated by flexural mode. Figure 1-1 and Figure 1-2, respectively, shows the typical shear mechanism for solid walls and walls with openings in terms of both experimental and numerical results. Comparing these two sets of diagrams, it is noted that the continuous stepped diagonal crack observed in the solid walls has changed into two short flatter stepped diagonal cracks around the openings for

the perforated walls since the existence of openings makes it impossible for the crack to progress from top-right to the bottom-left compressed toes. It is found that the introduction of openings dramatically decreases flexural and shear stiffness as well as the strength of masonry shear walls. Therefore, the response characteristics to lateral loading are altered.

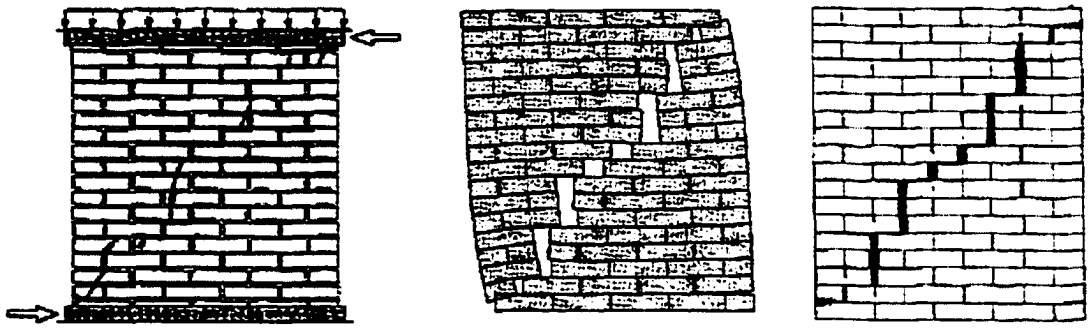

(a) Experimental Results (b) Numerical Results

Figure 1-1 Shear Failure Patterns for Solid Walls (Lourenço et al. 1997)

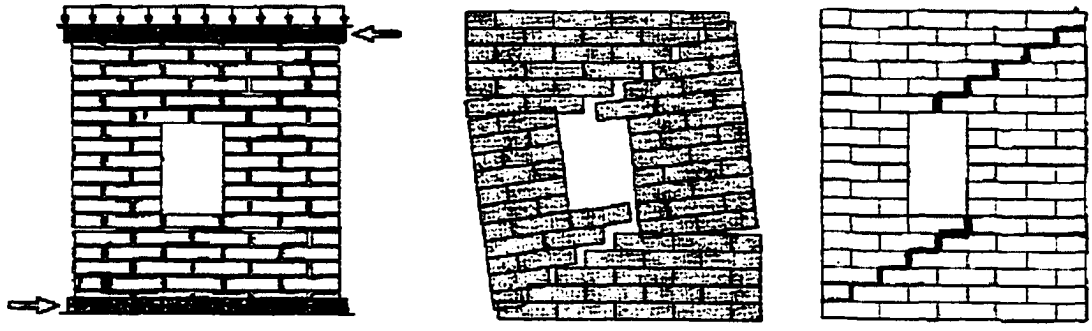

(a) Experimental Results (b) Numerical Results

Figure 1-2 Shear Failure Patterns for Perforated Walls (Lourenço et al. 1997)

Since masonry shear walls with openings are found to be easily damaged during earthquakes, optimum strengthening strategies for these structures have been pursued for many years. Fibre Reinforced Polymer (FRP) composites, which possess light weight,

high strength and excellent durability, may be internally or externally applied to strengthen masonry structure. However, most investigators have only concentrated on reinforcing concrete structure with FRP. Research work on FRP composites applied on masonry structure is very limited especially on partially-grouted masonry shear walls with openings. As a result, it is essential to develop efficient strengthening schemes for such masonry shear walls involving externally applied FRP composites. In order to achieve this ultimate objective, a good understanding of the structural behaviour of both masonry walls and FRP composites as well as the interaction between the two types of material subjected to lateral loading is of primary importance.

The University of Alberta program has investigated masonry walls under out-of-plane loads in the presence of CFRP (Carbon Fibre Reinforced Polymer) and GFRP (Glass Fibre Reinforced Polymer) sheets, respectively (Albert et al. 1998 and Kuzik et al. 1999). Miao (2004) conducted an ongoing experimental study on masonry shear walls strengthened with CFRP sheets subjected to in-plane loadings. In this program, four partially-grouted reinforced masonry shear walls with window openings were tested under the combination of constant axial loading and monotonic lateral loading. Three of the walls were externally strengthened with CFRP sheets and one served as a control wall. The experimental procedures and results were reported in detail. This thesis forms the numerical part of the study, which simulates and investigates the behaviour of the test specimens using finite element analysis.

1.2 Objectives

There are four objectives to be achieved in this research. The main objective of the program is to develop the corresponding finite element models that can simulate the behaviour of the specimens tested in the experimental program. The test results derived from the experimental program are used to verify the validity and reliability of the numerical models proposed in this research.

The second objective is to obtain a better understanding of the shear cracking and failure mechanisms of the partially-grouted masonry shear walls perforated with openings with and without strengthening with CFRP sheets based on the numerical analysis and discussion.

The third objective is to investigate the influence of different width and amount as well as locations of CFRP sheets on the overall structural behaviour of masonry shear walls and to determine the optimum strengthening scheme using CFRP sheets, which is more effective and makes it possible to cut down the overall construction cost.

The fourth objective is to propose some suggestions and recommendations for future research where further calibrations are needed to be conducted to improve the simulation results.

1.3 Thesis Outline

Chapter 2 presents a literature review of previous experimental programs and numerical simulations involving masonry shear walls with and without FRP composites. The test specimens, loadings applied to the walls, as well as the test results and conclusions obtained by previous researchers are described and discussed in brief. The finite element models for masonry walls including macro-modeling and micro-modeling, masonry material behaviour under static loadings and models for FRP composites as well as the interaction between masonry walls and FRP composites are all reviewed.

Chapter 3 details the simulation procedure for establishing numerical models for the masonry specimens tested in the experimental phase of the University of Alberta program. In order to better understand the numerical models for the specimens, the experimental program is reviewed briefly in the first part of the chapter. A brief description of test specimens, test set-up, test method, instrumentation and procedure is presented. In addition, the experimental observations and test results are discussed briefly as well. The rest of the chapter deals with the corresponding numerical models simulating

the test specimens described in the first part. The geometric modeling, boundary conditions and loading, and material properties for masonry material, CFRP and steel are all presented. Constitutive modeling of masonry, which involves concrete damaged plasticity, biaxial yield surface, compression hardening, tension stiffening and crack directions are focused in this chapter. Finally the analysis procedure is also described in detail.

Chapter 4 compares the results derived from the finite element analysis to those from the testing program. The deformation shapes, lateral load-displacement curves, stress contours and strain contour derived from the numerical models are described and discussed. In addition, stress and strain distribution of CFRP sheets along fibre directions is also presented. After the required data is obtained, comparison is made between the results from the experiment and simulation. Some conclusions are drawn based on the comparison and discussion.

Chapter 5 summarizes the whole numerical research program conducted in this study. Conclusions are drawn based on the analysis and discussion of the numerical models. Possible reasons to account for the difference between the numerical and experimental results are given. Some recommendations to improve simulation results for further research are proposed.

2. LITERATURE REVIEW

2.1 Introduction

This chapter presents a relatively comprehensive review of previous research work on masonry shear walls involving both experimental program and numerical analysis. The overview includes masonry shear walls with and without openings, as well as shear walls strengthened with FRP composites.

2.2 Experimental Research

In this section, a number of experimental research programs on masonry shear walls with and without openings are addressed in brief. Some conclusions are drawn based on the test results.

2.2.1 Masonry Shear Walls without Openings

A number of investigators have studied the structural behaviour of the masonry shear walls without openings for decades. Woodward et al. (1985) investigated parameters that might influence the shear resistance of unreinforced hollow concrete block masonry walls. Thirty-two wall panels were tested under vertical compressive stress in combination with in-plane lateral displacement. The parameters investigated included the amount of applied vertical compressive stress, wall aspect-ratio, block strength, and mortar type. The test results revealed that the relationship between applied vertical compressive stress and shear resistance was almost linear. When analyzing the relationship between shear stress and diagonal wall strain, a common critical diagonal tensile strain was found to exist at the onset of diagonal cracking. This indicated the existence of a material criterion defining the onset of wall diagonal tensile cracking, which is independent of strength and vertical compressive stress.

Ghanem (1992) carried out a test program to evaluate the in-plane behavior of partially reinforced concrete block masonry shear walls. Fourteen 1/3-scale masonry shear walls were constructed and tested under in-plane lateral loads, with and without axial compression. The experiment results were then used to study the effect of axial compression on the behaviour of partially reinforced masonry shear walls (Ghanem et al. 1993). It was shown that the axial compression had a great influence on failure mode, cracking load, load-deflection curve and load carrying capacity. The higher the axial stress is, the more easily the walls fail in shear (brittle) mode. Increasing axial stress tends to reduce ductility, increases the cracking strength and changes the wall behaviour from flexure to shear mode.

Khattab et al. (1993) examined the effect of reinforcement on the shear response by testing five full-scale reinforced grouted concrete masonry panels under a state of pure shear stress along the mortar joint planes. It was concluded that increasing the amount of shear reinforcement, without paying proper attention to the details, could lead to a behavior similar to that of unreinforced masonry.

2.2.2 Masonry Shear Walls with Openings

The early literature (Chen et al. 1978, and Scrivener 1986) showed that masonry shear walls with openings were the most easily damaged structural elements during earthquakes. As a result, much research work has been carried out to investigate the behaviour of masonry shear walls with openings under combination of static and cyclic lateral loading. Leiva et al. (1993) studied six full-scale reinforced masonry walls with openings subjected to constant vertical loads and quasi-static, reversed in-plane shear loads at two floor levels. The specimens were of fully grouted hollow concrete masonry with a height of two storeies. Four specimens were pairs of walls, coupled by floor slabs with and without lintels. The other two were single walls with door and window openings, representing walls perforated by window and door openings in two-storey buildings. Based on the test results and analytical predictions, a general design approach including

four steps was proposed for coupled and perforated walls of reinforced masonry walls under seismic loadings. The proposed approach makes it possible to predict strength and produce stable load-deflection behaviour under many cycles of reversed cyclic load.

Vermeltfoort et al. (1993) performed shear tests on six solid and six perforated masonry walls of one meter square in size. The specimens were first loaded vertically and then horizontally by moving the upper edge with a jack. The authors also detailed the process of crack development and failure mechanisms for both types of walls. For the solid walls, the first cracks developed in the uppermost and lowest bed joints, then progressing in opposite corners. This resulted in force concentration and the formation of a compression strut in the cracked area. These cracks continued to propagate due to shear stress in the bed joints. The walls failed with the diagonal crack through the whole specimen, partly through the already cracked joints and partly through the middle bricks due to the tensile stresses perpendicular to the direction of the force in the strut. For the walls with openings, splitting cracks took place at the two opposite corners due to the relatively weak mortar, resulting in a reduced horizontal load. The walls were finally divided into four parts due to the development of cracks. Between the contact areas of the parts compression struts were recognized. The width of the cracks increased due to rotation of the piers. In both piers, a diagonal compression strut developed. It was found that the angle of the compression strut in the perforated walls was much steeper than that of solid walls. Compare the two sets of test data for the walls under similar vertical load, it is indicated that the perforated walls have lower lateral load capacity but softer than those of solid walls.

Elshafie et al. (1999) conducted a research program to investigate the lateral response of reinforced masonry shear walls with openings by testing eight 1/3-scale walls under in-plane loadings. Various sizes and locations of openings were taken into account in the test program. It was found that for shear walls with similar overall dimensions and flexural reinforcement arrangement, the effects of openings on reduction of the wall strength and stiffness were proportional. Solid shear walls and shear walls with openings would have similar displacements at 75% of the peak load provided they had the same

overall dimensions and flexural reinforcement arrangement, which was independent of opening size and location.

Based on the above literature review for both solid and perforate walls, it is concluded that the introduction of openings in masonry shear walls can significantly weaken the wall stiffness and strength, alter crack development and failure mechanisms, resulting in decreasing the lateral load carrying capacity of masonry shear walls. Thus, it is important to develop strengthening schemes for such walls. FRP composites are the superior alternative because of their excellent mechanical and physical properties, and more importantly easy to apply. The following section will deal with the application of FRP composites to masonry shear walls.

2.2.3 Masonry Shear Walls with FRP Composites

Albert et al. (1998) were the first to show that unidirectional FRP sheets could achieve proper bond and work compositely with concrete block masonry. The authors performed thirteen tests on ten full-scale unreinforced masonry (URM) walls. Each specimen was tested under two out-of-plane line loads. The test results showed that externally applied FRP greatly increased the strength and ductility of ungrouted and unreinforced masonry walls. Hamilton III et al. (1999) examined seven unreinforced concrete masonry walls subjected to out-of-plane flexure with carbon, aramid and glass tape reinforcing. It showed that depending on the strength of masonry strengthened with FRP, walls will fail either by fracture of the FRP, shear or tension failure in the masonry, or by delamination. Kuzik et al. (1999) studied the out-of-plane cyclic behaviour of masonry walls reinforced externally with Glass Fiber Reinforced Polymer (GFRP) sheets involving eight concrete masonry walls. It indicated that the performance for both strength and ductility of masonry walls strengthened with GFRP was improved significantly.

With respect to masonry shear walls reinforced with FRP composites subjected to in-plane loadings, Tumialan et al. (2001) tested six unreinforced masonry (URM) walls

made of concrete blocks. The specimens involved one control wall and five other walls strengthened with GFRP bars, GFRP laminates, or a combination of GFRP bars and laminates. The load was applied in cycles of loading and unloading, except for the control wall. The test results found that remarkable increases in shear capacity and pseudo-ductility could be achieved.

Fam et al. (2002) studied the performance of a masonry wall retrofitted with GFRP sheets under in-plane lateral cyclic loading. After epoxy injection of the cracks and patching of the missing portions, the original reinforced clay brick masonry wall was repaired with GFRP sheets. The repaired wall was tested to failure in the same manner of the original wall. The results indicated that the strength and displacement capacities of the wall were completely restored and even exceeded the original capacities.

Belarbi et al. (2003) conducted an experimental program dealing with retrofitting of Unreinforcd Masonry (URM) walls with FRP under in-plane loading. Six full-scale URM walls retrofitted with different strengthening schemes using GFRP rods were tested under monotonic lateral load until to failure during the research program. The experimental results showed that the shear capacity of URM walls could be considerably improved when strengthened with FRP composites.

Haroun et al. (2003) investigated the behaviour of full-scale masonry walls under in-plane cyclic lateral loads. Six wall specimens constructed with reinforced concrete masonry units were strengthened by unidirectional composite laminates involving Carbon, E-glass and pre-cured carbon strips bonded on one or both sides of the walls. The walls were subjected to a constant axial load and incremental cyclic lateral shear loads. The test results revealed that significant increases in strength, stiffness and ductility were achieved by the application of FRP laminates. The authors also recommended an FRP U-laminate be applied at the bottom ends and through the thickness of the walls to overcome the premature failure due to localized compression failure at the wall toe where high compression stress takes place.

Zhao et al. (2003) performed an experimental program. Three test specimens made of hollow concrete block units strengthened with continuous carbon fiber sheet before or after cracking under combined uniformly distributed constant vertical load and cyclic lateral load. The test results showed that the cracking load and the ultimate load were increased substantially and the obvious improvement in deformability was also reported. It was found that the action of carbon fiber sheet system was similar to that of the flexible diagonal braces in the truss model.

2.3 Finite Element Analysis

Numerical studies on the behaviour of masonry shear walls subjected to in-plane static and dynamic loads have been the focus of numerous researchers for many years. Since the numerical models to be established and analyzed in this research are subjected to quasi-static in-plane loadings, only numerical models involving in-plane static loadings will be reviewed. Many factors, such as dimensions and anisotropy of masonry units, joint width and arrangement of head and bed joints, material properties of both units and mortars, as well as quality of workmanship, contribute to the extreme complexity and difficulty of numerical simulation for masonry shear walls (Tzamtzis et al. 2003a).

2.3.1 Models for Masonry

Tzamtzis et al. (2003a) classified major constitutive models for masonry in two basic categories: (a) macro-modeling or one-phase material models; and (b) micro-modeling or two-phase material models. Macro models assume masonry as an ideal homogeneous material with constitutive equations different from those of the individual components. Macro models are relatively simple to use but with relatively complicated constitutive equations, indicating their suitability for studying global behaviour of masonry. Micro models take into account the units and mortar separately to account for the interaction between them. They are relatively costly to use compared to macro models because of the requirement of a great number of input data, implying that they are suitable

for studying local behaviour of masonry. A detailed discussion of the two approaches can be found in Lourenço (1996).

Macro-modeling

A number of investigators have studied the structural behaviour of masonry considering the material to be an assemblage of units and mortar with average properties. Rosenhaupt et al. (1965) and Saw (1974) both assume isotropic elastic behaviour for masonry to simplify the problem, neglecting the interaction between motar and units and the effect of weak mortar planes. Dhanasekar et al. (1984) presented a non-linear finite element model for solid masonry. The masonry was modeled as a continuum with average properties derived from biaxial tests on brick masonry panels. The model was able to simulate the effects of material non-linearity and progressive local failure. However, the model could not be used to predict the behaviour of masonry subjected to concentrated loads, implying the model had limitations when local effects are important. It was also not applicable to concrete block masonry walls.

Micro-modeling

Shing et al. (1997) analyzed six partially grouted reinforced masonry shear walls tested by Schultz (1994). The authors considered masonry as a composite material in finite element analysis, in which different types of elements were used for mortar joints and masonry units. The masonry units were modeled using four-node quadrilateral smeared crack elements to account for both tensile and compressive fracture of the units. The mortar joints were simulated with interface elements to account for the inherent planes of weakness. Reinforcing bars were modeled as an elastic-hardening plastic material in the manner of a smeared overlay superimposed on top of a smeared crack element. It was assumed that no bond slip existed between the reinforcing bars and concrete. In the numerical analysis, a plane-stress smeared crack formulation was used to model the behaviour of masonry units, in which cracks were assumed to be smeared over

an entire element. In addition, the units were assumed to be homogeneous and isotropic before cracking. The compressive failure and tensile fracture of masonry were governed by a von Mises failure surface with a Rankine-type tension cutoff. The behaviour of mortar joints and the vertical splitting of masonry units were simulated with an elastic-plastic interface model developed by Lotfi et al. (1994).

Lourenço et al. (1997) developed an interface elastoplastic constitutive model that includes all possible failure mechanisms of masonry structures. For the numerical analysis, mortar and units were discretized to account for cracking, slip, and crushing of the material. Bricks were modeled with plane stress continuum elements (8-noded); while joints were modeled with line interface elements (6-noded). Local and global Newton-Raphson methods were used as the base of numerical implementation. It is found that the model is successful to analyze masonry shear walls and predict the experimental collapse load and behaviour.

Tzamtzis et al. (2003b) proposed a three-dimensional (3D) nonlinear microscopic finite element model for masonry structures subjected to static and dynamic loadings. The model treated masonry as a two-phase material, thus allowing for non-linear deformation characteristics and progressive local failure of both bricks and mortar joints. The influence of the mortar joints was accounted for by using interface elements to simulate the time-dependent sliding and separation along the interfaces. The authors perceived that this model was more realistic to macro models.

2.3.2 Material Behaviour

Numerical models for material behaviour of masonry improved with the increased sophistication of numerical methods for stress analysis. In general, a complete numerical model for the analysis of material behaviour includes the elastic properties of masonry, a yield criterion, inelastic stress-strain relations, and a failure criterion (Tzamtzis et al. 2003a).

Elastic Properties of Masonry

Limited research was conducted to study the behaviour of concrete masonry under biaxial stress, which is commonly encountered by masonry shear walls due to in-plane loadings. Hegemier et al. (1978) carried out biaxial tests of full-scale concrete masonry panels under monotonic and cyclic stress histories. The test data revealed that the tensile strength of concrete masonry decreased with compressive stress and the tensile strength could be predicted from component strengths if grout flaw distribution is known. It was also found that initial macrocracking stresses had little relation with reinforcing steel in normal amounts.

Yield Criterion

Lourenço et al. (1998) presented a yield criterion including different strengths along each material axis. This anisotropic continuum model involved two yield criteria for both tension and compression — a Rankine-type yield criterion for tension and a Hill-type yield criterion for compression. It assumed that two failure mechanisms could be distinguished — one associated with localized fracture processes and the other associated with a more distributed fracture process. When verified against tests results of masonry shear walls using the proposed anisotropic model, good agreement was found.

Inelastic Stress-Strain Relationship

Pietruszczak et al. (2003) developed a continuum formulation for modeling the inelastic behaviour of structural masonry. The conditions at failure were defined by the introduction of a critical plane approach, where the orientation of the localized plane was specified for which the failure function reaches a maximum. The proposed continuum framework involved the deformation process associated with both homogeneous behaviour and localized deformation mode in addition to anisotropic material characteristics. The approach is suitable to be used for large-scale masonry structures.

Failure Criterion

The development of a general failure criterion for masonry is difficult since it is very difficult to propose a representative biaxial test and a large number of tests are involved. Ushaksaraei et al. (2002) proposed a macroscopic failure criterion for structural masonry based on a critical plane approach. This method is an extension of nonlinear Coulomb failure theory. It assumed that a critical plane or a localization plane exists, on which the failure function, which is expressed in terms of normal and tangential components of the traction vector, reaches a maximum. The orientation of the localization plane could be uniquely predicted by using this approach.

2.3.3 Masonry Shear Walls with FRP Composites

The modeling for FRP composites bonded to masonry shear walls is very scarce. Thus, relevant literature on FRP composites bonded to concrete structures is referred to as preliminary sources of information in this study. Kamel (2003) investigated bond behaviour of FRP sheets, which were externally bonded to concrete blocks. In the two-dimensional (2D) finite element models, the CFRP sheet mesh was built using four-node plane stress elements with reduced integration (ABAQUS element CPS4R), which are the first order quadrilateral elements. The CFRP sheets used have a linear-elastic stress-strain relationship failing with brittle failure. The CFRP sheet material was defined as orthotropic with strong tensile strength in the direction of fibres; while in the transverse direction, the tensile strength of the CFRP sheets is very low. Plane stress orthotropic failure measures were used in the models as indications of material failure. With respect to the interface between concrete and CFRP sheets, the CFRP sheets were initially assumed to be bonded to the concrete surface, then debonding occurred at the interface joints when the interface stresses reached a defined critical limit. The comparison between the test results and numerical output showed that this methodology appeared to work well.

2.4 Summary

In this chapter, previous research work in both experimental and numerical on masonry shear walls with and without FRP composites is presented and summarized. Experimental observations, results and conclusions from the test programs are depicted. The masonry elements modeled in the finite element analysis and constitutive numerical methods are described briefly as well. For the next chapter, the procedure for numerical models simulating the masonry specimens tested in the experimental program is to be dealt with in detail.

3. NUMERICAL MODEL

3.1 Introduction

A series of masonry shear walls with rectangular window openings were tested to failure under in-plane axial and horizontal loadings at University of Alberta (Miao 2004). The tested specimens included one control wall and three other walls externally bonded with Carbon Fibre Reinforced Polymer (CFRP) sheets. The primary objectives of the tests were to investigate the in-plane shear bahaviour and failure mechanisms of masonry walls with and without strengthening with CFRP sheets, to verify the effectiveness of CFRP sheets and to determine the optimum strengthening schemes with CFRP sheets to reinforce the masonry walls so that the construction cost can be reduced.

In order to verify the test results and develop analytical models to predict the behaviour of strengthened walls, as well as to provide provisional design and strengthening guidelines for masonry structure, a series of corresponding numerical models were established using the commercial finite element analysis program ABAQUS (2002). The simulations provide a theoretical insight into the structural behaviour and failure mechanisms for both masonry walls and CFRP sheets subjected to in-plane axial and lateral loadings.

This chapter starts with a brief description of the test program, including the test set-up, test method and procedure. The test results are briefly presented as well. Then the numerical models are depicted in detail, including geometric modeling, boundary conditions and loading as well as material properties. The focus will be on the constitutive modeling of masonry involving concrete damaged plasticity model, biaxial yield surface, compression hardening, tension stiffening and crack directions. The analysis procedure involving explicit dynamic analysis for the numerical simulation is also addressed in detail.

3.2 Review of the Experimental Program

3.2.1 Test Specimens

In the experimental program, four full-scale reinforced concrete masonry walls were designed, constructed and tested under a combination of constant axial load and incremental monotonic lateral (push) load. All specimens were made up of partially grouted hollow concrete masonry. All masonry walls had the same overall dimensions. The size and location of the window openings were also the same. As shown in Figure 3-1, each wall was 3800 mm (19 courses) high, 3990 mm long and 190 mm thick, and constructed in running bond pattern from one wythe of concrete blocks with 10 mm thick bed and head mortar joints. The concrete masonry units were standard hollow blocks and had nominal dimensions of 390 mm x 190 mm x 190 mm. Type S mortar was used in constructing the specimens.

Each wall was perforated by a window opening with a size of 1200 mm x1200 mm. A lintel of 1600 mm long and 390 mm high was placed above the opening. At the top of the wall, there was a two-course bond beam with a height of 390 mm. Both the lintel and bond beam were fully grouted.

The wall was detailed with ten vertical reinforcing bars placed uniformly in the centre of the cores in the wall, and then the cores were grouted; while cores without vertical reinforcement were kept hollow. These bars were continuous from the bottom of the wall to the top of the bond beam without any lap splice in order to ease construction. The top ends of the rebars were welded to small steel plates to compensate for insufficient development length. At the bottom, the rebars overlapped with dowels, which were 600 mm long and welded to a 13 mm thick steel plate. Then the steel plate was bolted to a stiff W-shape steel beam with a depth of 312 mm. The dowels also served to prevent the specimen from base sliding failure. Each specimen had a vertical steel reinforcement ratio of 0.28%. There was no connection between the dowels and corresponding vertical rebars. Typical horizontal ladder type bed joint reinforcement was used every second course with

a diameter of 3.77 mm.

As mentioned before, the wall specimen was built with a height-to-length aspect ratio of 0.95 to present a shear dominated behaviour under in-plane loadings. The first wall without CFRP sheets on it, denoted by W1, was built as a control wall and as a comparison basis for the other three walls with CFRP sheets. The second wall, denoted by W2, had two horizontal and two vertical strips of 156 mm-wide CFRP sheets bonded around the opening on each side of the wall. The third wall, denoted by W3, was similar to the second wall, but the width of the CFRP sheets was only 78 mm, one half of those used in the second wall. The fourth wall, denoted by W4, was similar to the third wall; while it had one additional vertical CFRP sheet at the middle of each pier beside the opening. Therefore the fourth wall (W4) totally had 12 strips of CFRP sheets. All the horizontal CFRP sheets were continuous along the whole length of the walls; all the vertical CFRP sheets were bonded from the bottom of the walls to the bottom of the C-channels, which were used to uniformly transfer the lateral load to the walls. Perfect bonding was assumed between the CFRP sheets and masonry walls. Figure 3-2 shows the different schemes of CFRP sheets bonded to the specimens.

3.2.2 Test Set-up

As shown in Figure 3-3, the overall test set-up assemblage mainly consisted of a vertical loading system and a lateral loading system. Full details can be found in Miao (2004).

The vertical loading system was made up of four vertical steel tension rods, which were bolted to two small Hollow Structural Section (HSS) on top of a steel beam. The rods penetrated the strong floor and were connected to four hydraulic jacks underneath the strong floor. The vertical loading system was attached to a stiff W-shape steel beam on top of the specimen. The steel beam was used to uniformly distribute the vertical load to the wall. The base of the wall was connected to a steel plate by dowels; while the plate

was bolted to a base steel beam, which was situated on the strong floor.

3.2.3 Test Method, Instrumentation and Procedure

Each specimen was subjected to a monotonically increasing lateral loading combined with a constant axial loading. The vertical load, representing the floor and roof gravity load, was first applied to the top steel beam through two steel tension rods at each side of the wall, and then was uniformly distributed by the top steel beam and transferred to the upper course of the bond beam in the wall. The lateral loading, representing the seismic load or wind load, was applied to the lower course of the bond beam by a hydraulic jack through two C-shape channels connected to the wall by 6 bolts. A knife edge was incorporated in the lateral load system in order to eliminate any moment at the loading point.

The in-plane wall lateral displacement was monitored by four Linear Variable Differential transducers (LVDTs) along the height of the wall. In addition, there were two diagonal LVDTs to detect the diagonal change of tensile strain caused by diagonal cracking. Four sets of demecs were mounted around the four opening corners to monitor the change of strain and the development process of cracking.

The test was controlled using a computer-based data acquisition system and all electronic readings were recorded using this system. When the experiment started, the vertical load was increased from zero to 25 kN per vertical jack to a total of 100 kN and was maintained constant during the testing. Then the lateral load was monotonically slowly increased under load control system from zero up to the panel failure. At each load level all readings were electronically recorded. The readings acquired from the demecs were recorded manually for each load level throughout the test.

In general, the tests were terminated when complete destruction of the wall occurred.

3.2.4 Test Results

As described in Chapter 1, depending on aspect ratio, loading conditions as well as the amount of vertical and horizontal reinforcement, two distinct failure mechanisms can be identified for masonry shear walls under lateral loading — flexural mechanism and shear mechanism. With respect to the specimens investigated in this research, they had an aspect ration of 0.95 and vertical steel reinforcement ratio of 0.28%. Hence, shear mechanism for inelastic behaviour is expected to dominate load-deformation behaviour. It was observed from experiment that all walls exhibited distinct inelastic behaviour modes with significant diagonal tensile cracking at ultimate loading stage. The cracking initiated from the opening corners and progressed diagonally to the compressed toes. Therefore, it is evident that the ultimate strength of the walls was governed by shear failure and the test results coincided with the prediction. The failure modes for the specimens are shown from Figure 3-4 to Figure 3-7.

Another observation was that both shear capacity and ductility of the masonry walls have been substantially improved when strengthened with CFRP sheets as shown in Figure 3-8. The control wall failed at a lateral load of 225 kN. Depending on the arrangement of the CFRP sheets on the walls, the extent of increase for the three walls with CFRP sheets was different. The wall W2 failed at 360 kN with the capacity increased by 60% compared to the control wall. The wall W3 and W4 failed at 330 kN and 353 kN, respectively. The shear capacity for the two walls has been increased by 46.7% and 56.9%, respectively. From Figure 3-8, it can also be seen that the ductility for wall W2, W3, and W4 has been increased significantly when compared to the control wall W1. The detailed description and discussion of the test results can be found in Miao (2004).

3.3 Numerical Simulation of Test Specimens

Masonry is a type of composite material that comprises units and mortar joints. It exhibits distinct directional properties because of the presence of vertical and horizontal

mortar joints, which act as weak planes. As described in Chapter 2, there are two different approaches to model such anisotropy, namely, 'micro-modeling' and 'macro-modeling'.

Micro-modeling focuses on the individual components, e.g. mortar, units, and the unit /mortar interface. The major disadvantage of micro-modeling is that it requires a dense and complicated mesh. That precludes its application to large structures.

Macro-modeling deals with masonry structure as a whole composite and focuses on the global structural behaviour. The knowledge of the interaction between units and mortar is generally neglected. Macro-modeling assumes that the masonry structure is a homogenous continuum to be divided by finite element mesh, which does not need to represent the fine detail of the actual structure.

In this finite element analysis, macro-modeling was used since the global lateral load - displacement relationship is more important for this study. Here the masonry wall was modeled as an initially isotropic material with average properties. A numerical model using ABAQUS program was developed for each corresponding wall. There are two modules available in ABAQUS finite element analysis program — ABAQUS/Standard and ABAQUS/Explicit. ABAQUS/Standard is used to solve a wide range of linear and nonlinear problems involving the static, dynamic, thermal, and electrical response of components. ABAQUS/Explicit uses an explicit dynamic finite element formulation based on central difference method. This module is suitable for modeling brief, transient dynamic events, such as impact and blast problems (ABAQUS 1998). However, it also can be used to simulate quasi-static processes through control of the mass and velocity. The lateral loading to be described in the following simulated the seismic or wind loading in a quasi-static manner. The module of ABAQUS/Explicit was used throughout the numerical analysis.

3.3.1 Geometric Modeling

All elements used in ABAQUS utilized numerical integration to allow complete generality in material bahaviour. The elements used in this thesis were formulated in a global Cartesian coordinate system. There were three types of elements used to model the walls: two-dimensional (2D) solid elements for the masonry walls and CFRP sheets; two-dimensional (2D) truss elements for vertical and horizontal reinforcement; and in-plane linear interpolation beam elements for the top steel beam. In addition, spring elements were used to model the boundary conditions of the walls. Multi-point constraints (MPCs) of BEAM or LINK type were employed to simulate the connection conditions between the walls and top steel beam or the CFRP sheets.

The four masonry walls were simulated with 4-node bilinear plane stress elements with reduced integration and hourglass control (CPS4R). It should be pointed out that the same mesh was used for all the specimens for the purpose of simplification and uniformity. The 50 mm x 50 mm dimension was the minimum mesh size and 100 mm x 100 mm was the maximum size. The maximum aspect ratio was less than 2.0. In order to soften the behaviour, reduced integration was adopted because numerical solutions using 4-node elements are generally stiffer than the results observed in the experiments (Bathe 1996).

For the three walls with CFRP sheets, the CFRP sheet mesh was also built of CPS4R elements, which had the same mesh sizes as the corresponding elements in the walls. Although they had the same coordinates, different node numbers and element numbers were given to the elements of CFRP sheets. Thus, node to node correspondence and compatibility was established and MPC's LINK type was used to model the connection between the walls and CFRP sheets. However in this case, it was impossible to simulate the debonding process between the walls and CFRP sheets because they were both in the same plane. Therefore, this failure mode was precluded.

The horizontal and vertical steel reinforcement embedded in the walls was

modeled using two dimensional (2D) 2-node truss elements (T2D2), which use linear interpolation for position and displacement and have constant stress along the axis or the centerlines of the elements. These elements were superposed on the mesh of the wall elements. The dowels were neglected in the simulation; instead the bottom nodes of the vertical rebars were modeled as pinned.

The W-shape top steel beam used to uniformly distribute the vertical load to the wall was modeled with two dimensional (2D) beam elements (B21). The element dimensions were divided in order to match the corresponding wall elements. Standard I-section was chosen for the beam cross-section and defined by geometric input data. The fundamental assumption that should be noted is that the beam section cannot deform in its own plane. Figure 3-9 shows the mesh for the specimen.

3.3.2 Boundary Conditions and Loading

The boundary conditions of the four edges of the specimen were quite different. The two side edges were not supported and were left free. At the upper edge of the wall, the connection between the nodes of the top steel beam and the top nodes in the specimen was modeled with a Multi-Point Constraint (MPC) of BEAM type. This type of connection provides a rigid beam between two nodes to constrain the displacement and rotation at the first node to those at the second node (ABAQUS 2002). That means both of them had the same node displacement and rotation even during the wall deforming resulting from the vertical and lateral loading.

At the lower edge of the wall, the boundary conditions for the vertical rebars were modeled as pinned connection, assuming that the dowels were welded to the steel plate and the plate was tightly bolted to the bottom steel beam and assuming that there was no bending moment. For those bottom nodes not corresponding to the rebars, the boundary conditions were modeled by a series of spring elements (SPRINGA) that had nonlinear spring behaviour. The springs were adjusted to have only compressive strength but

without tensile strength in order to simulate the mortar between the masonry units and the steel plate, whose tensile strength is very low.

Two loading phases were included in the process. The first phase applied the vertical load to the top steel beam. The second phase applied the lateral load using a displacement control mode keeping the vertical load constant. When modeling the lateral load, six nodes, representing the six bolts used to connect the C-channels to the specimen, were chosen and connected to a reference node (contact node) at the end of the wall using MPC's of BEAM type. The reference node was then forced to move along the lateral direction at a specified displacement. This movement resulted in the corresponding reaction force occurring at the individual bottom elements of the wall. Then the individual forces were summed up together to form the total magnitude of the lateral load used for lateral capacity analysis. This procedure simulated the lateral load transfer process in the experiment, in which the lateral load was uniformly transferred to the top portion of the walls by six bolts in the C-channels and eventually to the whole wall. As a result, the modeling of the lateral load transfer through the channels in the experimental testing was successfully achieved. The boundary conditions and loading are also shown in Figure 3-9.

3.3.3 Material Properties

The material properties in the models were taken similar to the test results obtained from the experimental program; while properties that were not available from the tests were reasonably assumed. The materials used in the experiments included concrete blocks, grout and mortar, which are the essential components of masonry walls. In addition, the properties for vertical and horizontal reinforcement and CFRP sheets that are used to strengthen the walls are also stated in detail. The simulation of each material property in the numerical models is to be discussed in the following sections.

3.3.3.1 Masonry

A series of ancillary material tests were conducted by Miao (2004). They included testing for mortar cubes, grout cubes, block units and prisms. However, since macro-modeling was used, the masonry walls were treated as a whole composite material having average properties in spite of the diverse materials they really had in the construction. The material properties of masonry used in the models are listed in Table 3-1.

Compressive Strength

The compressive strength of the masonry walls was adopted according to the data from the prism tests. Five grouted and five ungrouted concrete block prisms constructed in running bond with type S mortar, which was the same as used in the masonry walls, were tested in the laboratory after curing for at least 28 days. The compressive strength from grouted prisms was used for grouted masonry elements and the compressive strength from ungrouted prisms was used for ungrouted masonry elements.

Tensile Strength

Drysdale et al. (1979) conducted an experimental study to investigate the strength characteristics of ungrouted and grouted concrete masonry assemblages under various tensile stress orientations. The tensile strength of masonry is an important parameter in the behaviour of shear walls, in which horizontal forces will cause tension or shear stress, or both. The diagonal tensile failure is mainly governed by the tensile strength of the combined masonry material. Due to the time and space limitation in the laboratory, the tensile tests were not conducted in the experiment. Following Drysdale's work and taking into account the stiffness difference between bed joints and head joints, the tensile strength of masonry adopted in the models was taken as 8% of the compressive strength of the masonry prisms.

Modulus of Elasticity

Modulus of elasticity of masonry is known as an important parameter to calculate relative stiffness of masonry elements to determine lateral load distribution and deflection. Wolde-Tinsae et al. (1993) studied the data base that included published and unpublished data from the U.S. and Canada from 1960 to 1992. The authors recommended that the elastic modulus of masonry can be either based on masonry prism testing or the unit strength method as:

(a) Prism testing:

For grouted concrete block masonry: $E_m = 550\ f'_m$

For ungrouted hollow concrete block masonry: $E_m = 700\ f'_m$

(b) Unit strength method:

For grouted concrete block masonry: $E_m = 800\ f_{mu}$

For ungrouted hollow concrete block masonry: $E_m = 950\ f_{mu}$

As a result, the Modulus of elasticity for grouted and ungrouted masonry elements used in the numerical models was calculated based on the two methods for grouted and ungrouted hollow concrete block masonry, respectively.

3.3.3.2 CFRP

The CFRP used in the three specimens were in the form of sheets bonded to the masonry wall surface on both sides. The CFRP sheets have a linear elastic stress-strain relationship ending up with brittle failure. They were defined as an orthotropic material with strong strength in the fiber direction but with weak strength in the transverse direction. The general stress-strain behaviour for the CFRP sheets is shown in Figure 3-10. The material properties of CFRP sheets used in the models are listed in Table 3-2.

The CRFP sheet was defined as orthotropic elastic material using *ELASTIC, TYPE=LAMINA option. This requires four parameters: the modulus of elasticity in the fiber direction, E_{P1}; the modulus of elasticity in the transverse direction, E_{P2}; Poisson's ratio, ν_{12}, and shear modulus, G_{12}. The values of E_{P1} and ν_{12} were taken as 150,000MPa and 0.49, respectively, which match the coupon test results from the experiment (Miao 2004). The values of E_{P2} and G_{12} were taken as 15,000 MPa and 10,000 MPa, respectively.

3.3.3.3 Steel

The steel used in the specimens was in the form of reinforcement and steel beams. The material properties of steel used in the models are listed in Table 3-3. The specific modeling is to be discussed in the following sections.

Reinforcement

The reinforcement used in the walls included both vertical and horizontal bars, as well as horizontal joint wire reinforcement. The rebars with 15 mm in diameter were divided into two groups: weldable and regular. For the vertical reinforcement, weldable rebars were used due to their good weldability and ductility. In the horizontal direction two types of reinforcement were used. One was the regular rebars used in the lintels and bond beams, and the other was the joint reinforcement with the diameters of 3.77 mm used in the horizontal mortar joints with the spacing of 400 mm.

The rebars were defined as an elastic-plastic material. The elastic behaviour was governed by the modulus of elasticity (E_s) and Poisson's ratio (ν_s). The E_s values were taken from the rebar tests conducted in the laboratory. For weldable rebars, E_s was 214400 MPa and for regular ones, E_s was 214600 MPa. Poisson's ratio was taken as 0.3 for both groups of rebars. Beyond the elastic range, the rebar behaviour was defined by yield strength (f_{sy}), ultimate strength (f_{su}) and the plastic strain at ultimate strength (ε_{sp}); all based on the test results. The values of f_{sy} and f_{su} for both weldable and regular rebars

are listed in Table 3-3. The typical stress-strain curve for the rebars is shown in Figure 3-11.

There were no testing data for the horizontal joint reinforcement. Reasonable values were assumed in the models. The values for E_s and ν_s were taken as 210,000 MPa and 0.3, respectively. The material was defined as elastic.

Steel Beam

Since there were no test data available for the top steel beam from the laboratory, the values for E_s and ν_s were taken as 210,000 MPa and 0.3, respectively. The yield strength was taken as 350 MPa because the steel beam was known to be a 350W beam. The material was also defined as elastic.

3.4 Constitutive Modeling of Masonry

The masonry elements in the specimens were divided into two categories. One was grouted masonry elements with the thickness of 190 mm and the other was ungrouted masonry elements with the thickness of 68 mm, which comprises the face shell thickness. Figure 3-12 shows the distribution of the two types of masonry elements used in the numerical analysis. Concrete damaged plasticity model was used as the constitutive model for masonry elements in this research, which involves biaxial yield surface, compression hardening, tension stiffening and crack directions. They will be addressed in detail below.

3.4.1 Concrete Damaged Plasticity

There are two different constitutive models available in ABAQUS /Explicit for concrete subjected to low confining pressures: brittle cracking model and concrete damaged plasticity model. Brittle cracking model is used to model structures with

dominant tensile cracking. Concrete damaged plasticity model is used for structures subjected to arbitrary loading conditions. This model defines a biaxial yield surface mainly including an initial yield surface and a bounding surface. The model allows the degradation of the elastic stiffness under cyclic loading (ABAQUS 2002). The concrete damaged plasticity model defines the stress-strain behaviour of plain concrete in uniaxial compression outside the elastic range using compression hardening. It also defines the strain-softening behaviour for cracked concrete using tension stiffening.

The *CONCRETE DAMAGED PLASTICITY option is used to define flow potential and yield surface parameters in terms of dilation angle, which was taken as 15 degrees in the numerical models.

With regard to plastic flow, the concrete damaged plasticity model assumes nonassociated potential plastic flow. As for the yield function used in the simulation, the model adopts the yield function of Lubliner et al. (1989), with the modification proposed by Lee et al. (1998) to depict different evolution of strength under tension and compression.

3.4.2 Biaxial Yield Surface

The biaxial yield surface in plane stress for masonry elements is shown in Figure 3-13. At the beginning of loading, there is an initial yield surface and within this surface the element is elastic. With the development of compression hardening, the initial yield surface expands outward until eventually gets to the bounding surface. Between the initial yield surface and bounding surface, the element exhibits elastic-plastic behaviour. Beyond the bounding surface, the element fails.

3.4.3 Compression Hardening

The stress–strain behavior of masonry beyond the elastic range is defined by

using the option of *CONCRETE COMPRESSION HARDENING. Compressive stress data are provided as a tabular function of inelastic (or crushing) strain $\tilde{\varepsilon}_c^{in}$. The stress-strain curve can be defined outside the ultimate stress σ_{cu} into the strain-softening regime.

As described in ABAQUS (2002), an inelastic strain, $\tilde{\varepsilon}_c^{in}$, rather than plastic strain, $\tilde{\varepsilon}_c^{pl}$, is used for hardening data. The compressive inelastic strain is defined as the total strain minus the elastic strain corresponding to the initial undamaged material, $\tilde{\varepsilon}_c^{in} = \varepsilon_c - \varepsilon_{0c}^{el}$, in which $\varepsilon_{0c}^{el} = \sigma_c / E_0$. Figure 3-14 shows the compression hardening curves for grouted and ungrouted masonry elements in terms of yield stress and inelastic strain. The starting points and peak points show the yield strength and ultimate strength, respectively. The curves between these points are the process of compression hardening. The elements exhibit elastic-plastic behaviour at these ranges.

3.4.4 Tension Stiffening

The tension stiffening is defined as the effect of cracking followed by bond-slip of reinforcing bars (Atkinson et al. 1993). The authors pointed out that before tensile cracks occur, the behaviour of reinforced masonry subject to direct tension is approximately linear elastic. The steel bars and other materials (grout, unit and mortar) experience the same strain levels, which are proportional to their individual elastic moduli. When tensile cracking forms, it leads to a stress redistribution — the load portion previously carried by the masonry materials is now transferred to the steel across the crack.

In this research, it can be assumed that the tension stiffening effect is even more substantial for the masonry elements close to the CFRP sheets. Although there is no relevant literature referring to the tension stiffening effect of CFRP, it is reasonable to make such an assumption since to some extent the CFRP sheets behave similarly to the steel rebars. Figure 3-15 to Figure 3-17 illustrate the masonry elements affected by CFRP sheets. It was assumed that the masonry elements within a range of about 200 mm outside

the boundary of CFRP sheets were affected by CFRP and the tension stiffening curves to be stated below were also changed accordingly compared to those masonry elements unaffected by CFRP.

The postfailure behaviour for direct straining was modeled with the option of *CONCRETE TENSION STIFFEING. This also simplifies the simulation for the effect of the reinforcement interaction with masonry, as well as the interaction between the masonry and CFRP sheets. To specify tension stiffening, two options are provided in ABAQUS. One is to determine a postfailure stress-strain relation, and the other is to apply a fracture energy cracking criterion. The latter option was chosen for this study.

The fracture energy, G_f, is defined by Hilleborg et al. (1976) as the energy required to open a unit area of crack. It is an important material parameter. With this method the masonry brittle behaviour is characterized by a stress-displacement response rather than a stress-strain response. The facture energy cracking model can be defined by using the option of *CONCRETE TENSION STIFFENING, TYPE=DISPLACEMENT and specifying the postfailure stress as a tabular function of cracking displacement. Figure 3-18 gives the tension stiffening curves for specimen W1. In the diagrams, "Grouted" refers to grouted masonry elements; "Ungrouted" refers to ungrouted masonry elements.

For the three models with CFRP sheets, the tension stiffening effect was even more pronounced not only due to the existence of reinforcement but also the strengthening provided by the CFRP sheets. The influence of CFRP sheets on the tensile strength of masonry affects a much wider band of masonry than rebars, requiring very different data lines to be used for the models with and without CFRP sheets. For the models with CFRP, the data have been adjusted because of the different arrangement of CFRP on the walls. The tension stiffening curves adopted for the models are illustrated in Figure 3-19 and Figure 3-20. In the diagrams, "Grouted 1" and "Grouted 2" refer to the grouted masonry elements unaffected and affected by CFRP sheets, respectively; "Ungrouted 1" and "Ungrouted 2" refer to the ungrouted masonry elements unaffected and affected by CFRP sheets, respectively. Although the CFRP arrangement is different

for specimen W2 and W4, the same tension stiffening curves were assumed for the two specimens.

3.4.5 Crack Directions

The concrete damaged plasticity model does not have the concept of cracks developing at the material integration point, which is different from concrete models based on the smear crack approach. Referred to the research work of Lubliner et al. (1989), it is assumed in ABAQUS (2002) that the cracking takes place at points where the tensile equivalent plastic strain is greater than zero, $\tilde{\varepsilon}_t^{pl} > 0$, and the maximum principal plastic strain is positive. The normal vector direction of the crack plane is assumed to be parallel to that of the maximum principal plastic strain.

3.5 Analysis Procedure

Introducing an opening into shear walls reduces the shear strength and alters the deformation characteristics (El-Shafie et al. 1996). A nonlinear finite element analysis procedure was used to determine the response of the models with openings.

An analysis history in ABAQUS/Explicit is defined in three parts: 1) dividing the problem history into steps; 2) specifying an analysis procedure for each step; and 3) prescribing loads, boundary conditions, and output requests for each step.

The history data were divided into two steps: firstly the vertical loading and secondly the lateral loading, keeping vertical loading constant. For the second part, three procedures are available in ABAQUS/Explicit: explicit dynamic procedure, anneal procedure, and fully coupled thermal-stress procedure. The explicit dynamic procedure was chosen for the numerical analysis in this research. For the first step of loading, the time for vertical loading to increase from zero to the specified value was set to 50 seconds. For the second step of loading, the time for lateral displacement to increase from zero to

the specified value was set to 800 seconds, thus eliminating the inertial effects and modeling the quasi-static loading process in the experiment. The explicit dynamic analysis procedure is based upon the implementation of an explicit integration rule together with the use of diagonal ("lumped") element mass matrices (ABAQUS 2002). The explicit solution strategy used is conditionally stable. The critical time step size for the problem should be larger than the time it takes a sound wave to propagate through the smallest element. Since the load application was quasi-static, proper dynamic characteristics were not an important issue. Thus, to control the number of time steps and preserve accuracy, the speed of sound was reduced by increasing the density by a factor of 10^6 for all elements including masonry, steel reinforcement and CFRP sheets.

For the third part, a distributed vertical load was applied to the top steel beam for the first loading step; the direct format of *BOUNDARY, TYPE=DISPLACEMENT was used to specify the node set number to which the lateral displacement was applied, the degree of freedom in which the lateral displacement moved, and the magnitude of the specified lateral displacement for the second loading step. With respect to the output, node displacement for all elements, the displacement of top and bottom node, the reaction forces in the lateral direction for the bottom nodes, as well as the strain and stress in the fibre direction for CFRP sheets were requested.

3.6 Summary

In this chapter, the experimental program involving four masonry shear walls with window openings subjected to in-plane loadings were reviewed. The test set-up, procedure as well as test results were addressed briefly. Then the procedure of how the finite element models using ABAQUS program have been established was detailed from geometric modeling, boundary conditions and loading, material properties to constitutive modeling of masonry and analysis procedure. For the following chapter, the numerical results will be presented in detail and verification against the test results will be made. Some conclusions are to be drawn based on the discussion and comparison.

Table 3-1 Material Properties Used for Concrete Masonry

	Grouted	Ungrouted
Density (tonne/m^3)	2100.0x10^{-6}	2100.0x10^{-6}
Wall thickness (mm)	190	68
Modulus of Elasticity, E_m (MPa)	1000	1550
Poisson's ratio	0.15	0.15
Dilation angle for concrete damaged plasticity (degrees)	15	15
Compressive yield strength (MPa)	6.0	7.5
Ultimate compressive strength (MPa)	12.0	15.0
Ultimate tensile strength (MPa)	1.0	1.2

Note: The value of density is referred to Glanville et al. (1996)

Table 3-2 Material Properties Used for CFRP Sheets

Density (tonne/m^3)	2200.0x10^{-6}
Modulus of elasticity in fibre direction, E_{p1} (MPa)	150000.0
Modulus of elasticity in transverse direction, E_{p2} (MPa)	15000.0
Poisson's ratio	0.49

Table 3-3 Material Properties Used for Steel

	Reinforcement			Beam
	Rebars		Joint reinforcement	
	Weldable	Regular		
Density (tonne/m^3)	7800.0×10^{-6}			
Area (mm^2)	200	200/400	22.3	
Modulus of elasticity, E_s (MPa)	214400	214600	210000	210000
Poisson's ratio	0.30			
Tensile yield strength, f_{sy} (MPa)	454.5	474.5	450.0	350.0
Ultimate tensile strength, f_{su} (MPa)	617.5	779.0		

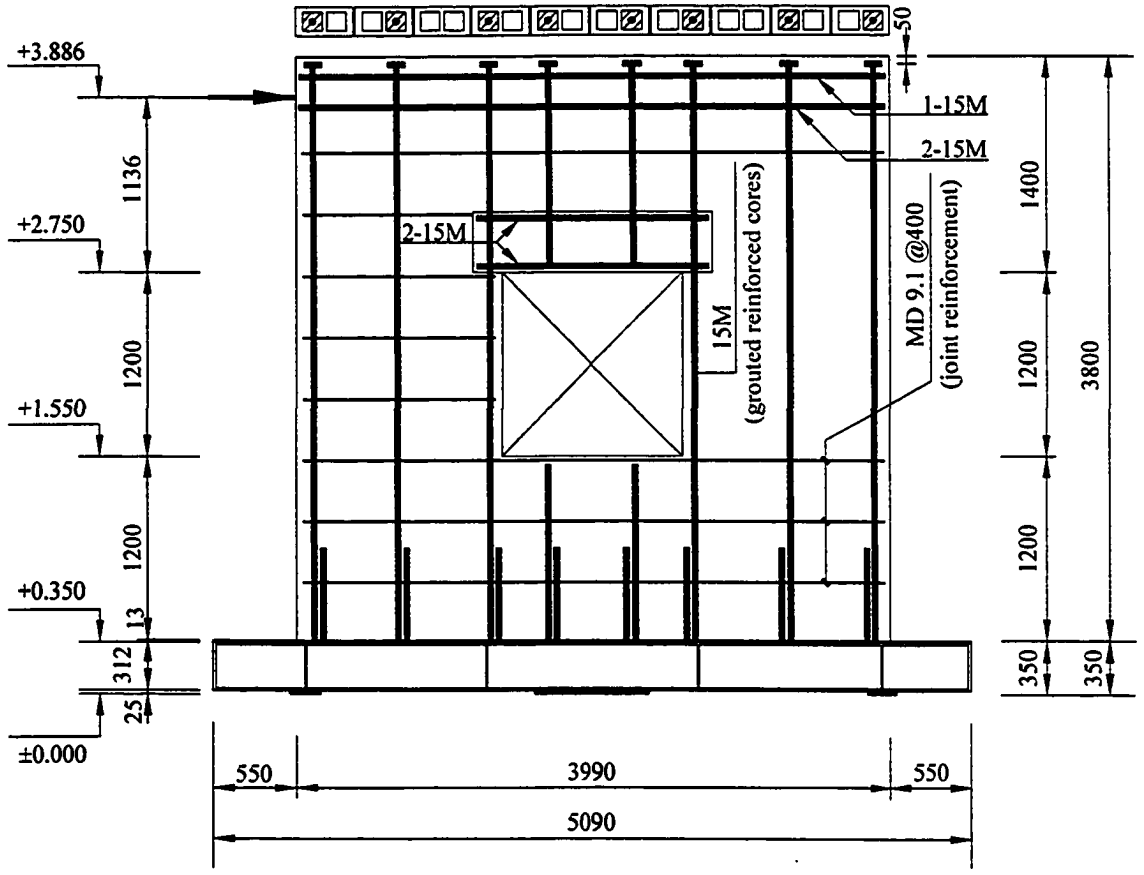

Figure 3-1 Reinforcement Details in the Specimens

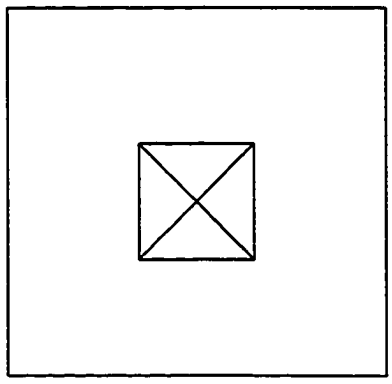

Specimen W1

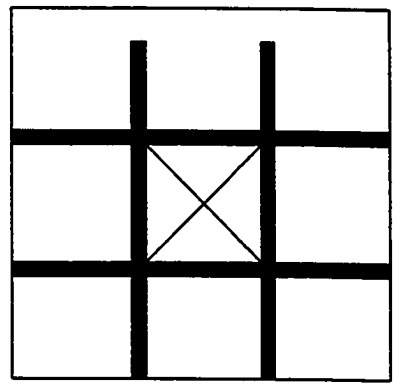

Specimen W2

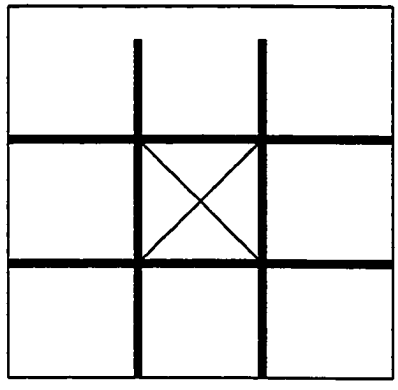

Specimen W3

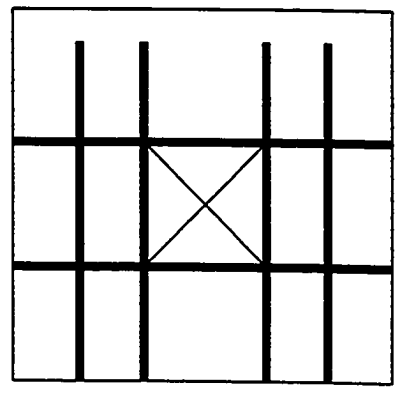

Specimen W4

Figure 3-2 CFRP Strengthening Schemes

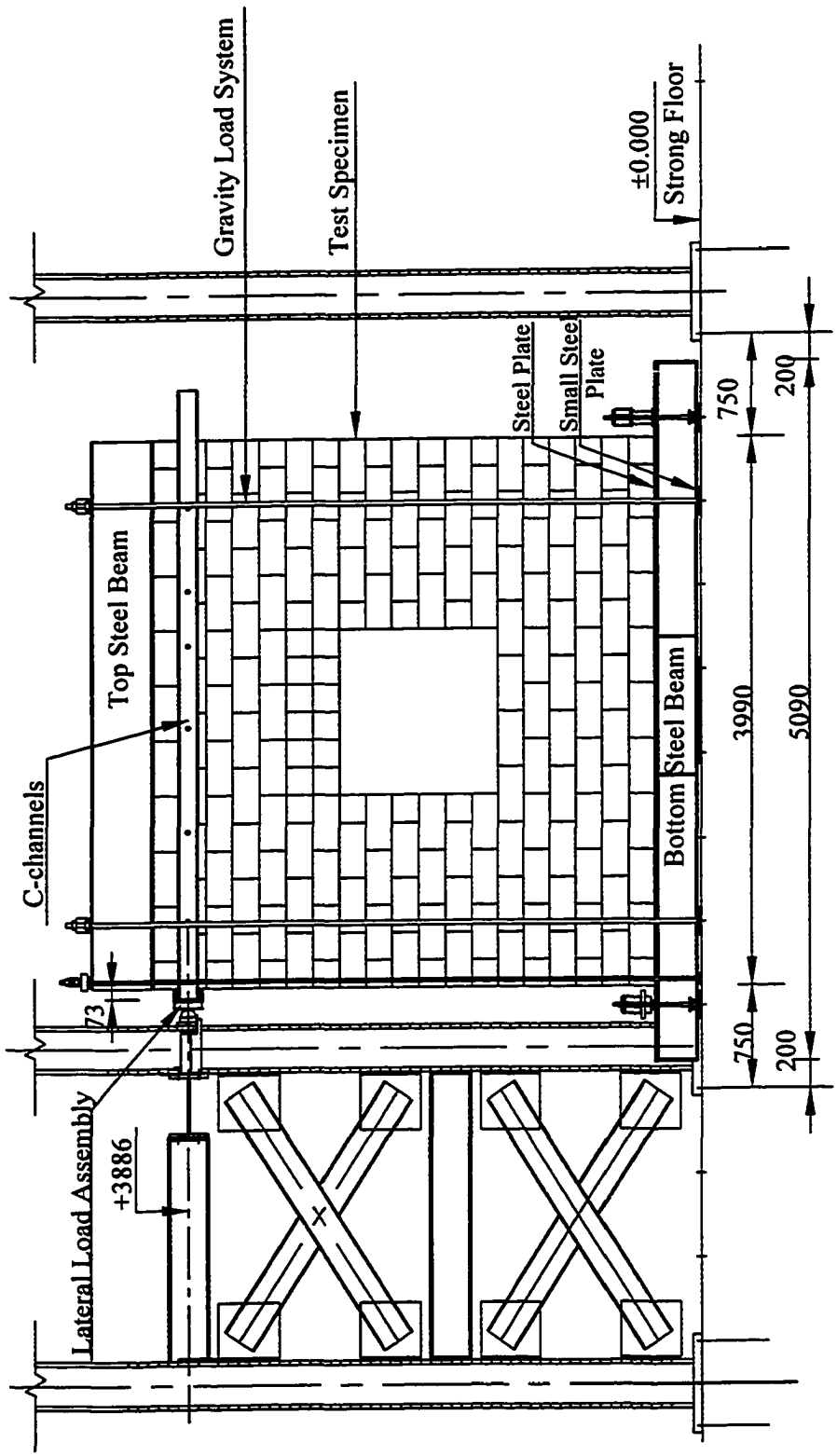

Figure 3-3 Test Set-up and Loading System

Figure 3-4 Failure Mode for W1

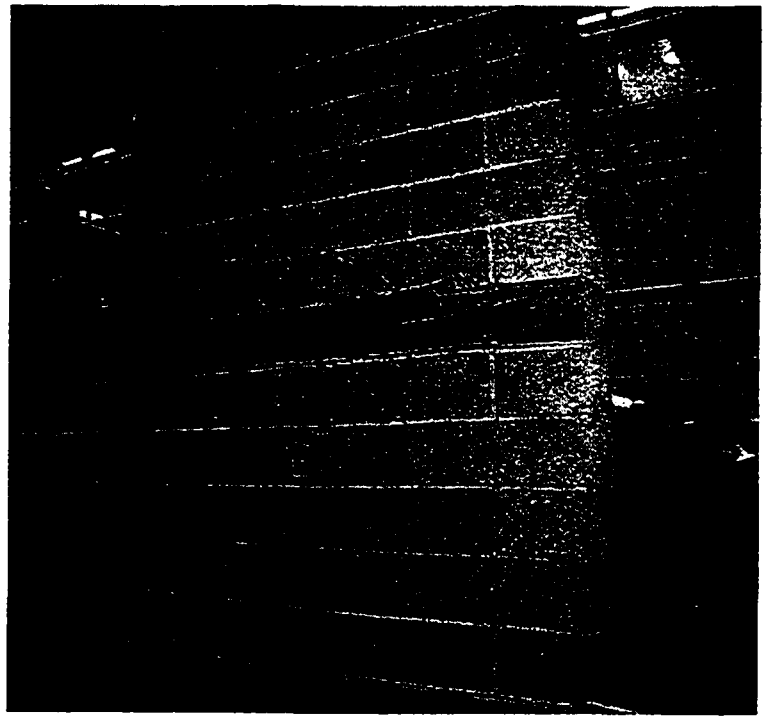

Figure 3-5 Failure Mode for W2

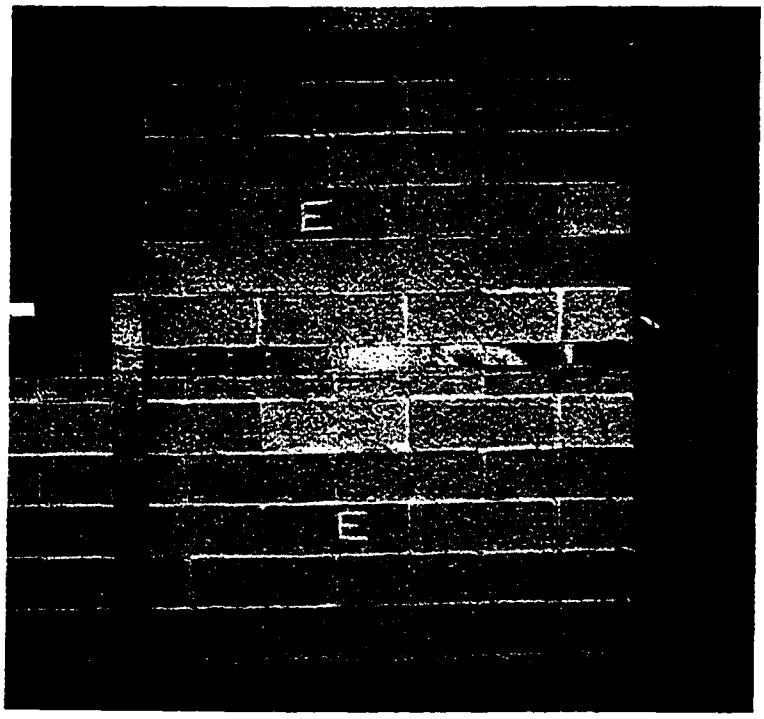

Figure 3-6 Failure Mode for W3

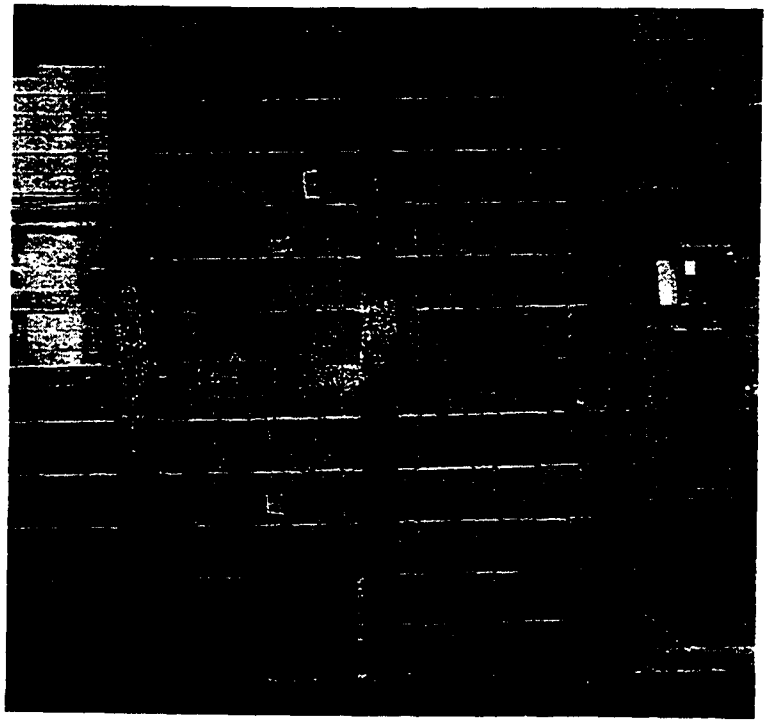

Figure 3-7 Failure Mode for W4

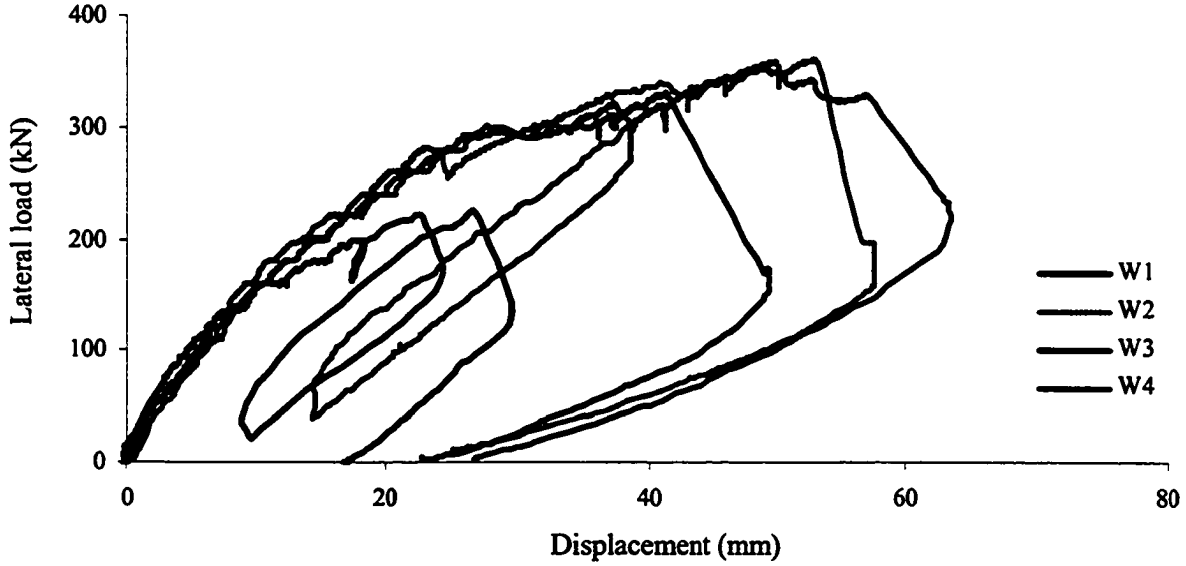

Figure 3-8 Lateral Load - Displacement Curves from Test

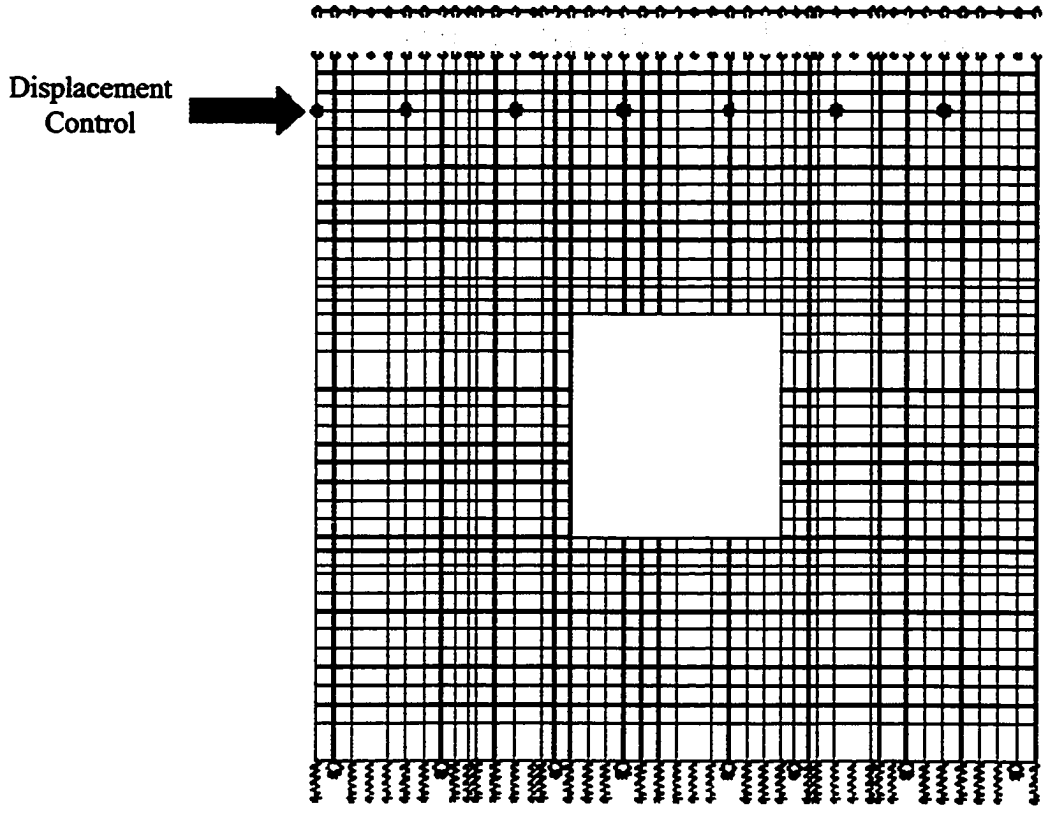

Figure 3-9 Mesh, B.C. and Loading

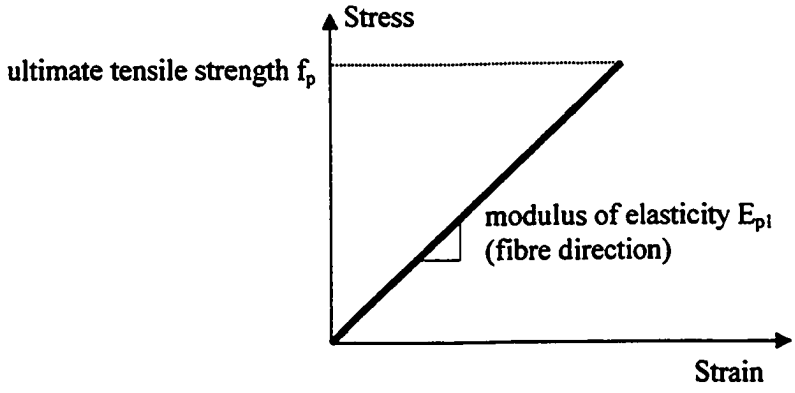

Figure 3-10 CFRP Behaviour

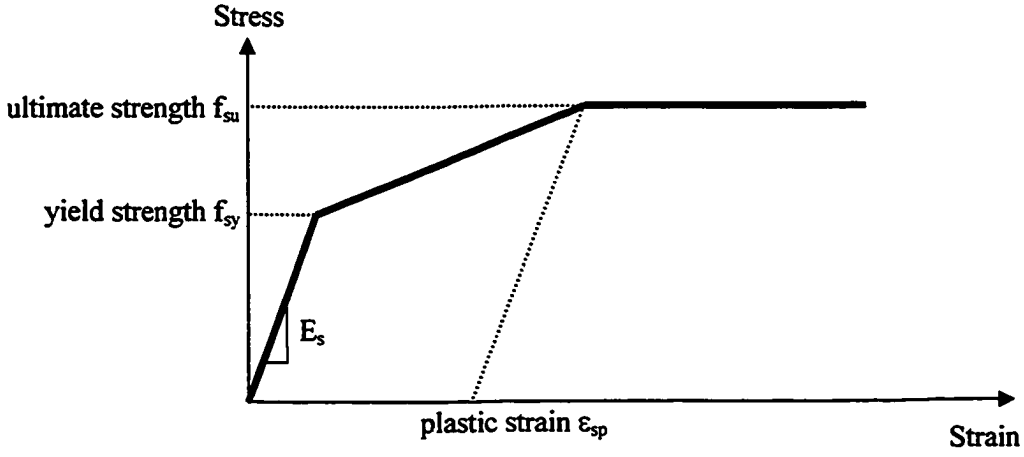

Figure 3-11 Steel Behaviour

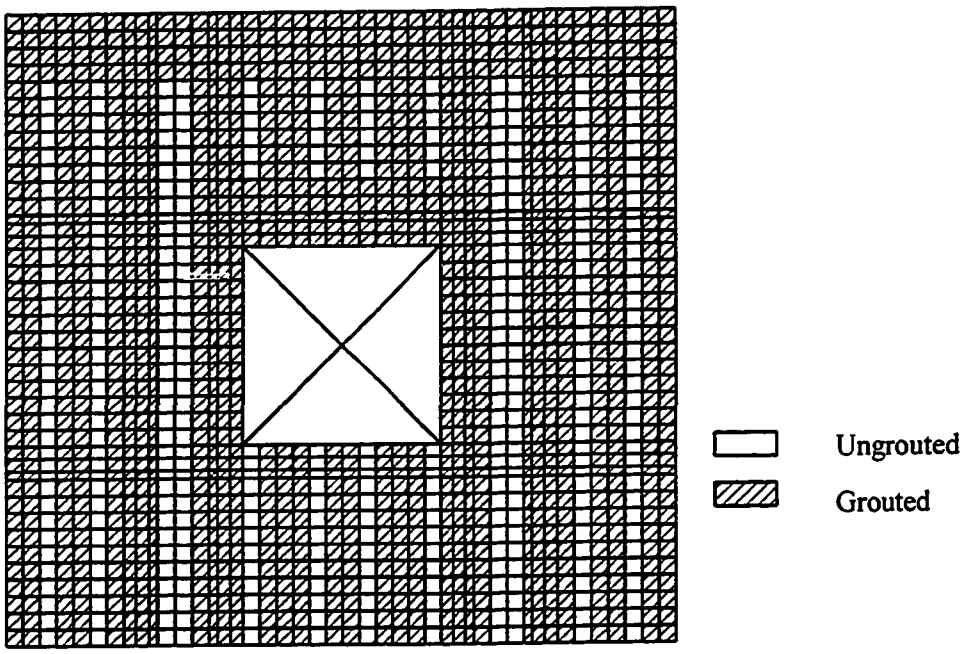

Figure 3-12 Distribution of Masonry Elements

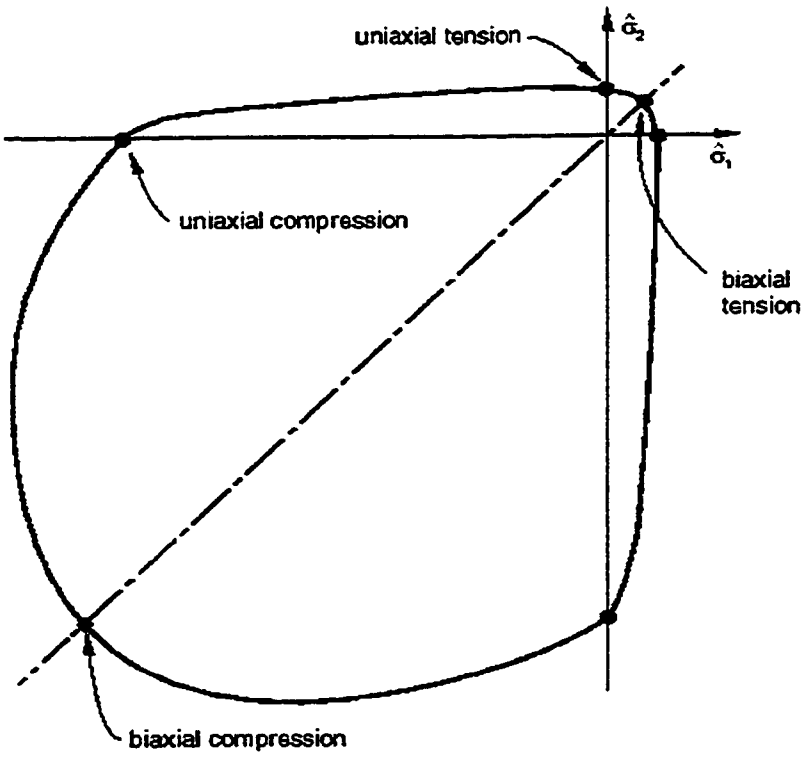

Figure 3-13 Yield Surface in Plane Stress (ABAQUS 2002)

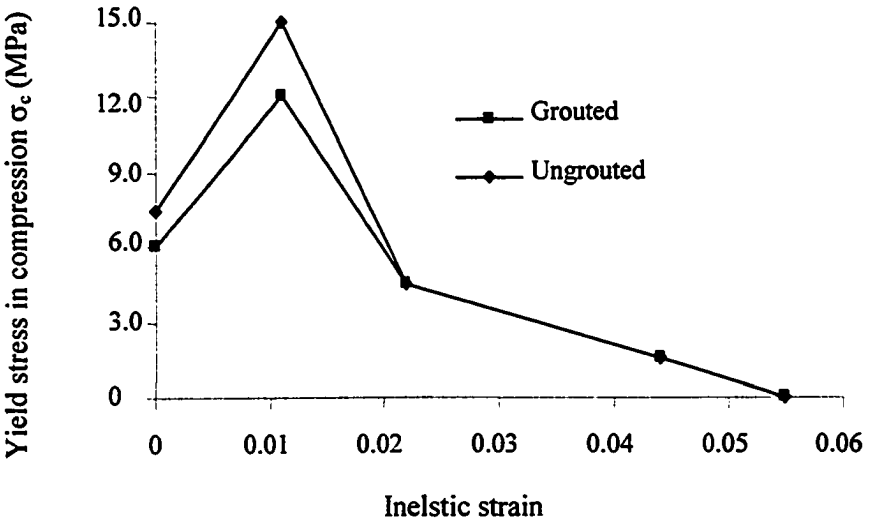

Figure 3-14 *CONCRETE COMPRESSION HARDENING Curves

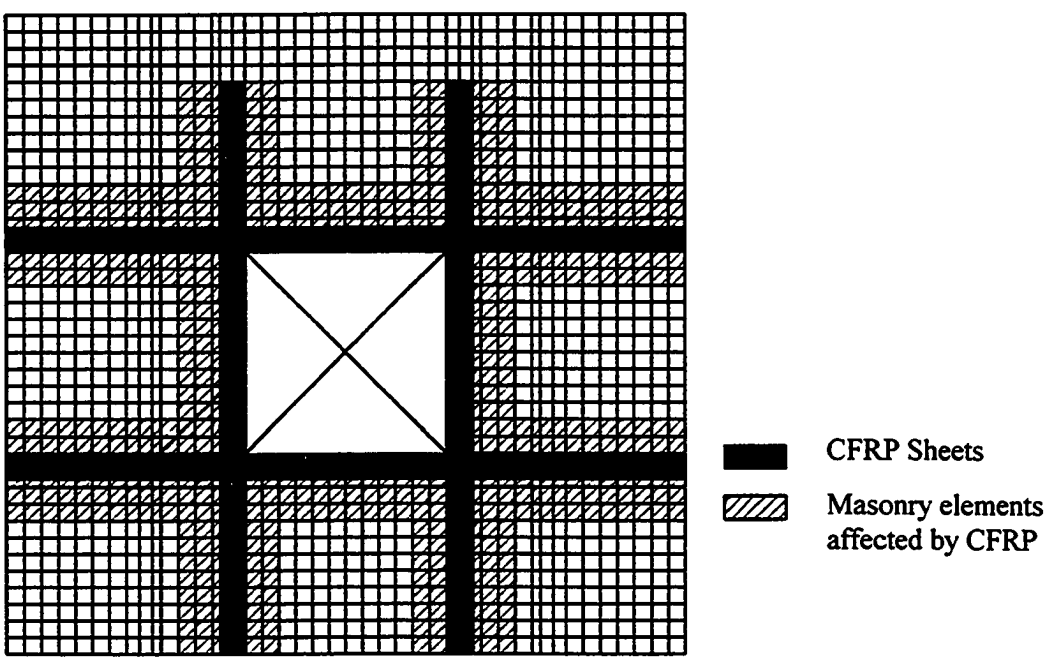

Figure 3-15 Masonry Elements Affected by CFRP for W2

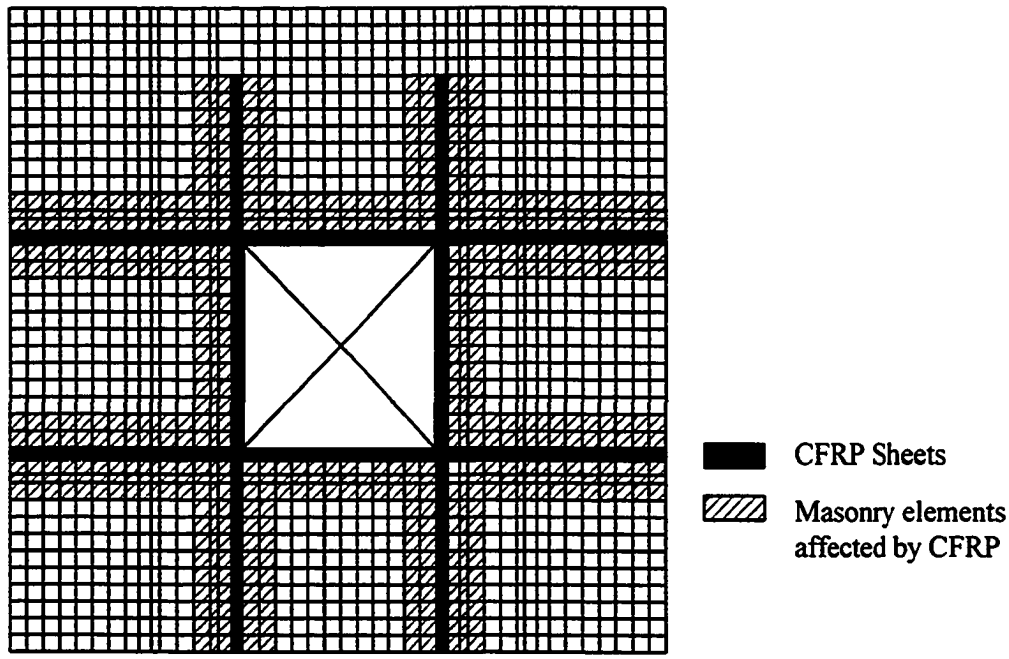

Figure 3-16 Masonry Elements Affected by CFRP for W3

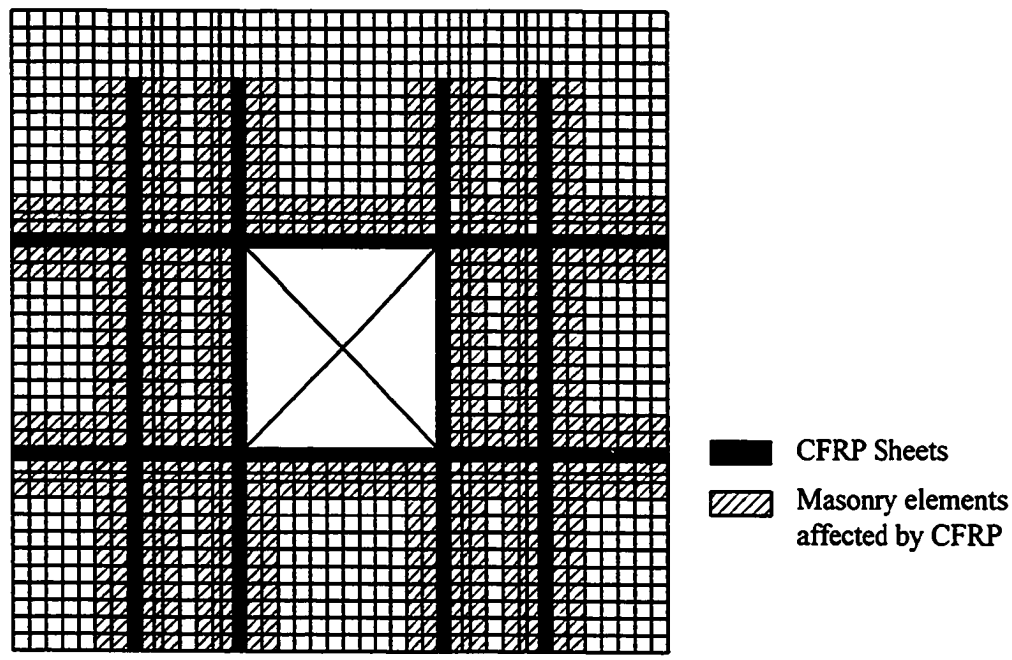

Figure 3-17 Masonry Elements Affected by CFRP for W4

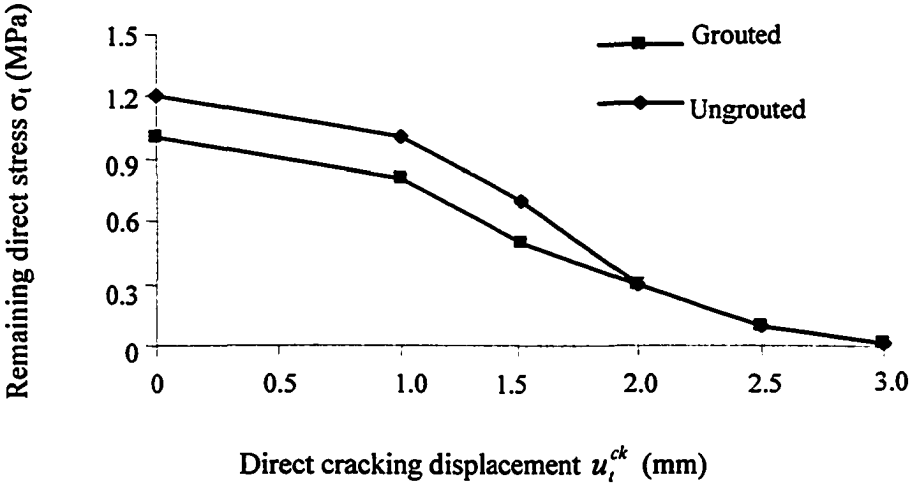

Figure 3-18 *CONCRETE TENSION STIFFENING Curves for W1

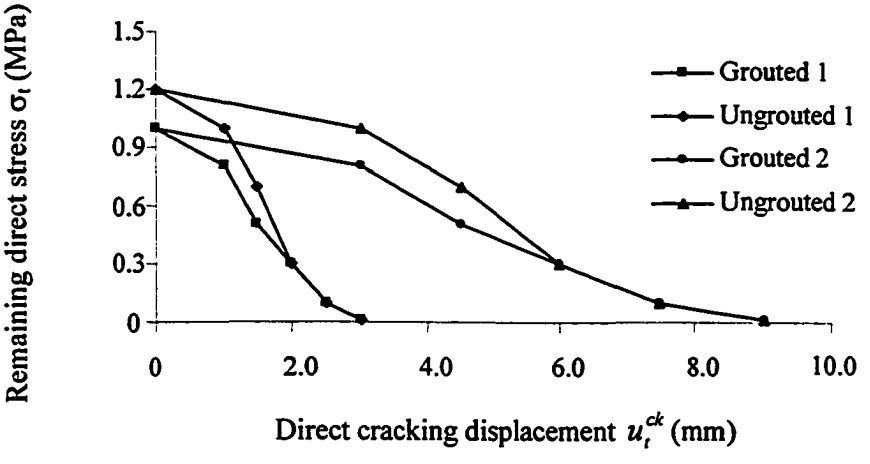

Figure 3-19 *CONCRETE TENSION STIFFENING Curves for W2 & W4

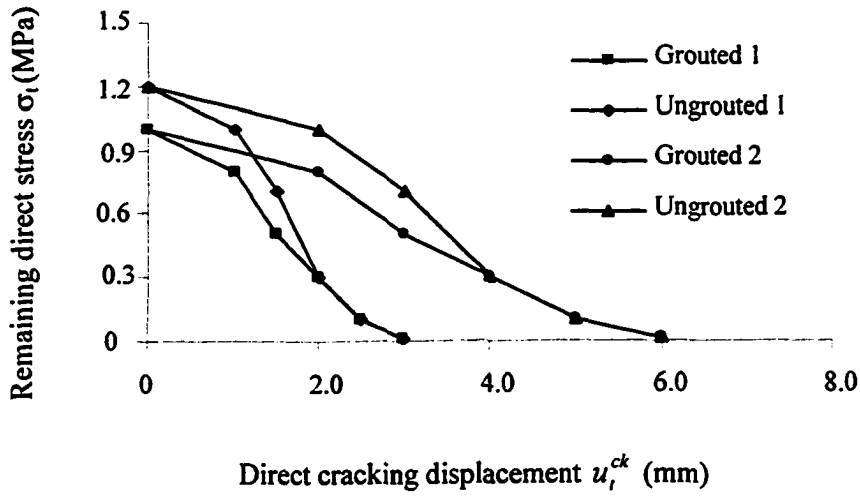

Figure 3-20 *CONCRETE TENSION STIFFENING Curves for W3

4. VERIFICATION AGAINST EXPERIMENTAL RESULTS

4.1 Introduction

In this chapter, the results of numerical models for the specimens tested at the University of Alberta are presented and discussed including deformation shapes, lateral load – displacement responses, stress and strain contours at failure, as well as the distribution of stress and strain of CFRP elements along fibre directions under different load levels. Verification is made against the test results and the comparison results between them are set forth. Conclusions are drawn based on the comparison and discussion.

4.2 Results of Numerical Analysis, Discussions and Verification

It should be pointed out that during the simulation process the same parameters for the masonry material and steel reinforcement were used for the four models of the tested specimens. In addition, the same parameters for CFRP material were employed for the three models containing CFRP sheets. As a result, the numerical models are representative and can be generalized to predict numerical results for other similar experimental programs if further calibration is to be made. The numerical models are verified by comparing their output with the experimental results that were discussed briefly in Chapter 3. The comparisons were performed on the overall lateral load – displacement behaviour of the specimens.

In order to obtain the overall lateral load – displacement responses of the specimens, the lateral reactions at the bottom elements and the displacement at the top and bottom elements of the walls at all time increments were recorded throughout the numerical analysis. The relative top lateral displacement of the walls was derived by deducting the bottom displacement from the top displacement. This procedure coincided with that used in experimental analysis. The overall lateral reaction was derived by

summing up the individual reaction in the lateral direction of every single element at the bottom of the walls. The overall lateral load was equal to the overall lateral reaction but with an opposite direction. The two sets of data for lateral load and displacement were then used to plot the lateral load – displacement curves and they were compared to the corresponding experimental curves derived from the test results.

The deformed shapes were automatically plotted by ABAQUS program based on the displacement output of every single element. The stress and strain contours for the masonry walls were also plotted and compared at failure. In addition, the strain and stress histories in the CFRP sheets were obtained and then the distribution curves of the strain and stress along fibre direction were plotted for both vertical and horizontal CFRP sheets and the results were compared at different lateral load levels. Some conclusions are drawn form these output results.

Figure 4-1 shows cracking patterns of the specimens at failure derived from experiment results. It can be seen that the main cracking developed diagonally in the right piers of the specimens. The detailed description can be found in Miao (2004). Figure 4-2 illustrates the distribution and designation of the CFRP sheets. Here "H' stands for Horizontal and "V" stands for "Vertical". For the horizontal CFRP sheets, from bottom to top the designation is given from H1 to H4, respectively. For the vertical CFRP sheets, from left to right the designation is given from V1 to V6, respectively. Figure 4-3 shows the lateral load verse displacement curves for the four specimens derived from the numerical models. It is evident to see that the lateral capacity and ductility of the masonry shear walls were substantially increased by CFRP strengthening.

4.2.1 Specimen W1

Deformation Shape

Specimen W1 was a control wall and there were no CFRP sheets on it. It served

as the comparison basis for the other three walls with CFRP. The behaviour of the wall at failure is depicted in Figure 4-4 in terms of deformed mesh with a deformation scale factor (DSF) of 10. It is noted that larger lateral deformation takes place at the elements around the opening, especially at the bottom-right corner of the opening. It is observed from Figure 4-1 (a) that diagonal cracking obviously developed at the right pier in the experiment, which is not obvious in the deformation shape derived from the numerical model.

Lateral Load - Displacement Curves

The comparison between numerical and experimental load – displacement diagrams, for specimen W1, is given in Figure 4-5. From a qualitative perspective good agreement is found because the same trend is observed in both diagrams. In particular, for the first approximately 80 mm displacement, the two diagrams are in good agreement. The lateral load capacity is also well predicted by the numerical analysis since the capacity from the experiment and model is 225 kN and 230 kN respectively with only 2.2% difference. Less agreement is found with respect to the displacement values corresponding to the peak load.

It is noted that in the curve of the test there was an unloading and reloading process at a displacement of about 23 mm during the experiment. This process resulted from the premature local failure of some portion of the wall at the bottom-left corner because of excessive tensile stress caused by wall uplifting when subjected to constantly increasing lateral load. As a result, the lateral load was decreased so that two external steel rods could be mounted to the wall to prevent further failure of the wall. Then the wall was reloaded until it failed. Failure took place when diagonal cracks developed in the right pier to such an extent that the tensile stress caused by monotonically increasing lateral load exceeded the ultimate tensile strength of the masonry wall. In the numerical analysis the process of unloading and reloading was not modeled.

It is also noticed that the numerical model is much stiffer than the test result. This was probably caused by the inability of the models to differentiate the stiffness and cracking patterns between head joint and bed joint. An initially isotropic elastic modeling and tensile strength were assigned to the models. Other possible factors may also result in this problem. Firstly, it can be accounted for by the boundary conditions at the bottom of the specimen. In the numerical model, the boundary conditions at the bottom of the wall were modeled as pinned or spring-connected; while in the actual experimental program, the wall was connected to the steel plate, which was directly under the wall, by welded dowels and the plate was bolted to the stiff steel beam, which was directly under the steel plate and just situated on the strong floor without any connection between the steel beam and the floor. Thus the boundary conditions for the experiment were not totally pinned or fixed. In addition, it was also showed that there was some sliding along the horizontal direction during the loading process from the test data recorded from the LVDTs mounted to the bottom of the wall. This sliding led to stiffness decrease of the specimen when subjected to in-plane loadings.

Secondly, the homogenous continuum macro-modeling was used for masonry material in terms of average strains and stresses, neglecting the existence of mortar joints which act as planes of weakness. As a matter of fact, the stiffness of mortar joints differs greatly from that of the masonry units.

Thirdly, the stiffness of the mortar joints differs between bed joints, which are reliable and head joints, which are less reliable.

In addition, the use of LINK connections of MPC rather than the modeling of debonding process between the masonry walls and CFRP sheets would also lead to the higher stiffness of the numerical model because the LINK constraints offer a pinned rigid link between two nodes to keep the distance between the two nodes constant; while it is impossible to take place under the experimental situation.

Strain and Stress Contour

Figure 4-6 shows the strain contour (maximum in-plane principal logarithmic strain) for specimen W1 at failure. It is evident that the critical areas with large strain are those beside the opening, especially at the bottom-right corner of the opening with the value of 0.09. This is because the increasing lateral loading caused diagonal tensile stress in the direction of bottom-left to top-right and results in the cracking in the direction perpendicular to the direction of the tensile stress. It agrees with the experimental observation that the cracking initiated at the similar areas during loading as shown in Figure 4-1(a).

The stress contour (Mises equivalent stress) for the wall at failure is given in Figure 4-7. It can be seen that higher equivalent stress occurs at the left pier of the wall. The lateral loading, applied from left to right (push), led to the distribution of tensile stress area in the left pier and compressive stress area in the right pier. The maximum equivalent stress is greater than 6 MPa, which exceeds the tensile strength of the masonry material, implying that the masonry cracked in some areas and some of the tensile stress was carried by the steel reinforcement.

4.2.2 Specimen W2

Deformation Shape

Specimen W2 had four vertical and horizontal 156mm-wide CFRP sheets around the opening at each side of the wall; while in the numerical analysis the width of the CFRP sheets was modified from 156 mm to 150 mm in order to simplify the mesh modeling. The behaviour of the wall W2 at failure is depicted in Figure 4-8 in terms of deformed mesh with a deformation scale factor (DSF) of 10. It is also seen that larger lateral deformation takes place at the right pier of the wall.

Figure 4-10 shows the deformation comparison for specimens W1 and W2 in terms of the same deformation scale factor (DSF) under the same load level (220 kN). It is obvious that specimen W2 with CFRP sheets deforms less than the control wall W1, indicating the substantial strengthening provided by CFRP sheets.

Lateral Load - Displacement Curves

The comparison between numerical and experimental load – displacement diagrams, for specimen W2, is given in Figure 4-9. More ductile behaviour and higher lateral load capacity resulting from CFRP strengthening have been observed when compared to the control wall in both numerical and experimental results. From a qualitative perspective good agreement is found because the same trend is shown in both diagrams. In particular, for the ascending part of the curves, the two diagrams are almost parallel. However the model is still stiffer than the test result. The lateral load capacity is overestimated by the numerical analysis at 445 kN; 23.6% higher than the value of 360 kN from the test. In addition, the model seems to be more ductile than the test result with 10.7% higher when comparing the displacements at the peak load. It should be pointed out that the model did not well simulate the descending part of the curve derived from the experiment, implying the model did not capture the characteristics of the structure failure mechanism right before and after failure. Thus further calibration needs to be conducted in the future.

Strain and Stress Contour

Figure 4-11 shows the strain contour (maximum in-plane principal logarithmic strain) for specimen W2 at failure. It is indicated that the critical areas with large strain are at the wall bottom as well as some parts of the two piers, which agrees with the cracking pattern in Figure 4-1 (b). The wall elements present relatively higher tensile strain with very small compression strain, indicating that tension predominated in the wall.

The strain contour of masonry elements and CFRP sheets under the same load level for specimen W1 and W2 is shown in Figure 13. Comparing Figure 13 (a) and (b) the maximum strain of masonry elements is 0.04 for W1 and 0.007 for W2. For the same areas, the strain in W2 is obviously much lower than that in the control wall W1. In addition, for W1 the critical elements are at the bottom-right corner of the opening; while for W2 the critical elements are at the bottom-left of the wall because of uplifting. As shown in Figure 13 (c), the maximum strain of CFRP sheets is 0.0007 for specimen W2.

The stress contour (Mises equivalent stress) for the wall at failure is given in Figure 4-12. It is indicated that high equivalent stress takes place at the elements of CFRP sheets around the opening, especially at the top-right and bottom-left corners because of the lateral loading. The maximum stress is 379 MPa, which is far below the ultimate tensile strength of 3800 MPa for CFRP provided by the manufacturer. Because of high tensile capacity provided by CFRP sheets, the overall lateral load capacity has been significantly increased.

Strain Distribution of CFRP Sheets

The strain distribution of horizontal CFRP sheets along the fibre direction at different load levels is shown from Figure 4-14 to Figure 4-17. It is shown that larger horizontal strain occurs at the opening corners due to the decreased wall stiffness by the introduction of the opening. The strain signs are opposite for the horizontal CFRP sheets below and above the opening (H1 & H4, H2 & H3) and even for the upper and lower sheets at the same side (H1 & H2, H3 & H4) because of frame action. The maximum tensile and compressive horizontal strain is about $1.5x10^{-3}$ at failure respectively.

The horizontal strain distribution of masonry elements for specimen W1 and the horizontal strain distribution of CFRP sheets for specimen W2 at the same location (H2) are given in Figure 4-18 and Figure 4-19, respectively. For W1 the critical elements are at the right corner of the opening with the maximum value of 0.04. For W2 the elements at the opening corners have much higher strain. The strain at the right corner of the opening

is only 0.0015, which is much lower than the strain in the control wall W1 at the same location. Similarly, when comparing Figure 4-18 with Figure 4-38 and Figure 4-18 with Figure 4-50, it can also concluded that the strain has been greatly decreased under the same load level due to CFRP strengthening.

The strain distribution of vertical CFRP sheets along the fibre direction at different load levels is shown from Figure 4-20 to Figure 4-23. It is shown that larger vertical strain still occurs at the opening corners. The strain signs are opposite for the vertical CFRP sheets beside the opening (V2 & V5, V3 & V4) and even for the sheets at the same side (V2 & V3, V4 & V5) because of frame action. The maximum tensile and compressive vertical strain is around $2.5x10^{-3}$ at failure respectively.

The vertical strain distribution of masonry elements for specimen W1 and the vertical strain distribution of CFRP sheets for specimen W2 at the same location (V4) are given in Figure 4-24 and Figure 4-25, respectively. For W1 the critical elements are at the top corner of the opening with the maximum value of 0.0027 and the infection point is at the location of 1300 mm high. For W2 the elements at the opening corners have much higher strain, especially at the top corner and the maximum value is similar to that in the control wall W1. However the infection point has shifted from lower location in W1 to the centerline of the opening in W2. Similar conclusions can be drawn when comparing Figure 4-24 with Figure 4-41 and Figure 4-24 with Figure 4-54.

Stress Distribution of CFRP Sheets

The stress distribution of horizontal CFRP sheets along the fibre direction at different load levels is given from Figure 4-26 to Figure 4-29. The stress distribution is found similar to the corresponding strain distribution and similar conclusions can be drawn from the analysis. The maximum tensile and compressive horizontal stresses are about 250 MPa respectively at failure. The reason why the compressive stress existed in the CFRP sheets is that the CFRP elements were connected with the corresponding elements in the masonry wall by MPC connections and they deformed together and

sustained the compressive stress together caused by the combination of vertical and lateral loading.

The stress distribution of the vertical CFRP sheets along the fibre direction at different load levels is shown from Figure 4-30 to Figure 4-33. Similar conclusions to the corresponding strain analysis can be drawn from the stress distribution. The maximum vertical tensile stress is around 360 MPa at failure.

4.2.3 Specimen W3

Deformation Shape

Specimen W3 had four vertical and horizontal 78 mm–wide CFRP sheets around the opening at each side of the wall. The behaviour of the wall W3 at failure is depicted in Figure 4-34 in terms of deformed mesh with a deformation scale factor (DSF) of 10. The elements in the two piers deform more than other elements.

Lateral Load - Displacement Curves

The comparison between numerical and experimental load – displacement diagrams, for specimen W3, is given in Figure 4-35. It is noted that the model is still stiffer than the test result. The lateral load capacity is underestimated by the numerical model at 292 kN, 11.5% lower than the value of 330 kN from the test. The displacement values at peak load are very close with 38.9 mm from the numerical analysis and 40.9 mm from the experiment. It should be noted that the numerical model did not agree with the descending part of the curve derived from the experiment.

Strain and Stress Contour

Figure 4-36 shows the strain contour (maximum in-plane principal logarithmic strain) for specimen W3 at failure. It can be seen that the critical areas with large strain are at the piers beside the opening, especially at the left pier, which agrees with the cracking pattern in Figure 4-1 (c). The maximum tensile strain is $1.105x10^{-1}$, which is higher than that for specimen W2 since narrow CFRP sheets were applied to the specimen W3.

The stress contour (Mises equivalent stress) for the wall W3 at failure is given in Figure 4-37. It is indicated that high equivalent stress happens at the left CFRP sheets. The maximum stress is 170 MPa, which is much lower than that in specimen W2.

Strain Distribution of CFRP Sheets

The strain distribution of horizontal CFRP sheets along the fibre direction at different load levels is shown in Figure 4-38 and Figure 4-39. It is shown that there is an obvious change at the elements close to the bottom-right corner, indicating that the cracking developed rapidly at this area. The minimum and maximum horizontal strain is about $-2.0x10^{-4}$ and $3.0x10^{-4}$ at failure, respectively. The strain signs are opposite for the two horizontal CFRP sheets.

The strain distribution of the vertical CFRP sheets along the fibre direction at different load levels is shown in Figure 4-40 and Figure 4-41. The minimum and maximum vertical strain is around $-7.0x10^{-4}$ and $10.5x10^{-4}$ at failure, respectively. The strain signs are approximately opposite for the two vertical CFRP sheets.

Stress Distribution of CFRP Sheets

The stress distribution of horizontal CFRP sheets along the fibre direction at different load levels is given in Figure 4-42 and Figure 4-43. The stress signs are

approximately opposite for the two horizontal CFRP sheets. The critical elements are at the bottom-right and up-left corners of the opening, which agrees with the experimental observation shown in Figure 4-1 (c). The maximum tensile and compressive stresses are around 40 MPa at failure, respectively, which are much lower than those derived from specimen W2.

The stress distribution of the vertical CFRP along the fibre direction at different load levels is shown in Figure 4-44 and Figure 4-45. The critical elements are at the opening corners. The maximum vertical tensile stress is around 160 MPa at failure, which is much lower than that at the same location for specimen W2.

4.2.4 Specimen W4

Deformation Shape

Specimen W4 had six vertical and horizontal 78 mm-wide CFRP sheets at each side of the wall. In the modeling the width was also changed from 78 mm to 75mm for simplicity. The behaviour of the wall W4 at failure is depicted in Figure 4-46 in terms of deformed mesh with a deformation scale factor (DSF) of 10. Large deformation occurs at the two piers.

Lateral Load - Displacement Curves

The comparison between numerical and experimental load – displacement diagrams, for specimen W4, is given in Figure 4-47. It is noted that the model is still stiffer than the test. The lateral load capacity is underestimated by the numerical model at 319 kN, 9.6% lower than the value of 353 kN from the test. In addition, the displacement values at peak load are very close with 52 mm from the numerical and 49 mm from the experimental results. The same problem exists that the numerical model does not agree with the descending part of the curve derived from the experiment. Therefore the model

needs to be further calibrated in both load capacity and the descending curve after the peak load is reached.

It is observed that in the test curve there is an unloading and reloading process at the displacement of about 37.4 mm during the experiment. This process resulted from the excessive load on the load cell used to record the load on the externally mounted steel rods, which were applied to prevent the wall uplifting. Hence the lateral load was decreased so that another load cell with higher capacity could be mounted to replace the load cell with lower capacity. Then the lateral load was increased and applied to the wall until failure. In the numerical analysis the process of unloading and reloading was not modeled.

Strain and Stress Contour

Figure 4-48 shows the strain contour (maximum in-plane principal logarithmic strain) for specimen W4 at failure. It is indicated that the critical areas with large strain are at both piers beside the opening, which agrees with the cracking pattern in Figure 4-1 (d). The maximum tensile strain at failure is 1.121×10^{-1}, which is slightly higher than that for specimen W3.

The stress contour (Mises equivalent stress) for the wall W4 at failure is given in Figure 4-49. It can be seen that high equivalent stress concentrates at some elements in the vertical CFRP sheets at the left pier. The maximum stress is 184 MPa after failure, which is slightly higher than that in specimen W3.

Strain Distribution of CFRP Sheets

The strain distribution of horizontal CFRP sheets along the fibre direction at different load levels is shown in Figure 4-50 and Figure 4-51. Obvious change happens to the elements around the bottom-right and top-left corners of the opening where the initial

cracking developed in the experiment. The minimum and maximum horizontal strain is about -2.2×10^{-4} and 3.5×10^{-4} at failure, respectively.

The strain distribution of the vertical CFRP sheets along the fibre direction at different load levels is shown from Figure 4-52 to Figure 4-55. It is shown that larger vertical strain still occurs at the opening corners. The strain signs are opposite for the vertical CFRP sheets beside the opening (V1 & V6, V3 & V4) and even for the sheets at the same side (V1 & V3, V4 & V6) because of frame action. The maximum tensile and compressive vertical strain is around 1.0×10^{-3} and -7.0×10^{-4} at failure respectively.

Stress Distribution of CFRP Sheets

The stress distribution of horizontal CFRP sheets along the fibre direction at different load levels is given in Figure 4-56 and Figure 4-57. Similar trend and conclusion to the strain analysis can be obtained. The maximum horizontal tensile and compressive stress is around 55 MPa and 40 MPa at failure respectively, which are similar to specimen W3 but far below than those derived from specimen W2.

The stress distribution of the vertical CFRP along the fibre direction at different load levels is shown from Figure 4-58 to Figure 4-61. They are very similar to the corresponding strain distribution of the CFRP sheets. The maximum vertical tensile stress is around 165 MPa at failure, which is also close to the value of specimens W3 but much lower than the value for specimen W2.

4.3 Summary

In this chapter, the numerical results for the corresponding experimental specimens are described in detail including deformation shapes, lateral load verse displacement curves, strain and stress contour, as well as the strain and stress distribution of CFRP sheets along the fibre directions. Verifications are performed against the

experimental results and relatively good agreements are found. However the numerical models still need to be calibrated in order to better coincide with the test results. The next chapter will sum up the numerical analysis and results derived in this study and conclusions will be drawn based on the comparison and discussion. In addition, some recommendations will be proposed for future research.

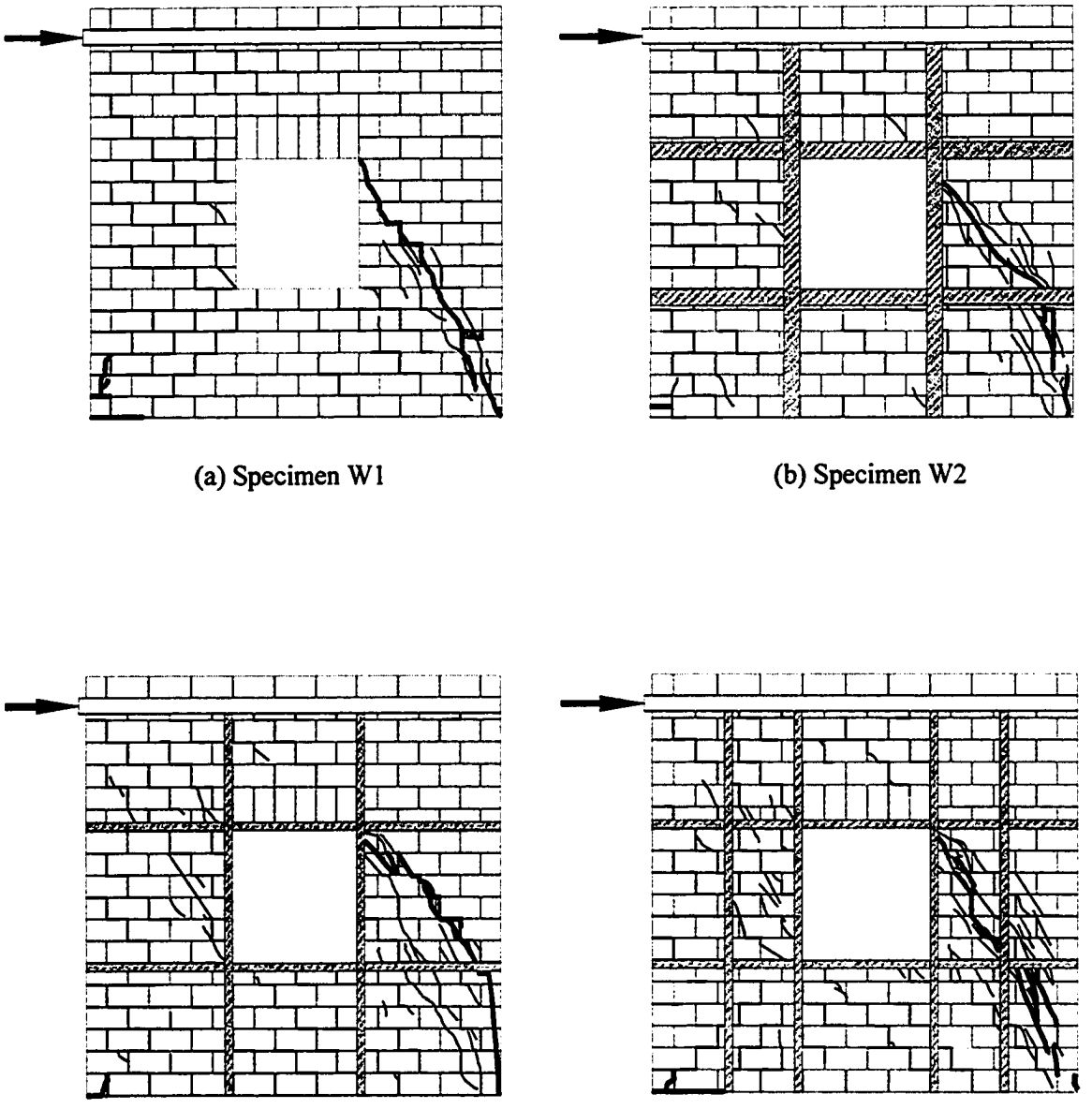

(a) Specimen W1

(b) Specimen W2

(c) Specimen W3

(d) Specimen W4

Figure 4-1 Cracking Patterns at Failure from Test

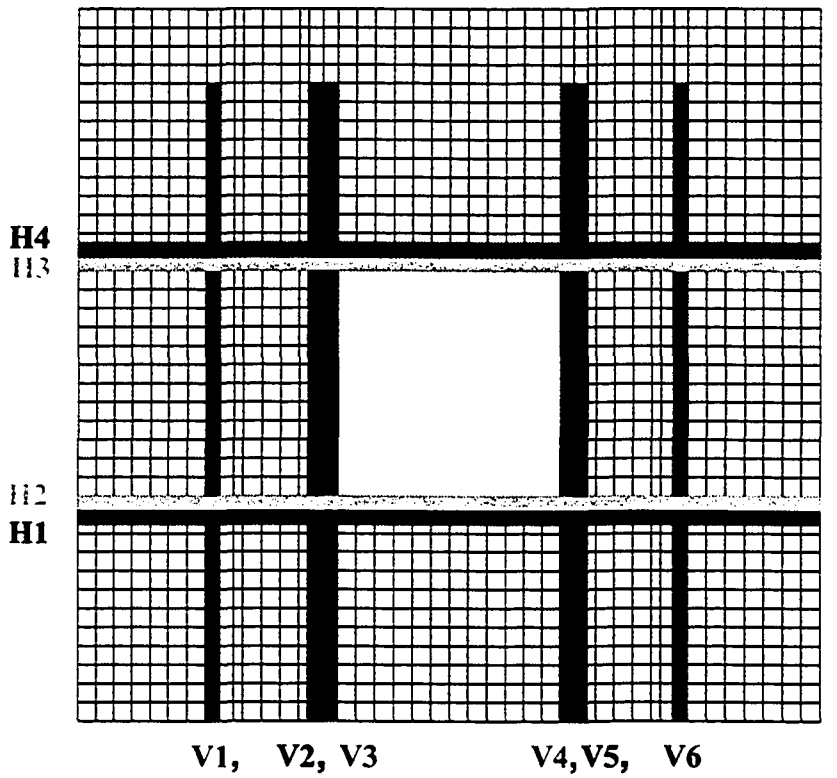

Figure 4-2 Distribution and Designation of CFRP Sheets

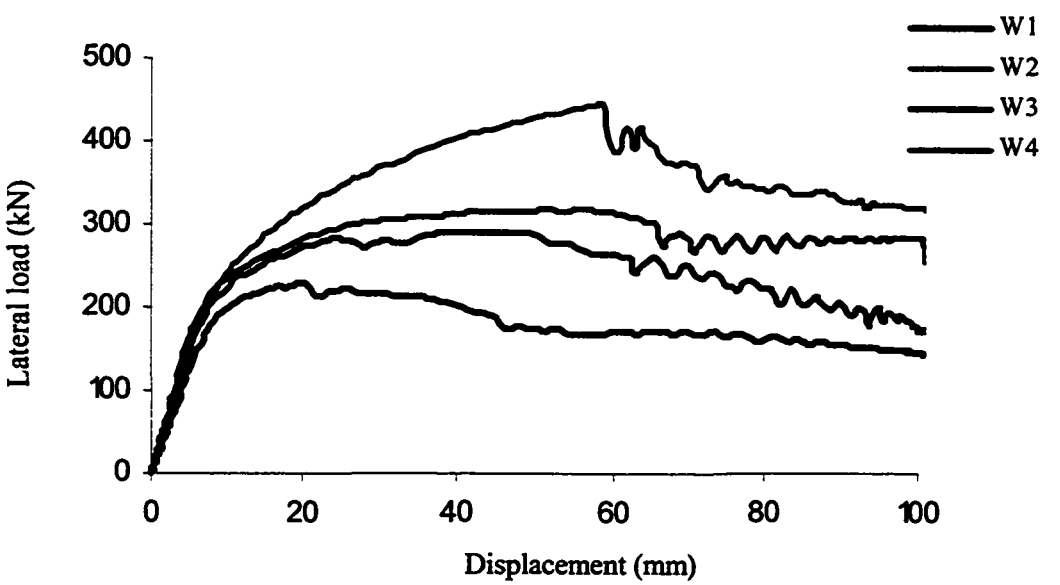

Figure 4-3 Lateral Load – Displacement Curves from Models

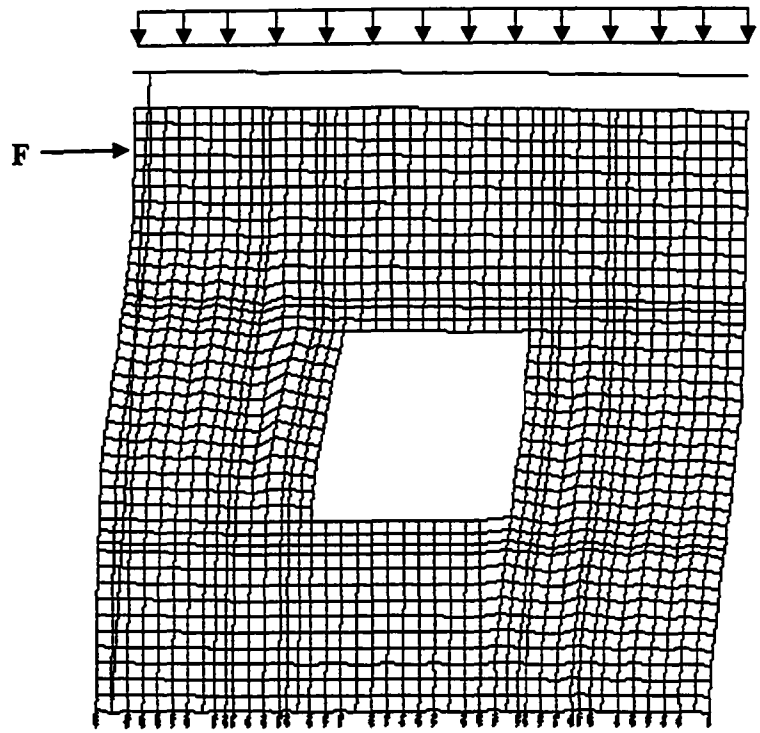

Figure 4-4 Deformed Mesh for Specimen W1

(DSF = 10)

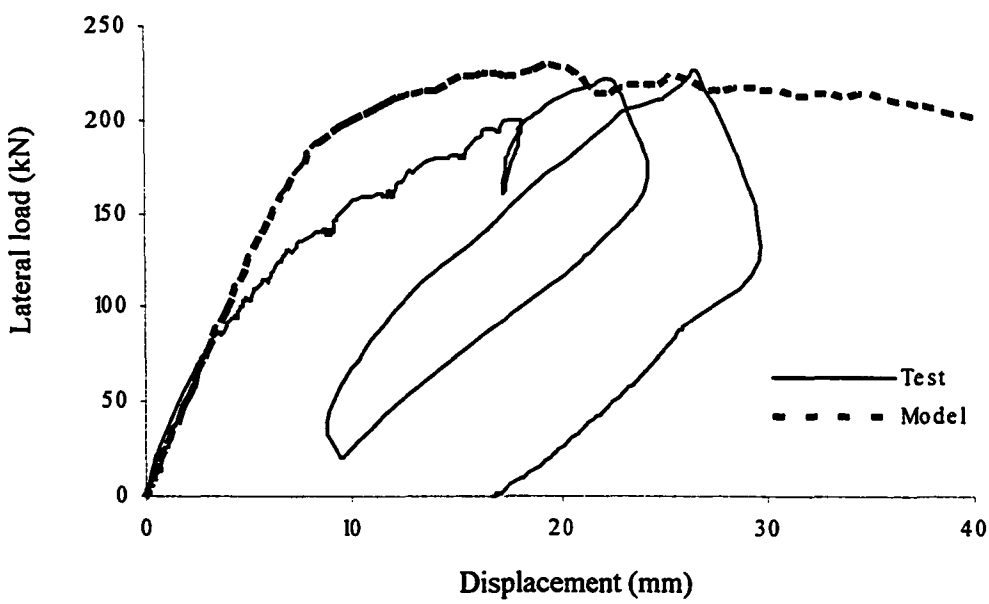

Figure 4-5 Lateral Load - Displacement Curves for W1

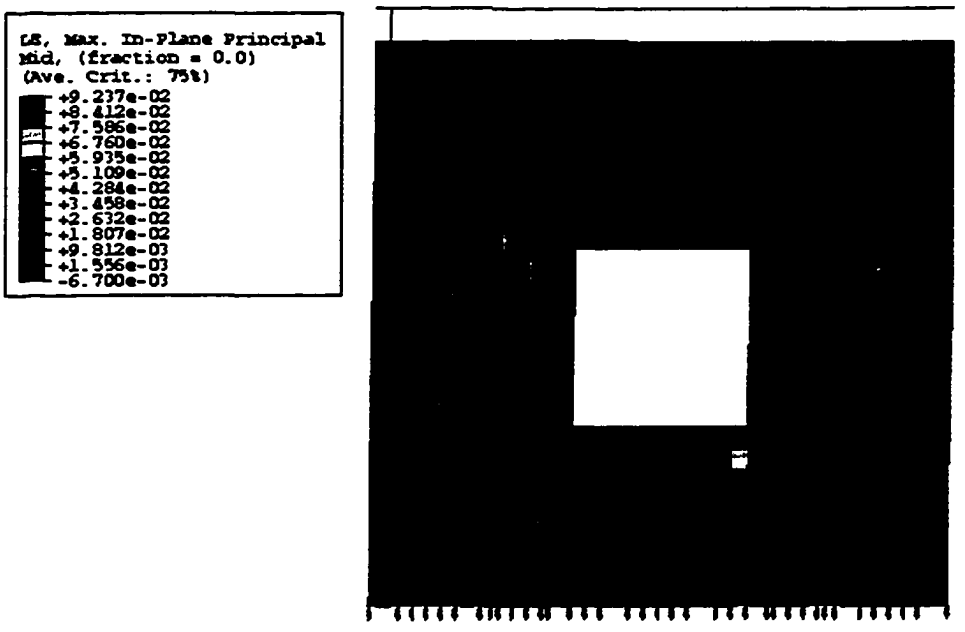

Figure 4-6 Strain Contour for W1 (at failure)

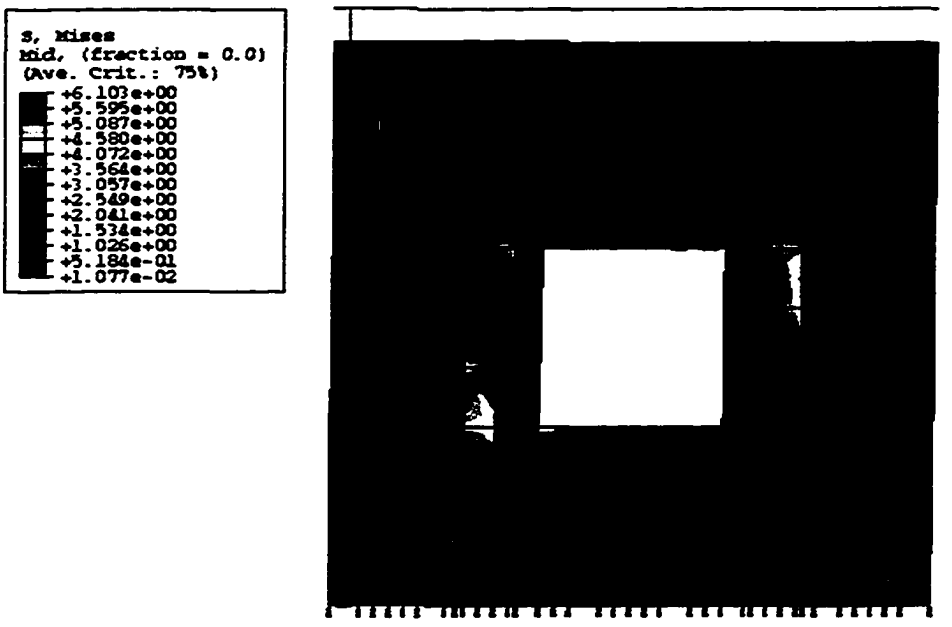

Figure 4-7 Stress Contour for W1 (at failure)

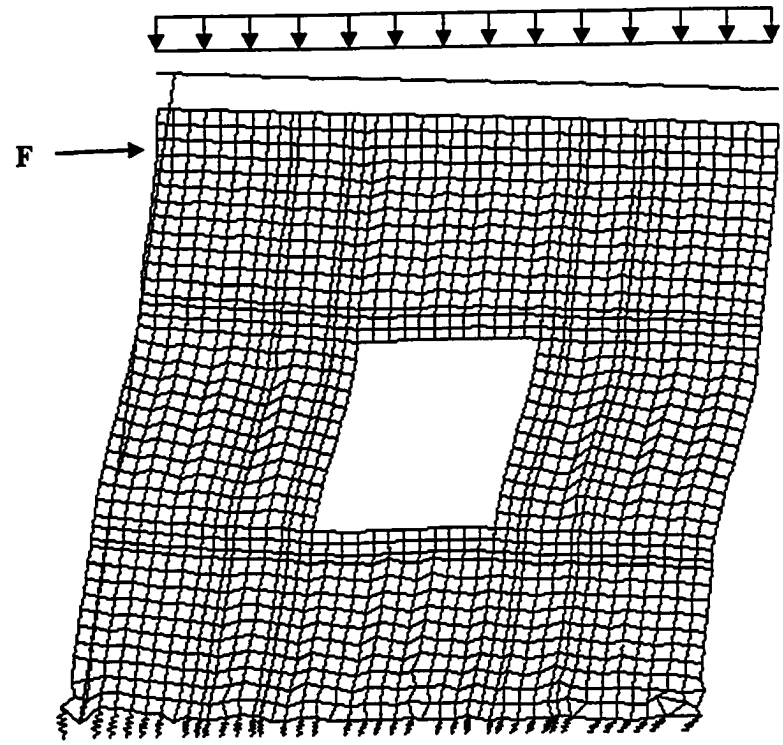

Figure 4-8 Deformed Mesh for Specimen W2

(DSF= 10)

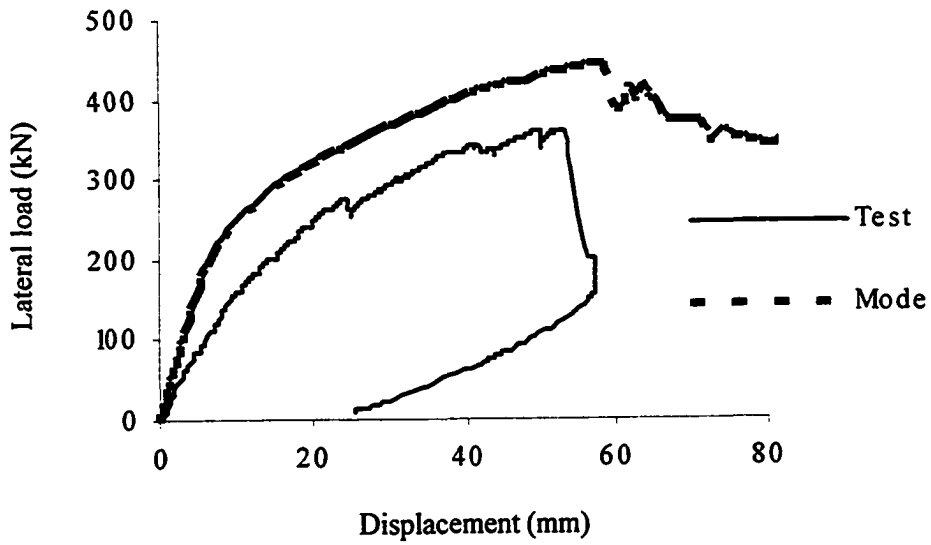

Figure 4-9 Lateral Load - Displacement Curves for W2

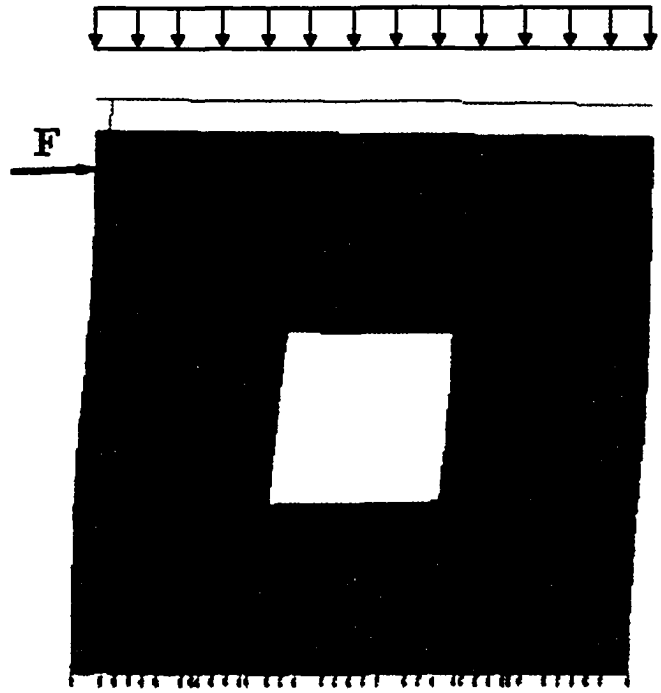

(a) Deformed mesh for W1
(DSF=10)

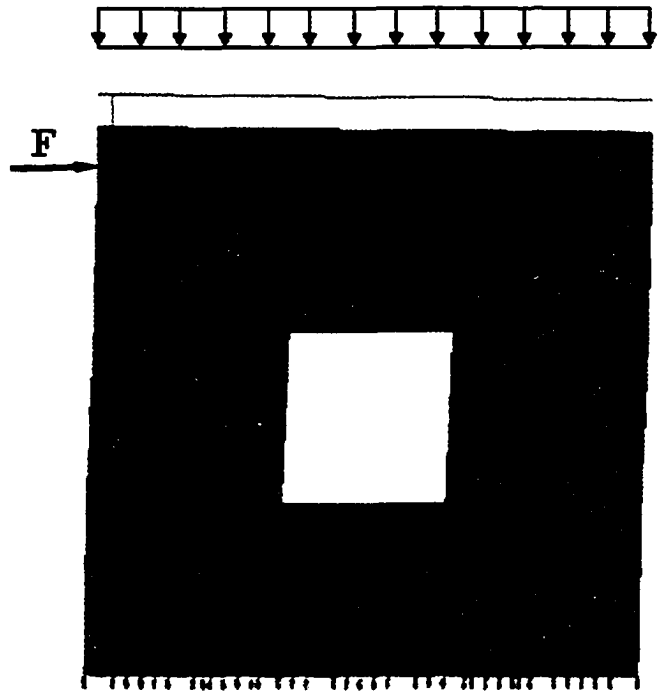

(b) Deformed mesh for W2
(DSF=10)

Figure 4-10 Deformation Comparison for W1 and W2

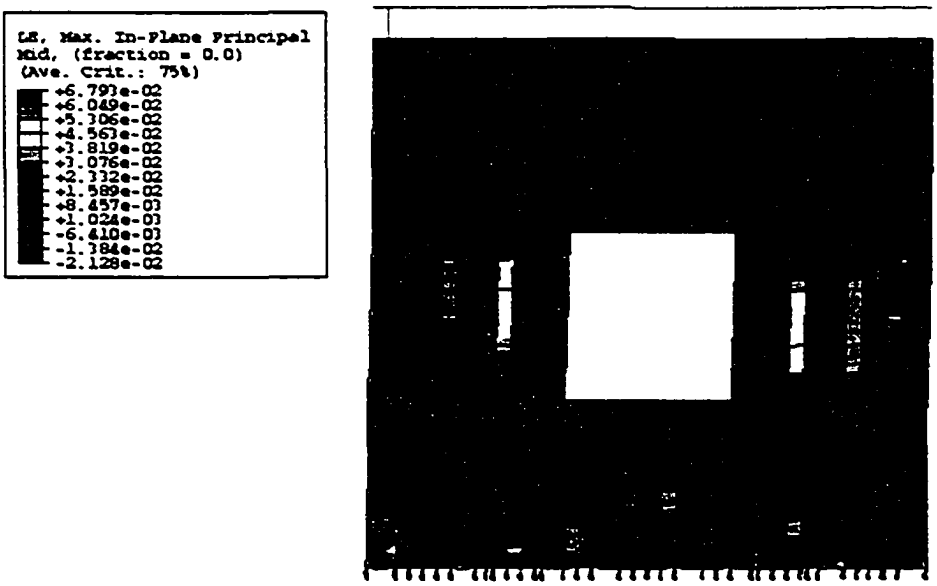

Figure 4-11 Strain Contour for W2 (at failure)

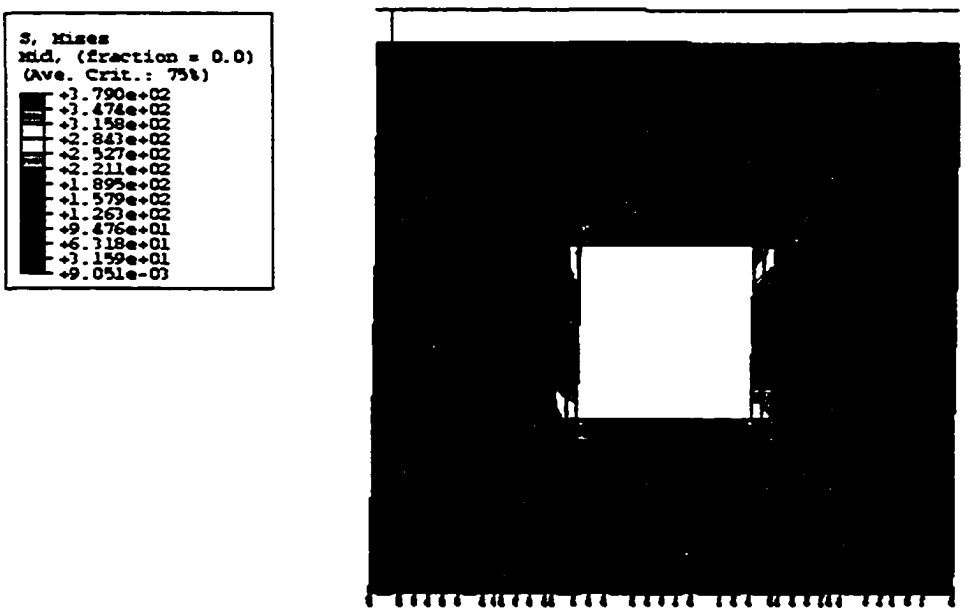

Figure 4-12 Stress Contour for W2 (at failure)

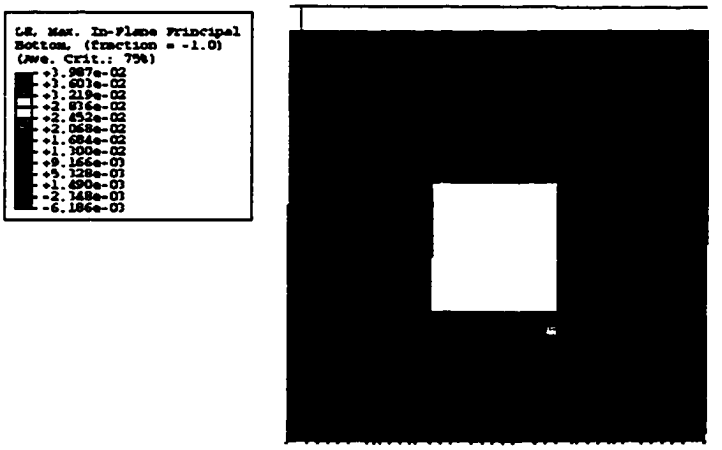

(a) Strain contour of masonry elements for W1

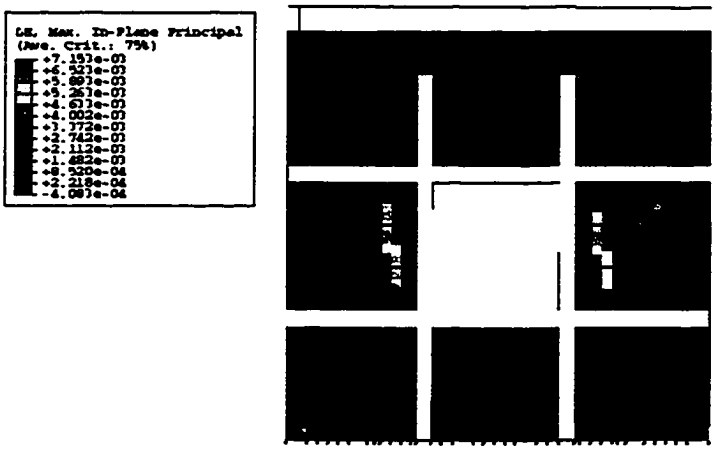

(b) Strain contour of masonry elements for W2

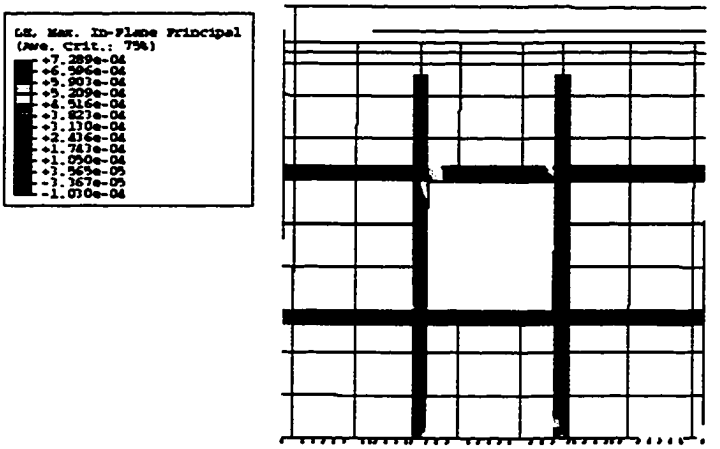

(c) Strain contour of CFRP sheets for W2

Figure 4-13 Strain Comparison for W1 and W2

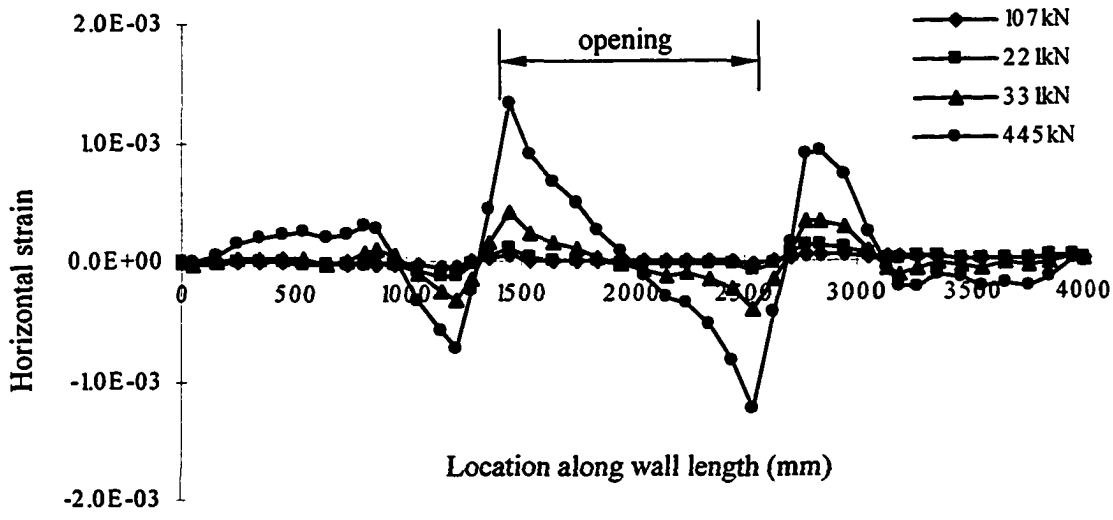

Figure 4-14 H1 Strain Distribution of Horizontal CFRP for W2

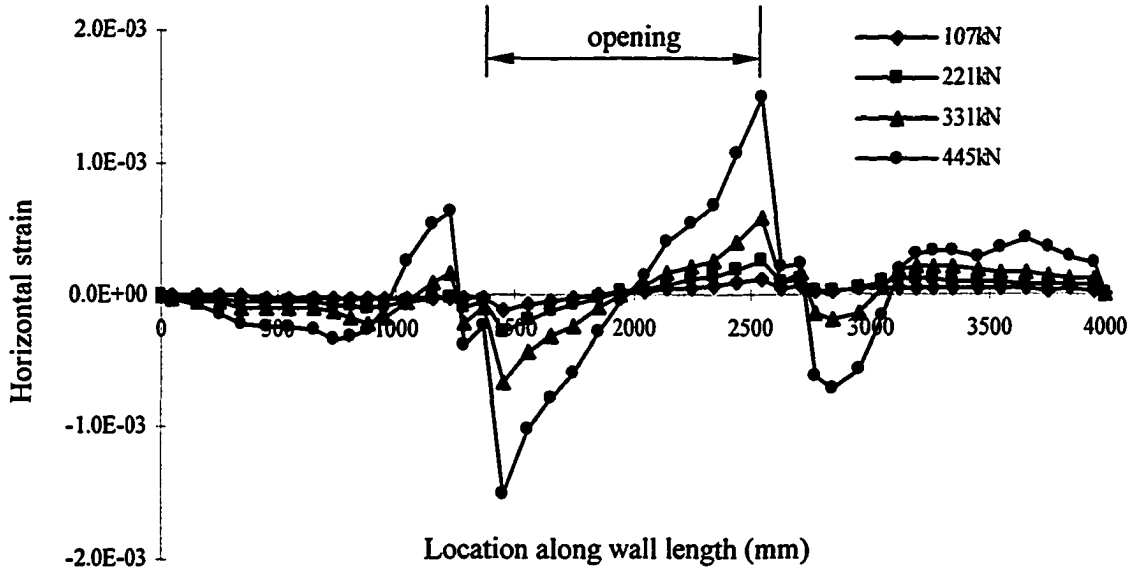

Figure 4-15 H2 Strain Distribution of Horizontal CFRP for W2

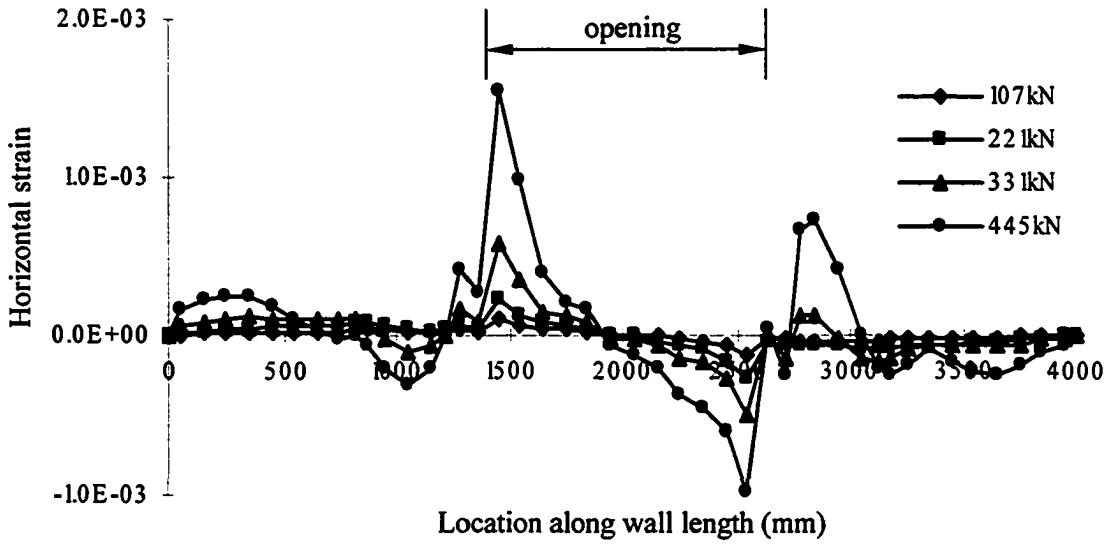

Figure 4-16 H3 Strain Distribution of Horizontal CFRP for W2

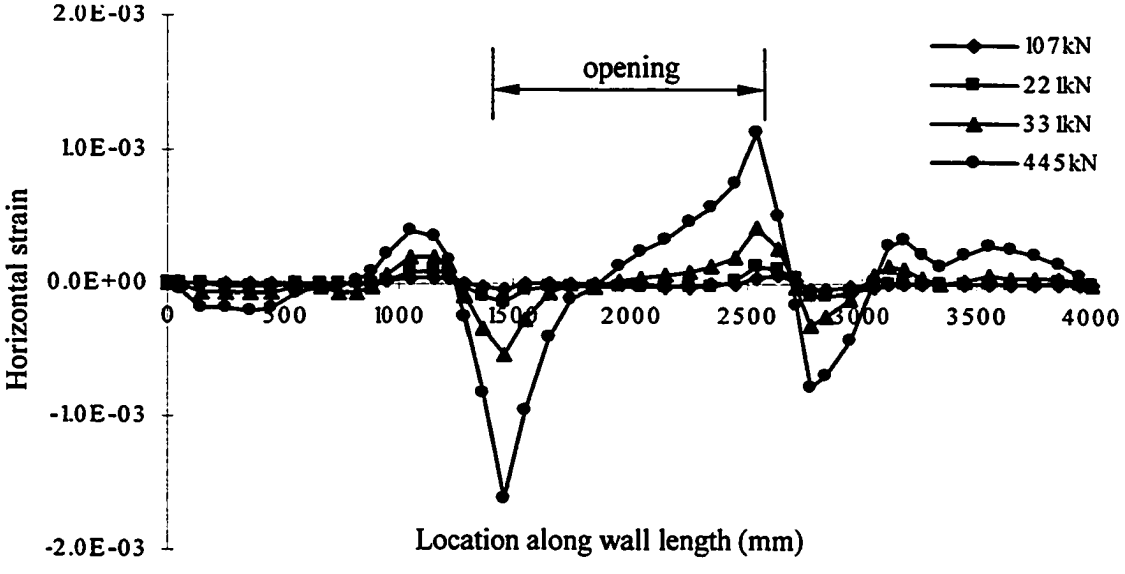

Figure 4-17 H4 Strain Distribution of Horizontal CFRP for W2

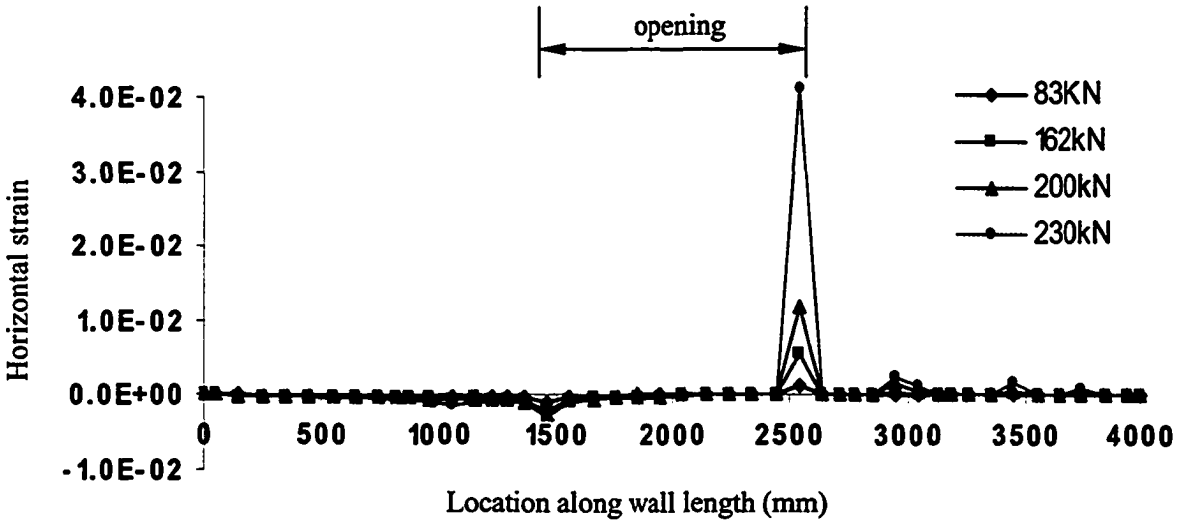

Figure 4-18 H2 Strain Distribution of Masonry Elements for W1

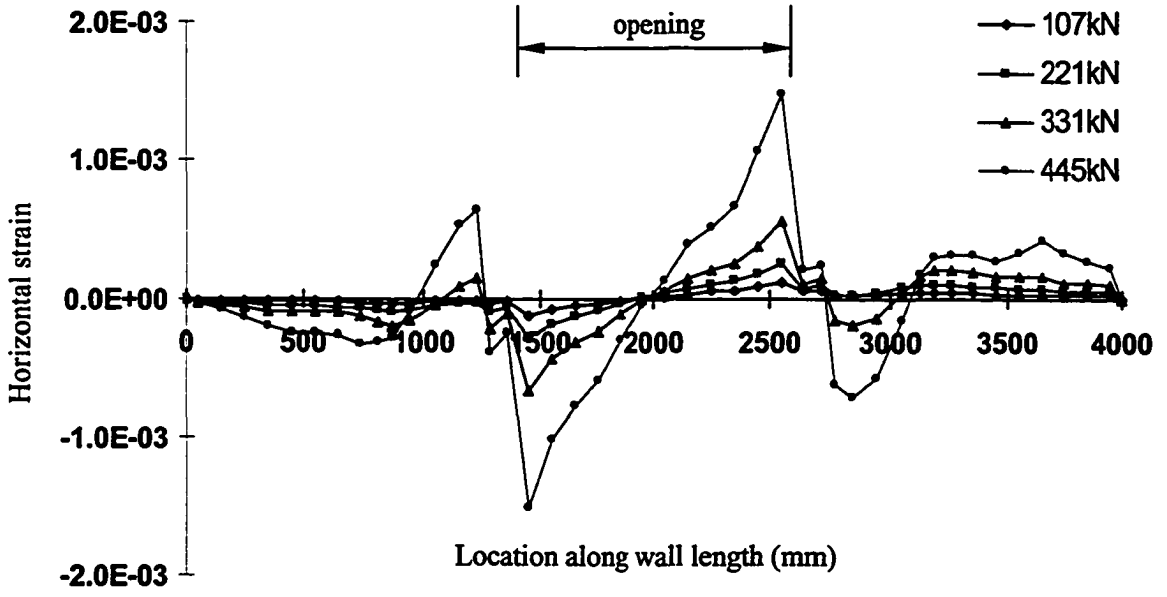

Figure 4-19 H2 Strain Distribution of Horizontal CFRP for W2

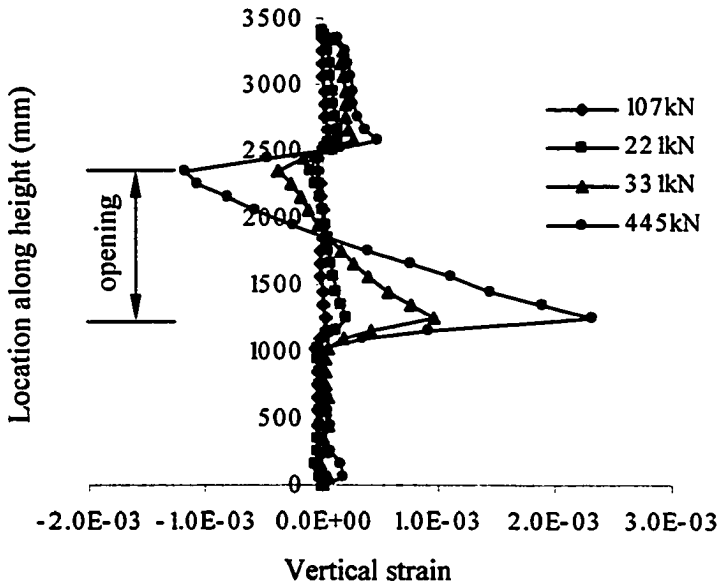

Figure 4-20 V2 Strain Distribution of Vertical CFRP for W2

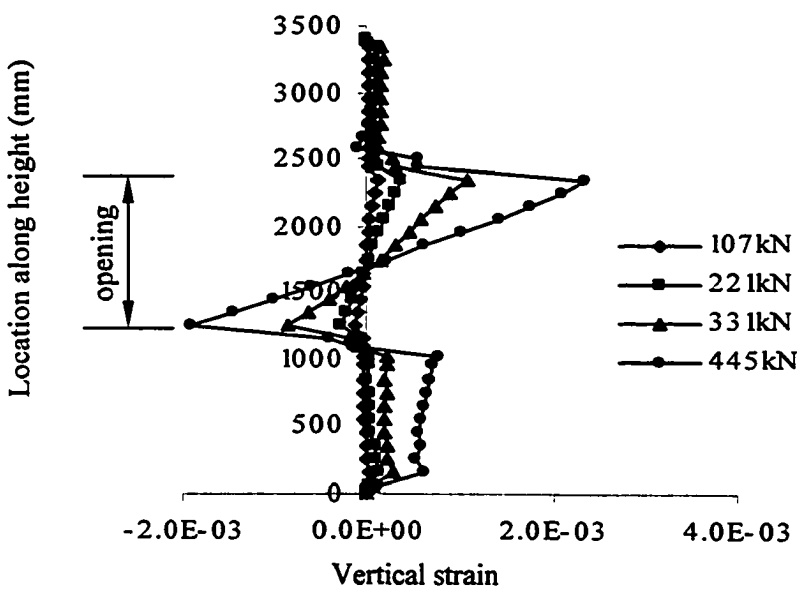

Figure 4-21 V3 Strain Distribution of Vertical CFRP for W2

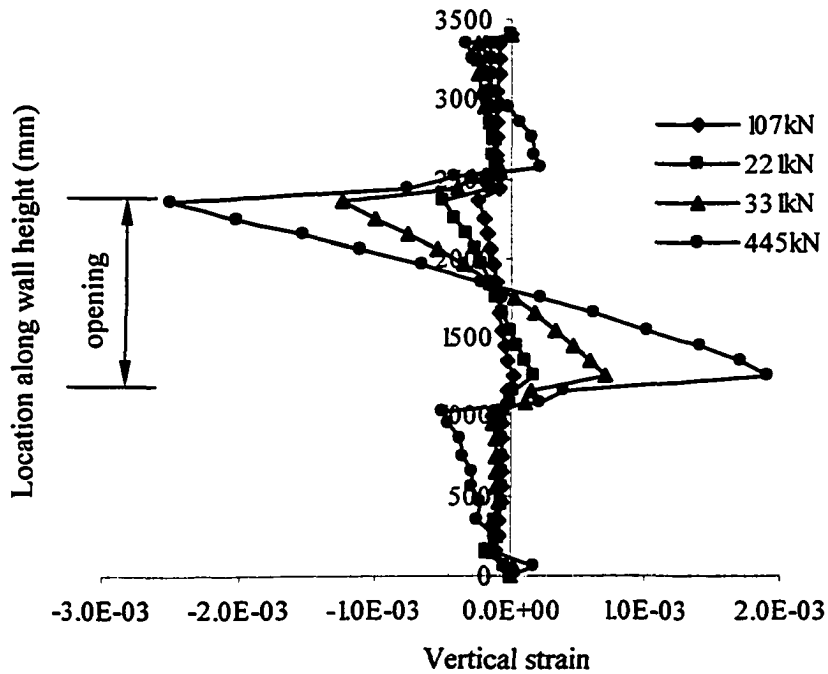

Figure 4-22 V4 Strain Distribution of Vertical CFRP for W2

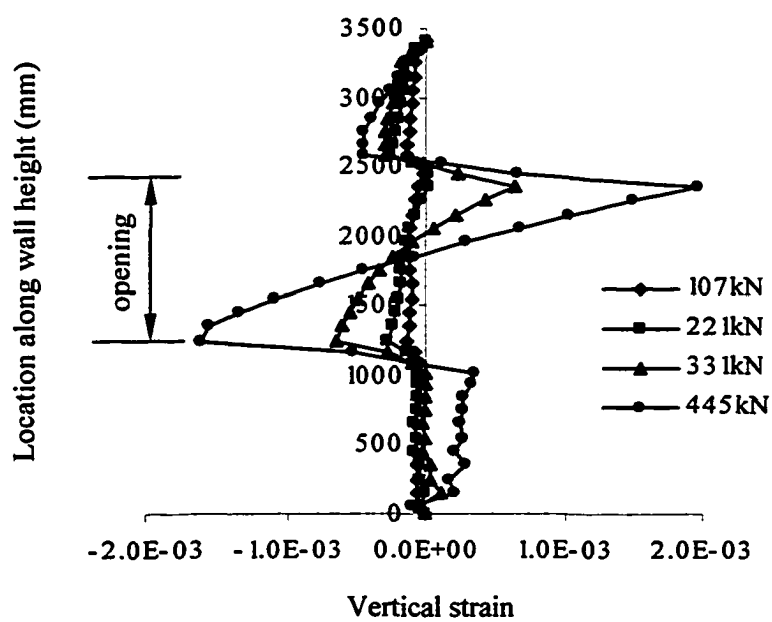

Figure 4-23 V5 Strain Distribution of Vertical CFRP for W2

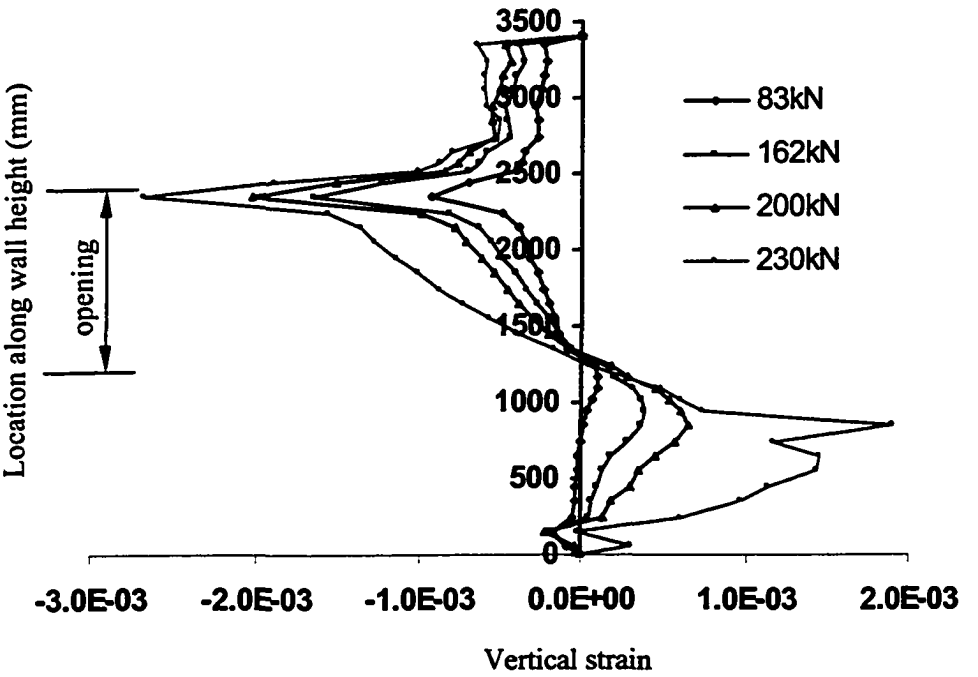

Figure 4-24 V4 Strain Distribution of Masonry Elements for W1

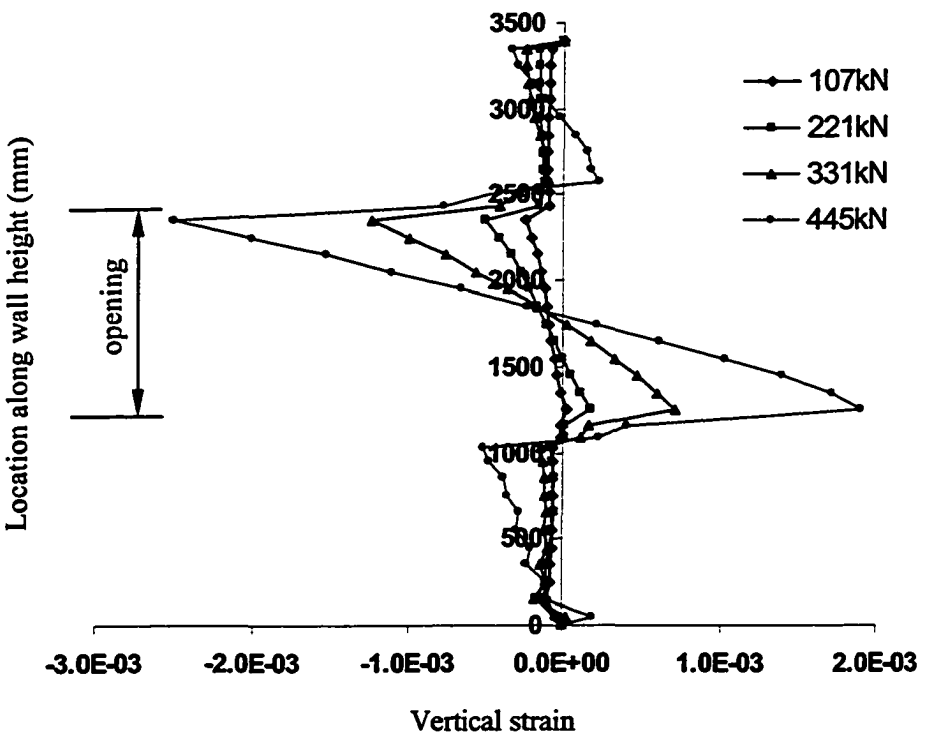

Figure 4-25 V4 Strain Distribution of Vertical CFRP for W2

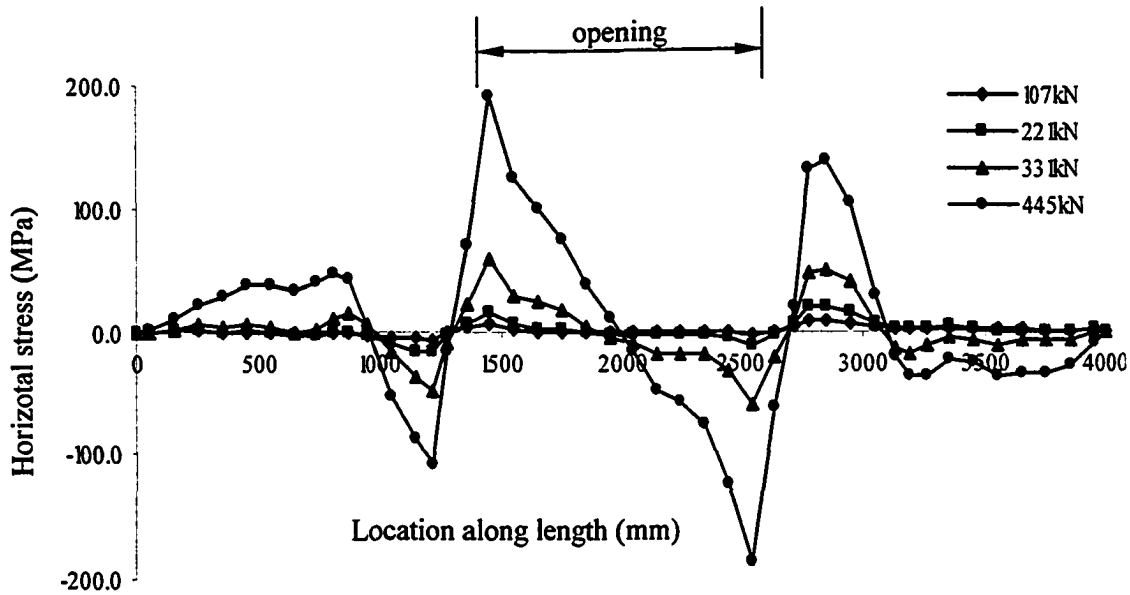

Figure 4-26 H1 Stress Distribution of Horizontal CFRP for W2

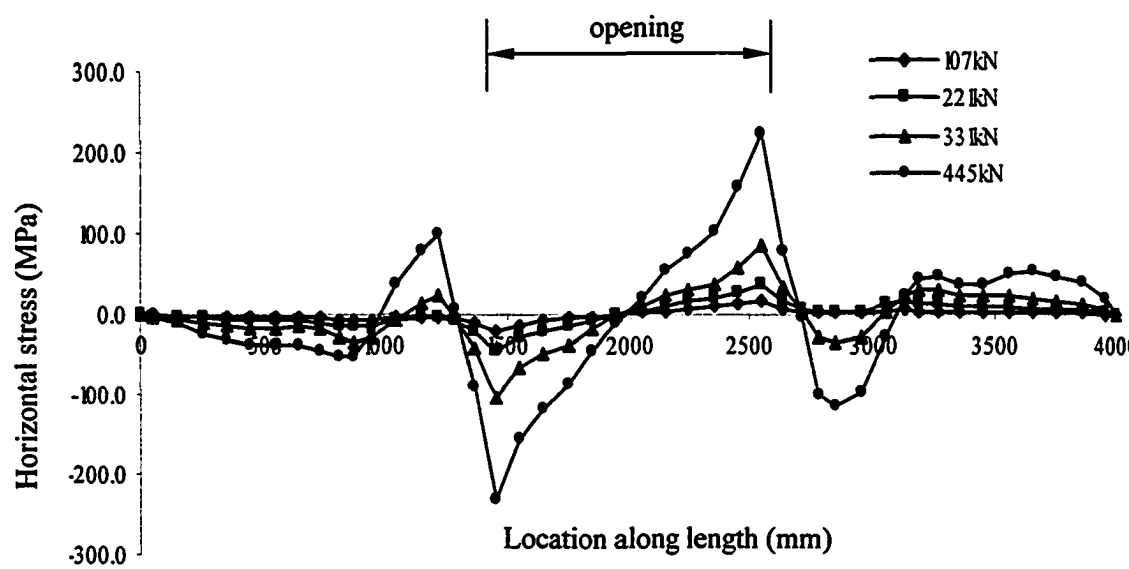

Figure 4-27 H2 Stress Distribution of Horizontal CFRP for W2

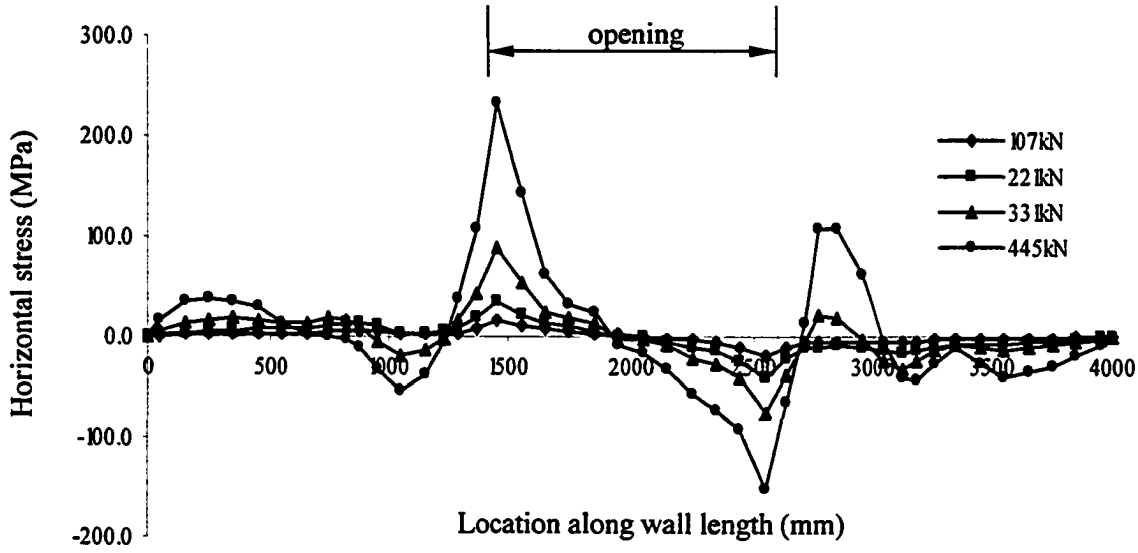

Figure 4-28 H3 Stress Distribution of Horizontal CFRP for W2

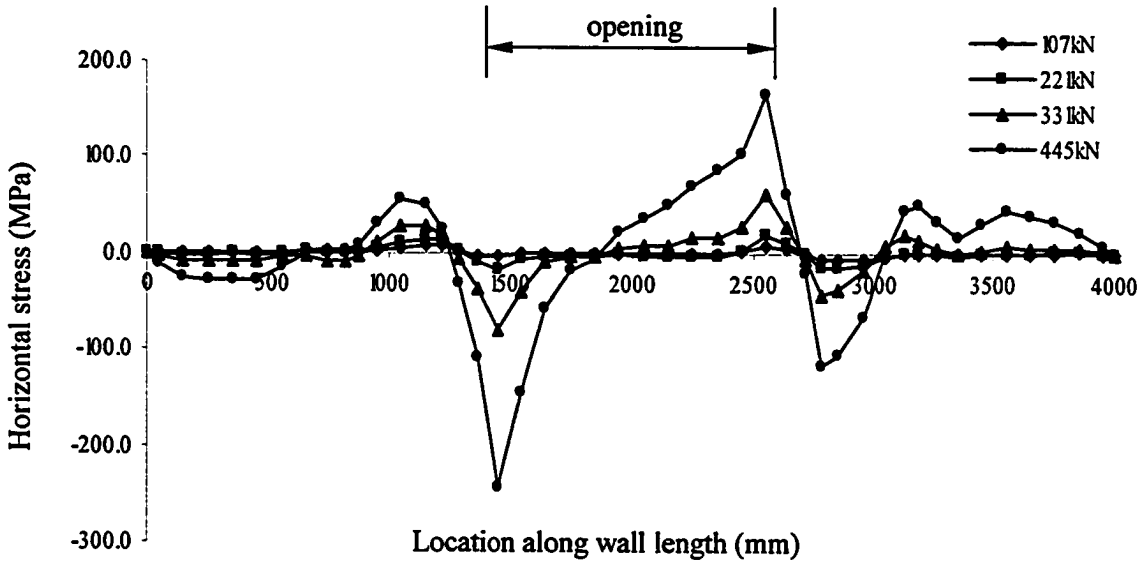

Figure 4-29 H4 Stress Distribution of Horizontal CFRP for W2

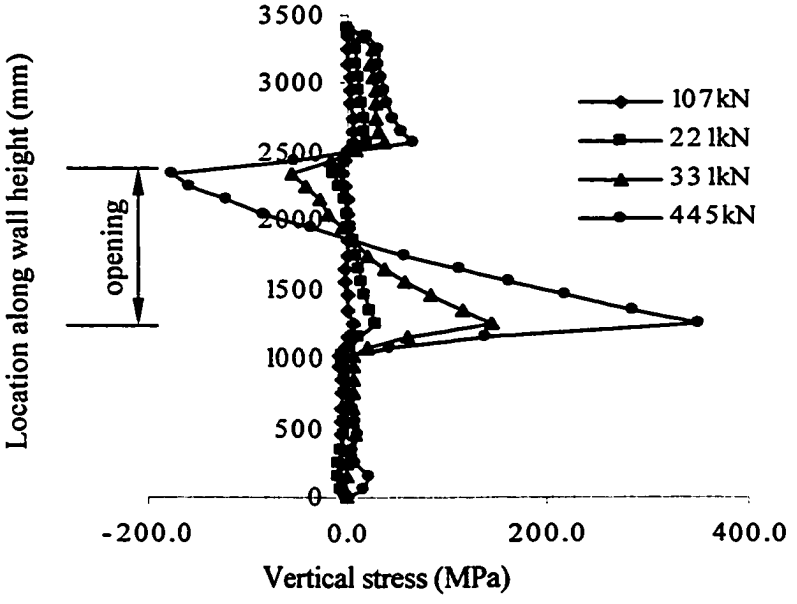

Figure 4-30 V2 Stress Distribution of Vertical CFRP for W2

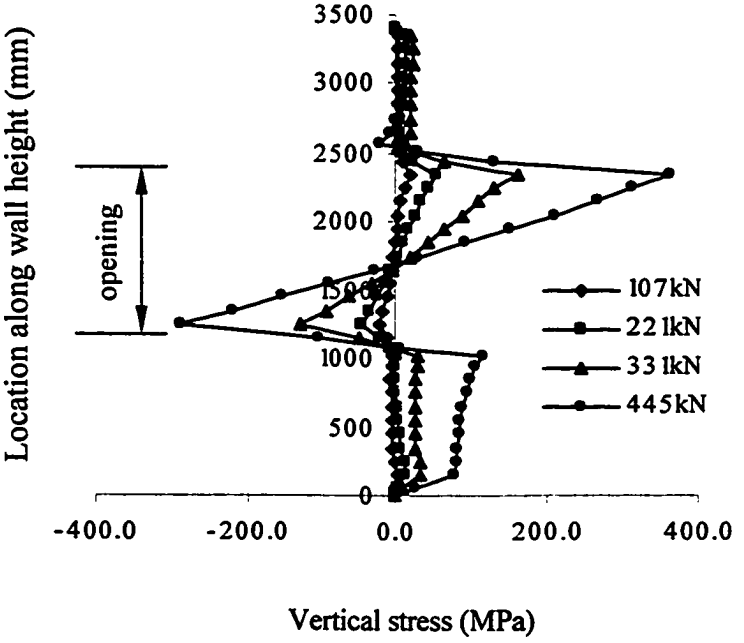

Figure 4-31 V3 Stress Distribution of Vertical CFRP for W2

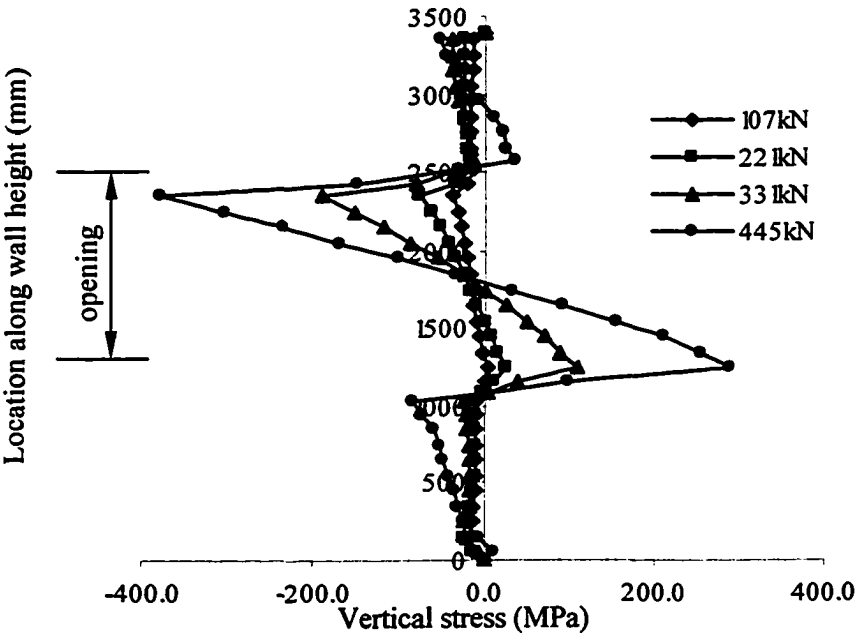

Figure 4-32 V4 Stress Distribution of Vertical CFRP for W2

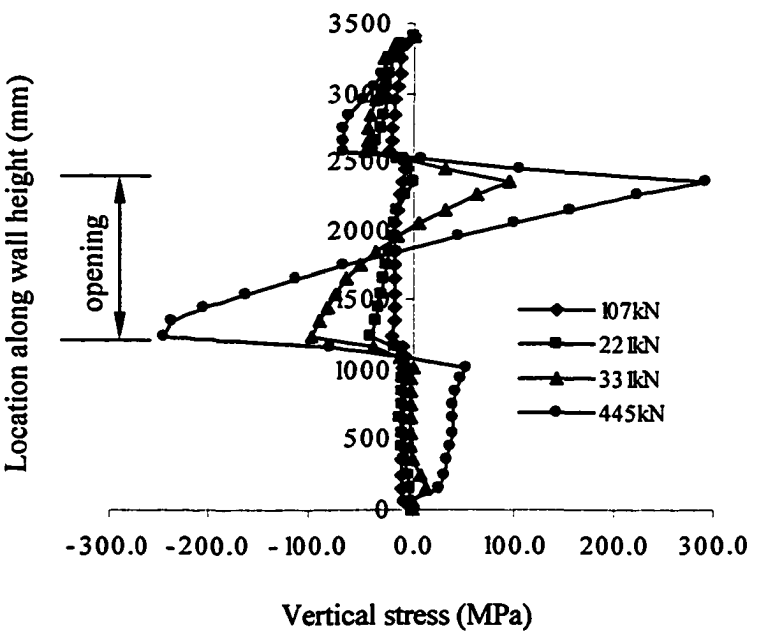

Figure 4-33 V5 Stress Distribution of Vertical CFRP for W2

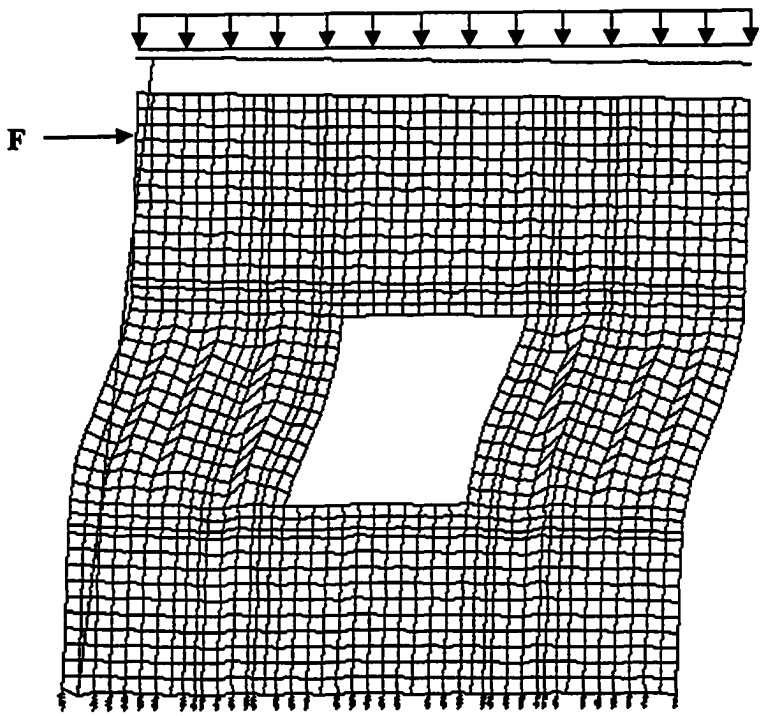

Figure 4-34 Deformed Mesh for Specimen W3

(DSF= 10)

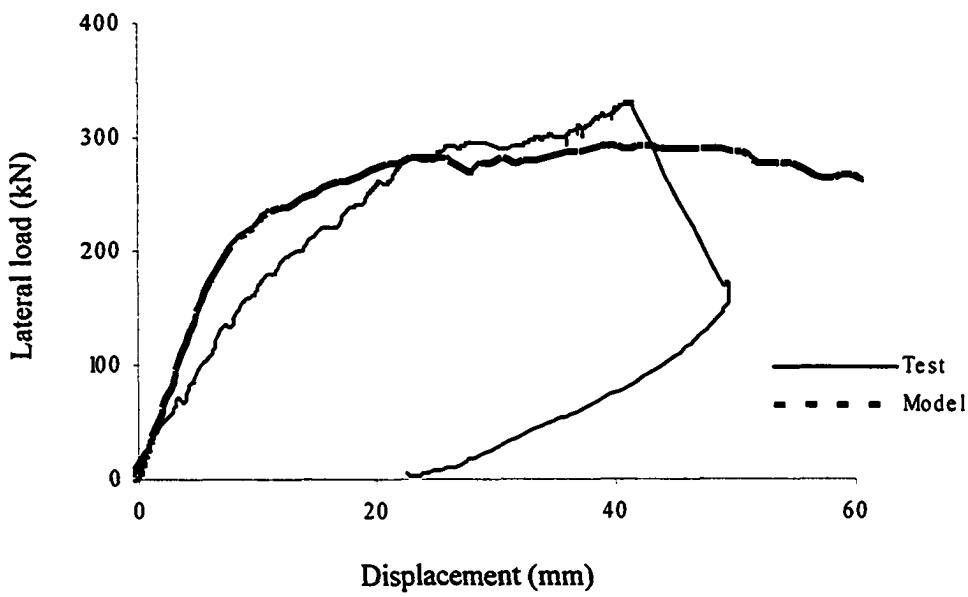

Figure 4-35 Lateral Load - Displacement Curves for W3

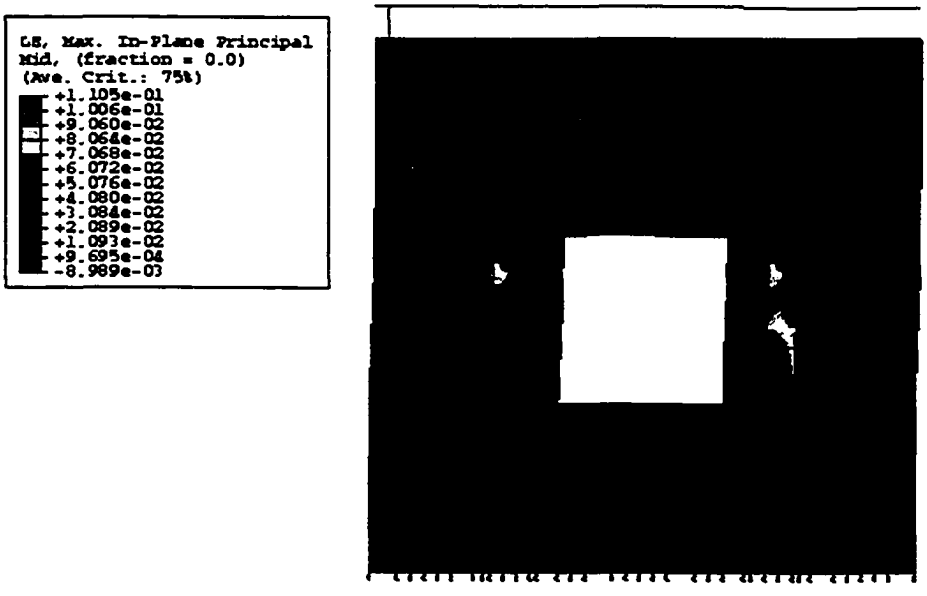

Figure 4-36 Strain Contour for W3 (at failure)

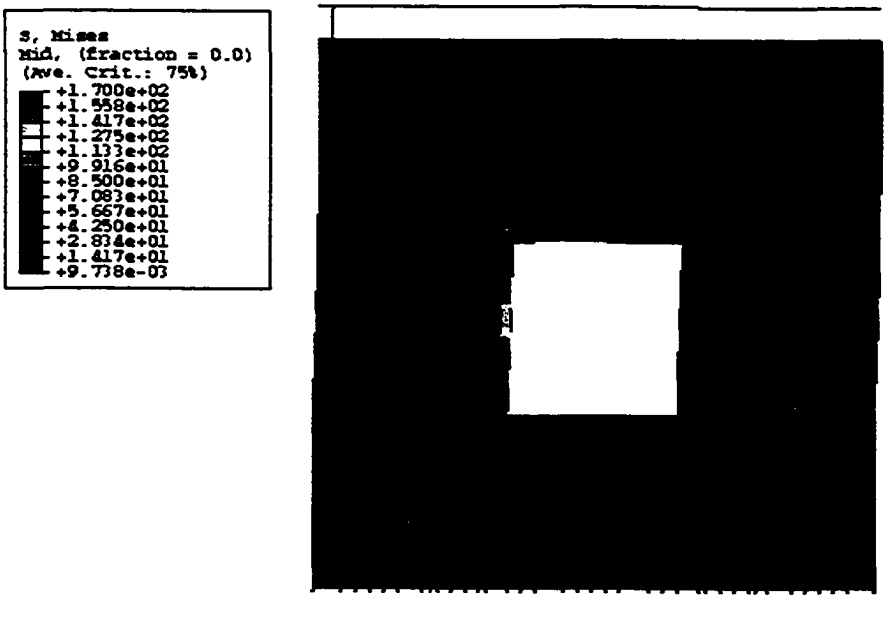

Figure 4-37 Stress Contour for W3 (at failure)

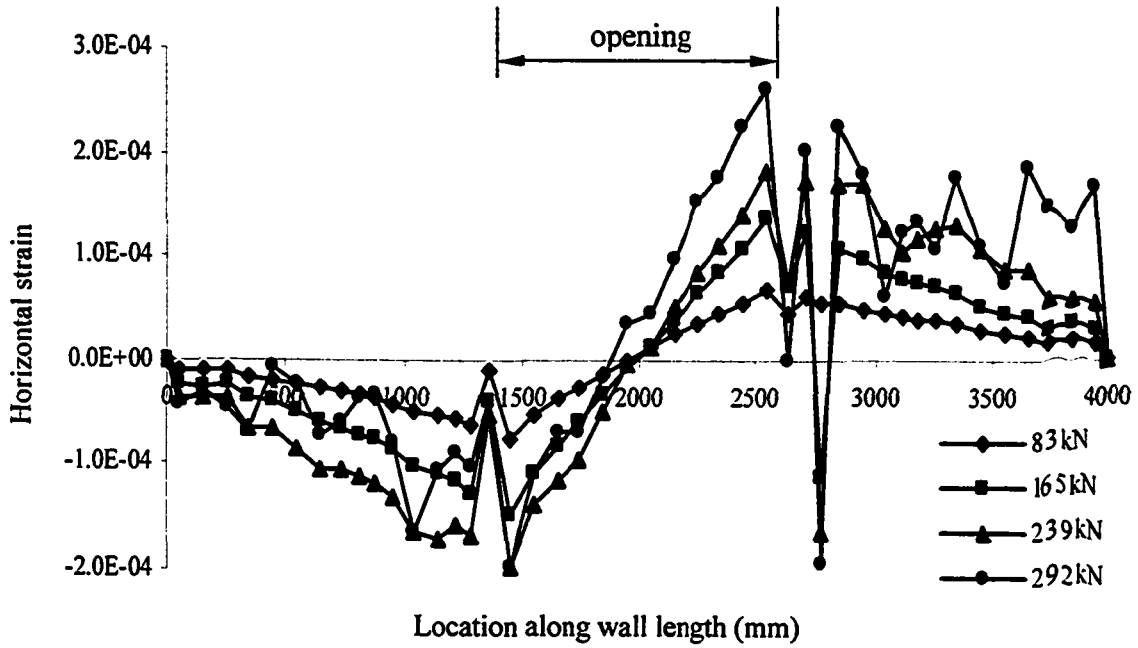

Figure 4-38 H2 Strain Distribution of Horizontal CFRP for W3

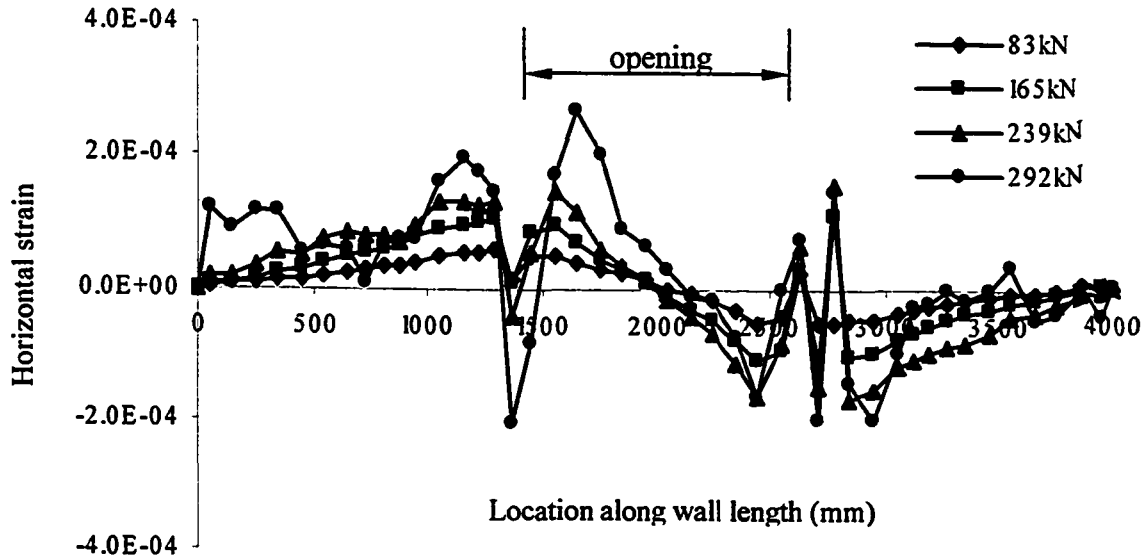

Figure 4-39 H3 Strain Distribution of Horizontal CFRP for W3

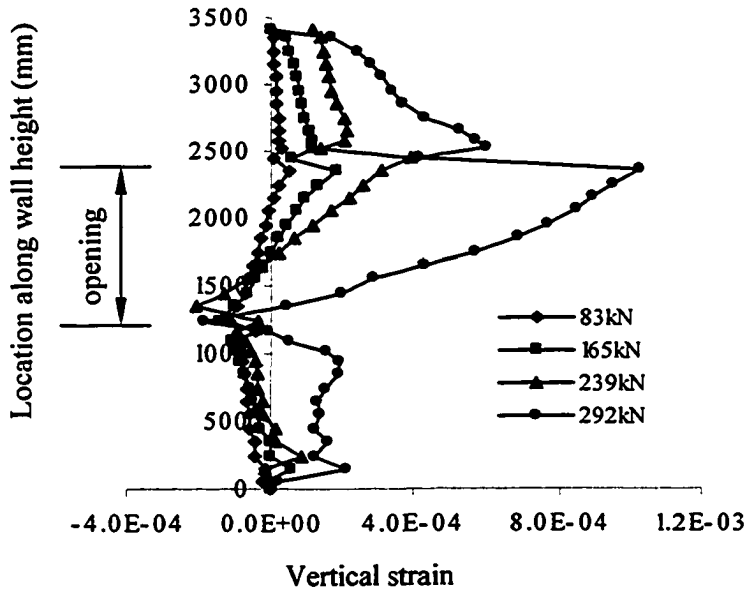

Figure 4-40 V3 Strain Distribution of Vertical CFRP for W3

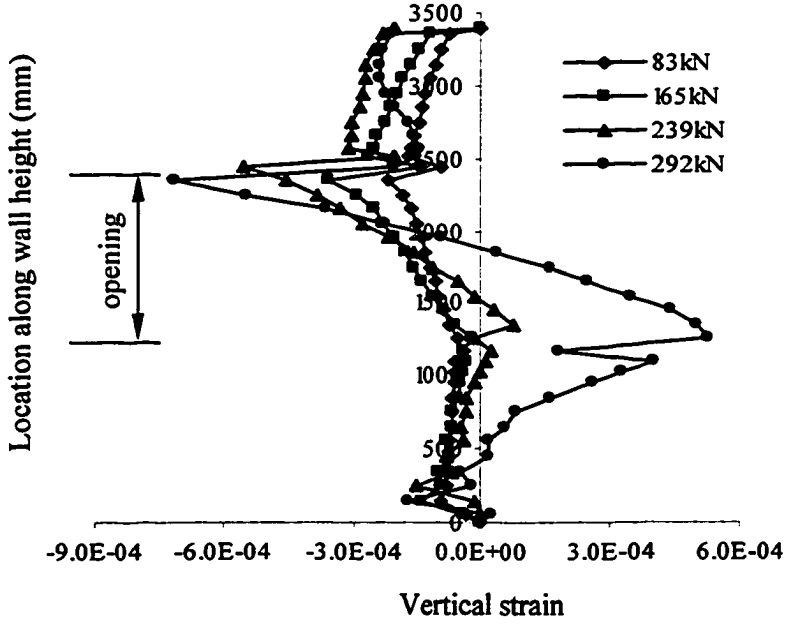

Figure 4-41 V4 Strain Distribution of Vertical CFRP for W3

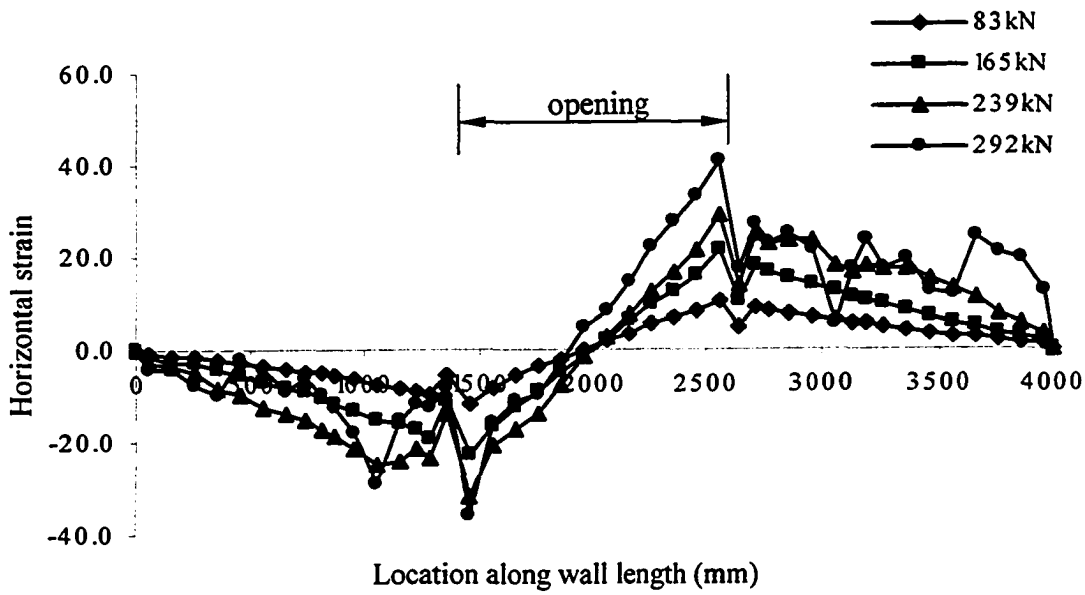

Figure 4-42 H2 Stress Distribution of Horizontal CFRP for W3

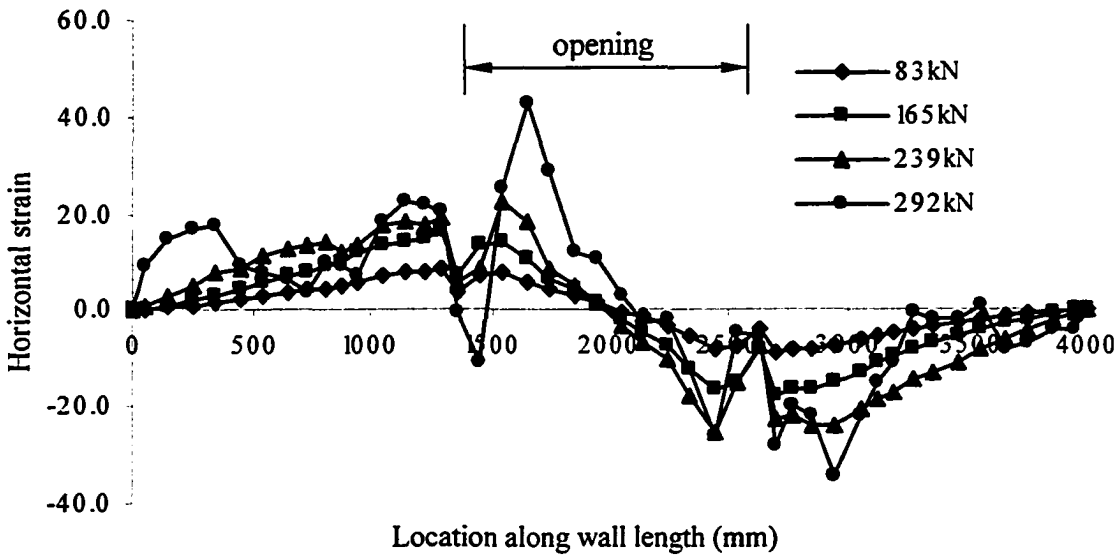

Figure 4-43 H3 Stress Distribution of Horizontal CFRP for W3

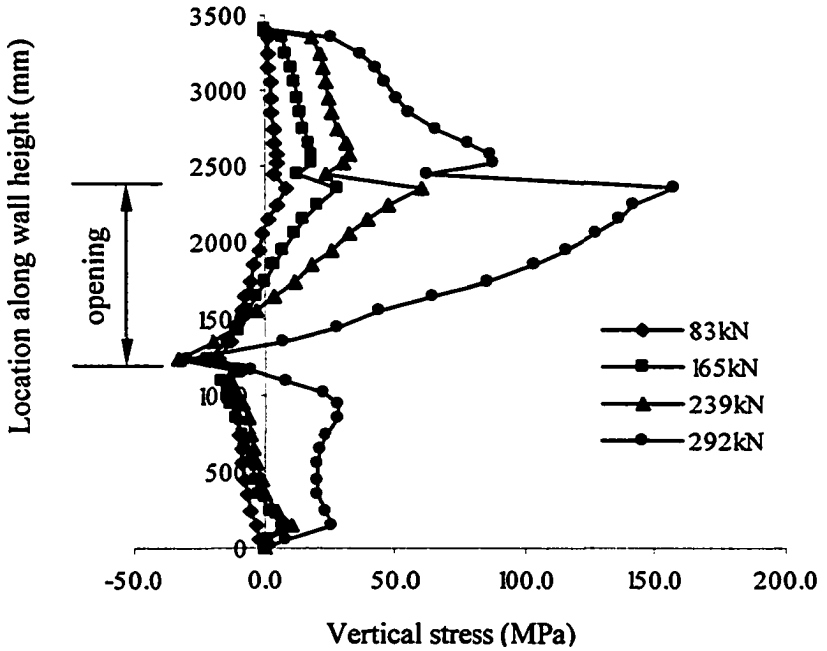

Figure 4-44 V3 Stress Distribution of Vertical CFRP for W3

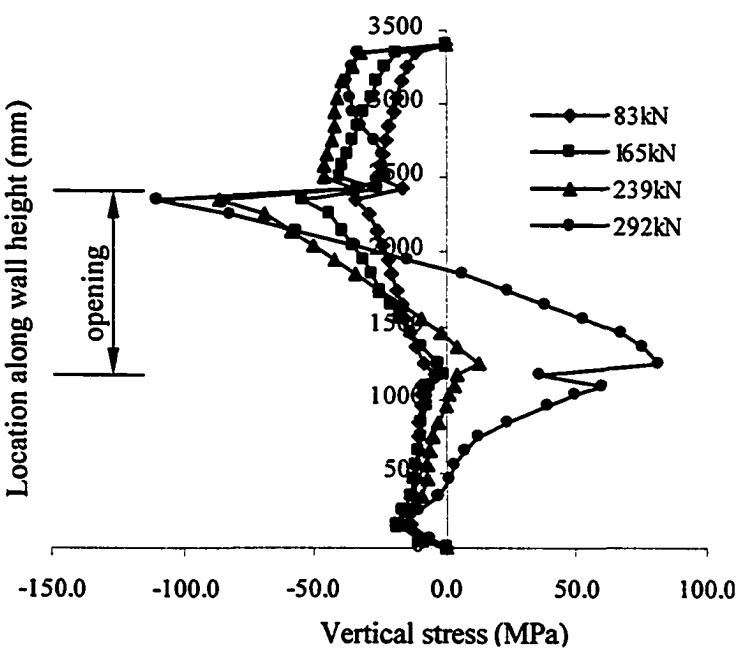

Figure 4-45 V4 Stress Distribution of Vertical CFRP for W3

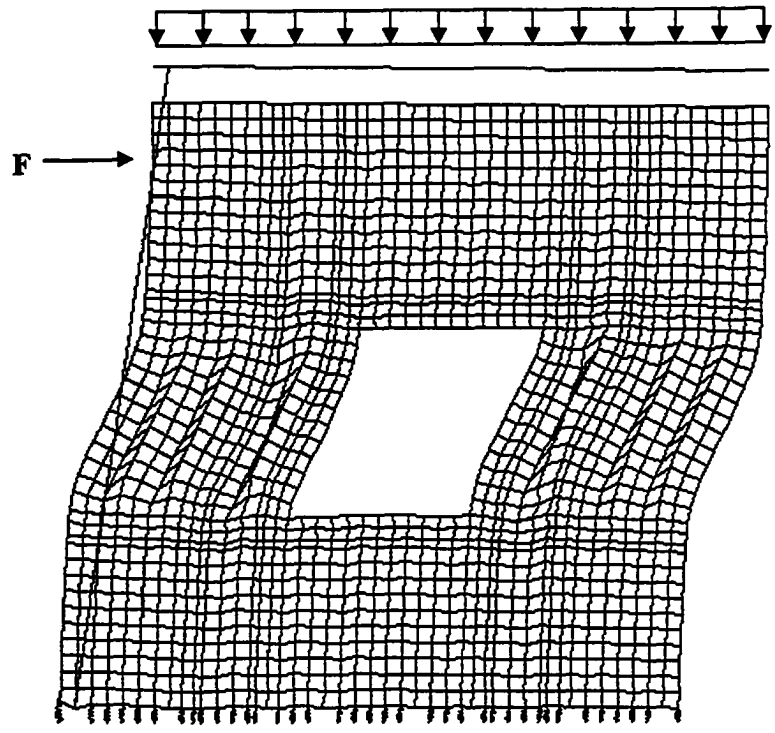

Figure 4-46 Deformed Mesh for Specimen W4

(DSF = 10)

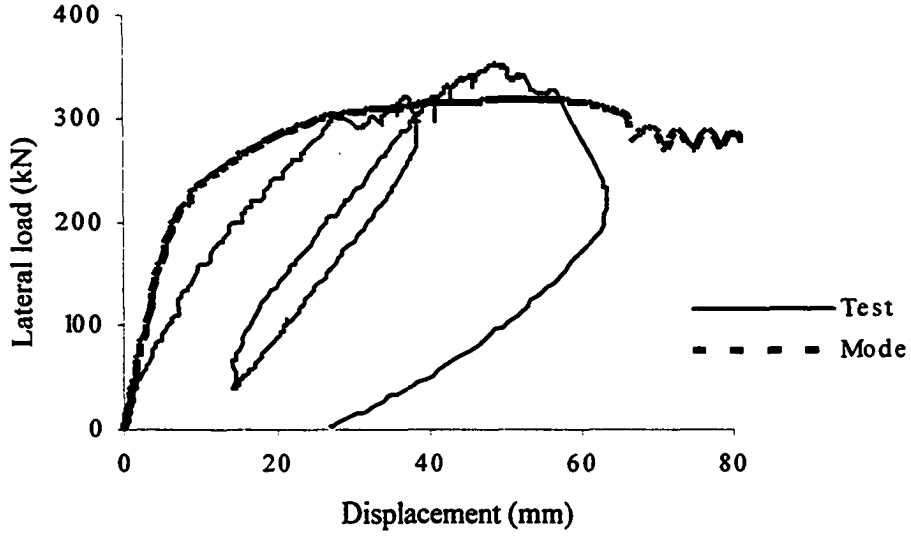

Figure 4-47 Lateral Load - Displacement Curves for W4

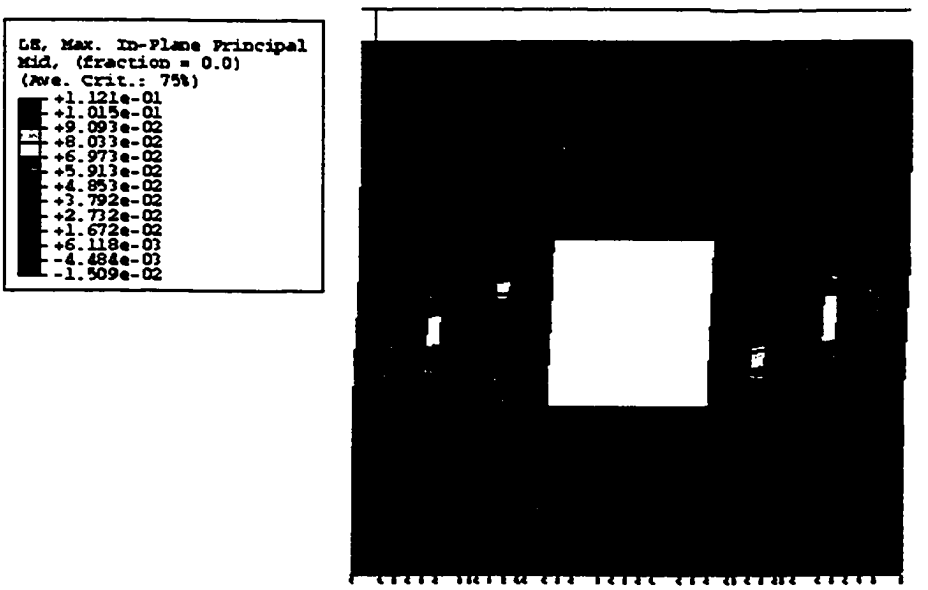

Figure 4-48 Strain Contour for W4 (at failure)

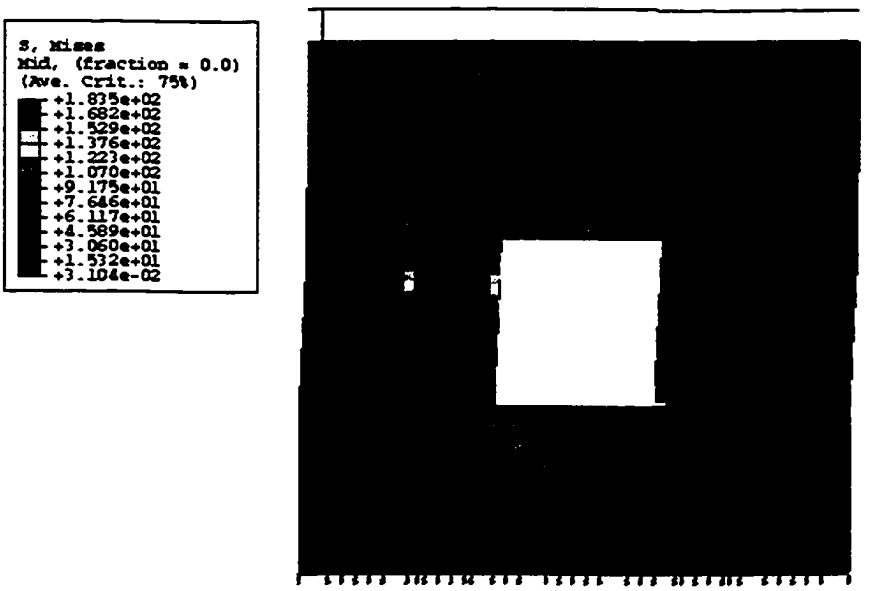

Figure 4-49 Stress Contour for W4 (at failure)

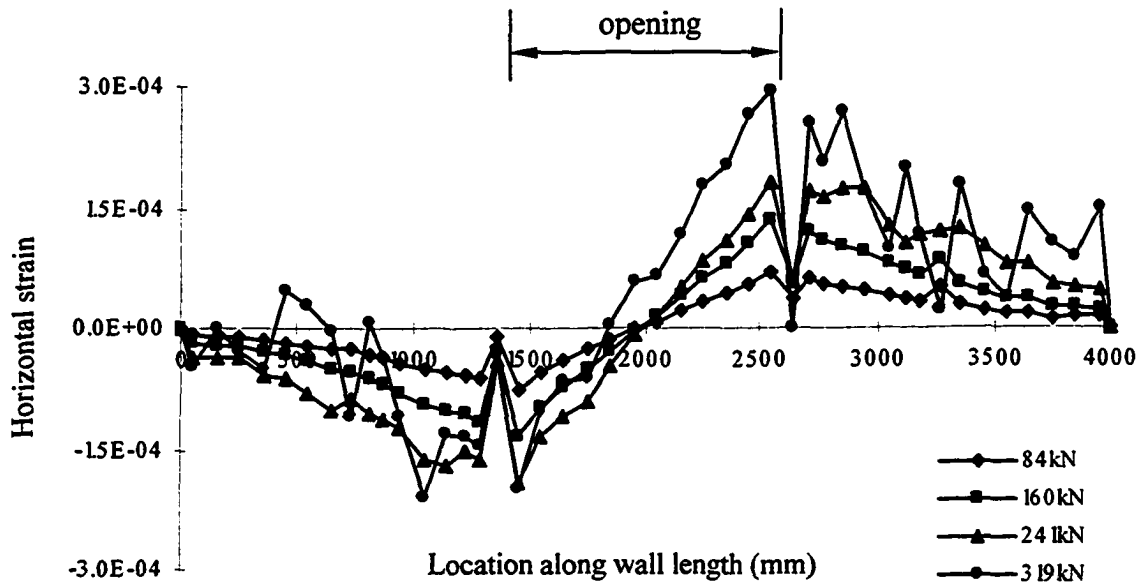

Figure 4-50 H2 Strain Distribution of Horizontal CFRP for W4

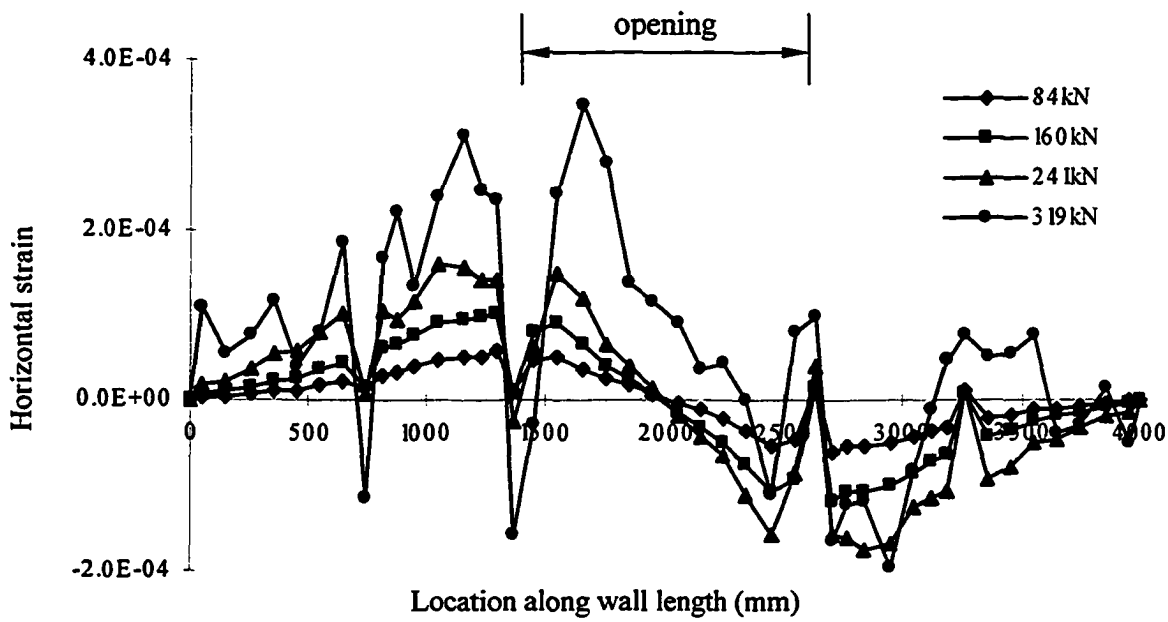

Figure 4-51 H3 Strain Distribution of Horizontal CFRP for W4

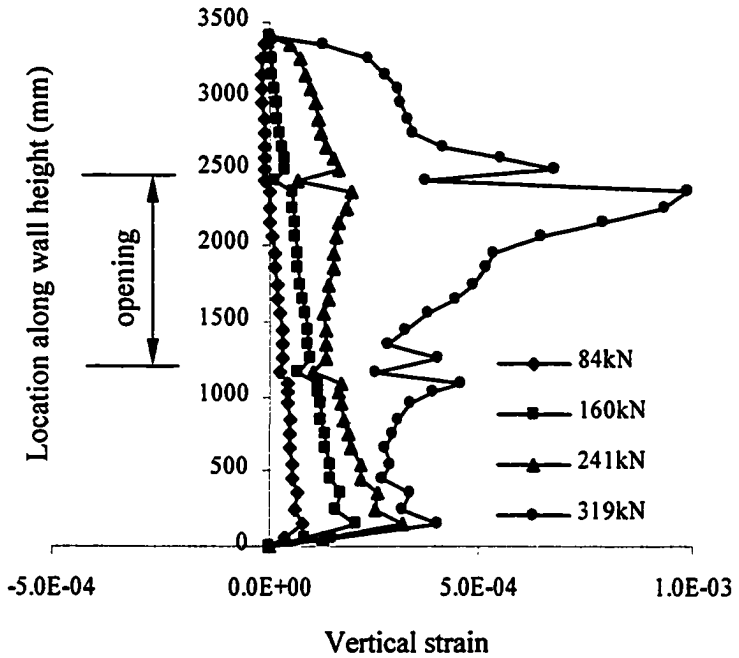

Figure 4-52 V1 Strain Distribution of Vertical CFRP for W4

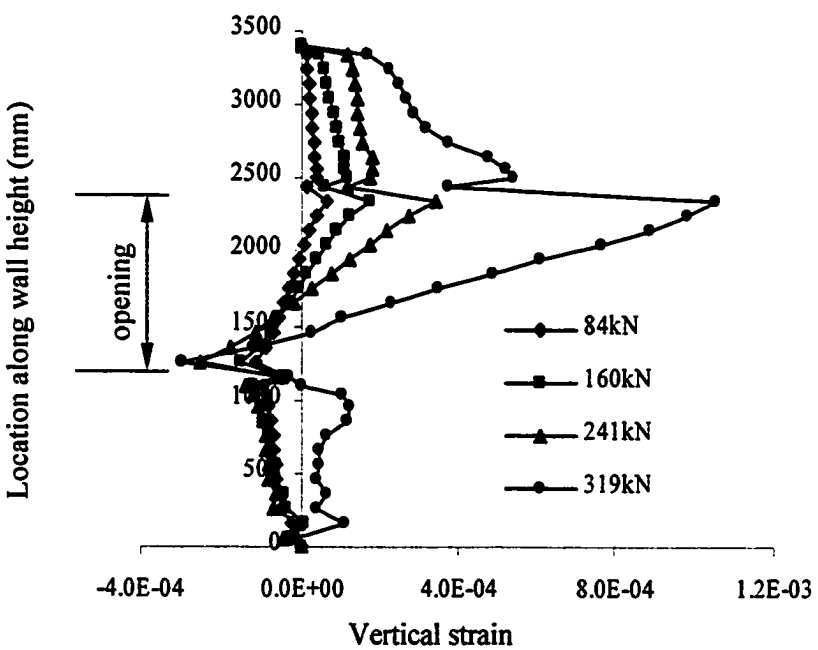

Figure 4-53 V3 Strain Distribution of Vertical CFRP for W4

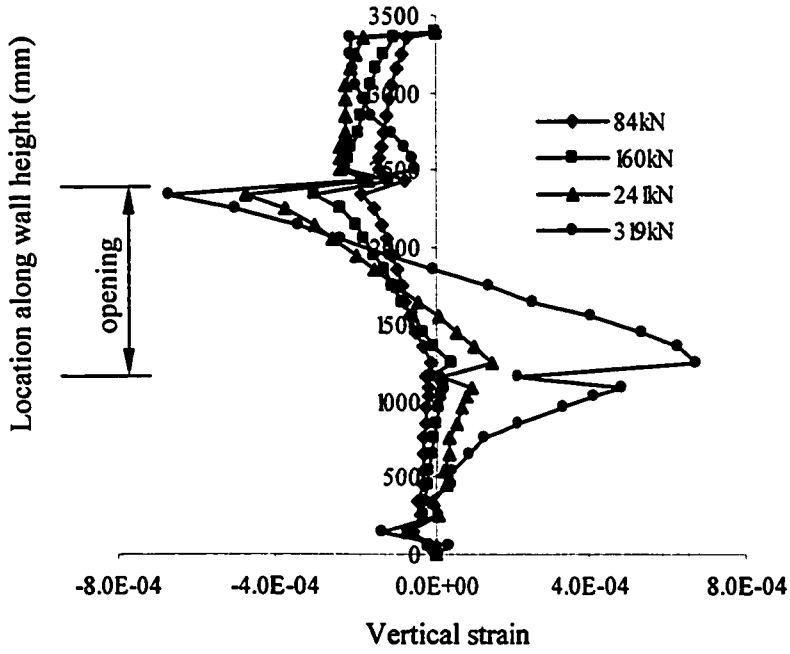

Figure 4-54 V4 Strain Distribution of Vertical CFRP for W4

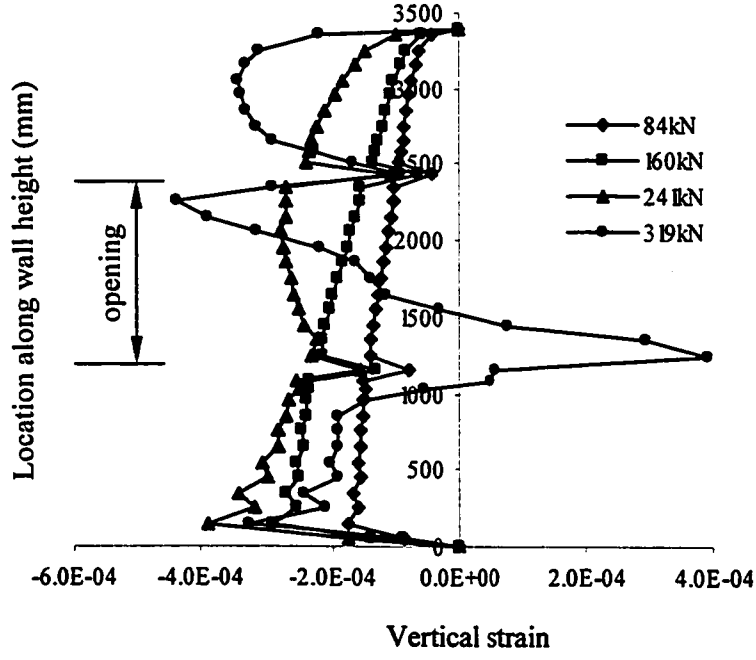

Figure 4-55 V6 Strain Distribution of Vertical CFRP for W4

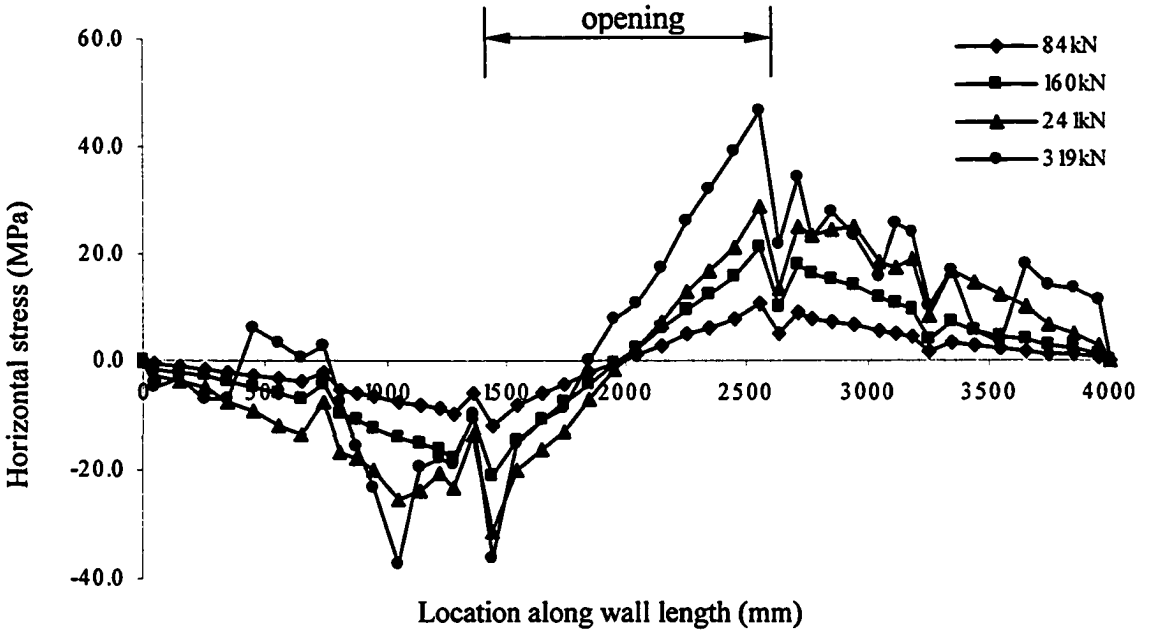

Figure 4-56 H2 Stress Distribution of Horizontal CFRP for W4

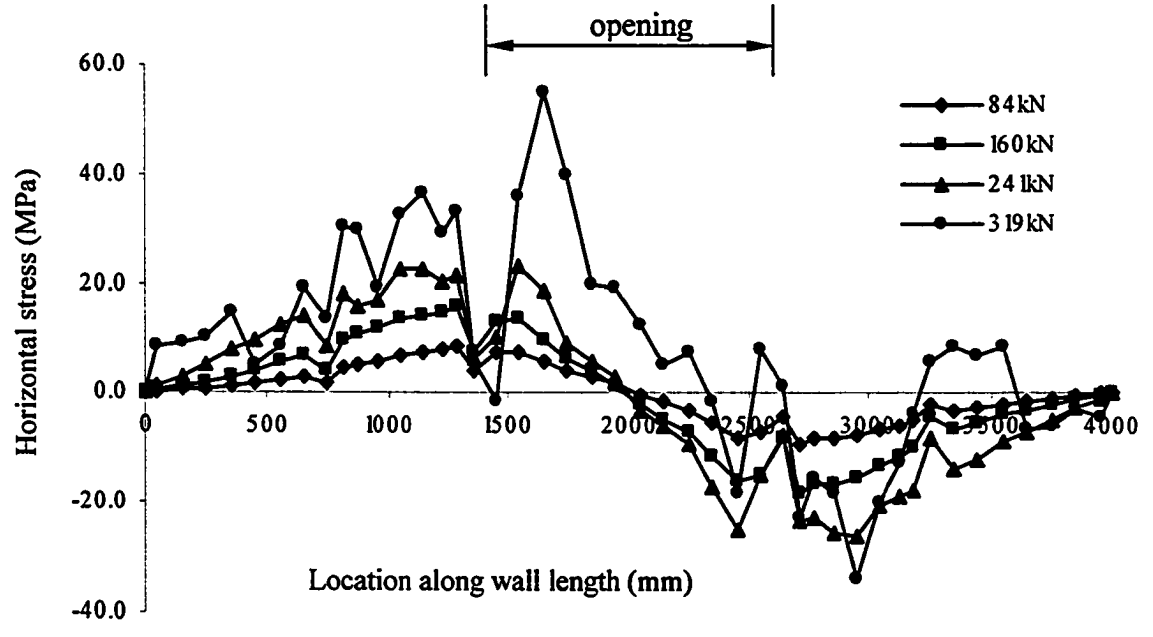

Figure 4-57 H3 Stress Distribution of Horizontal CFRP for W4

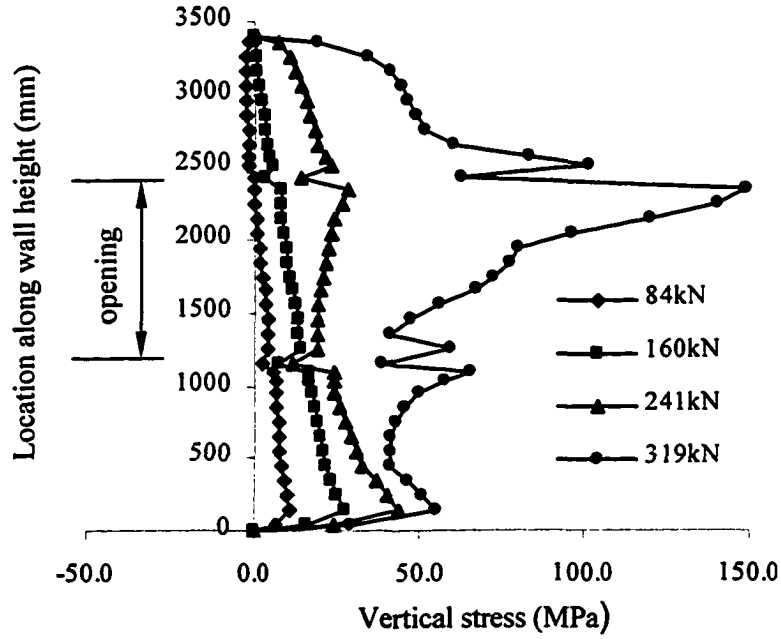

Figure 4-58 V1 Stress Distribution of Vertical CFRP for W4

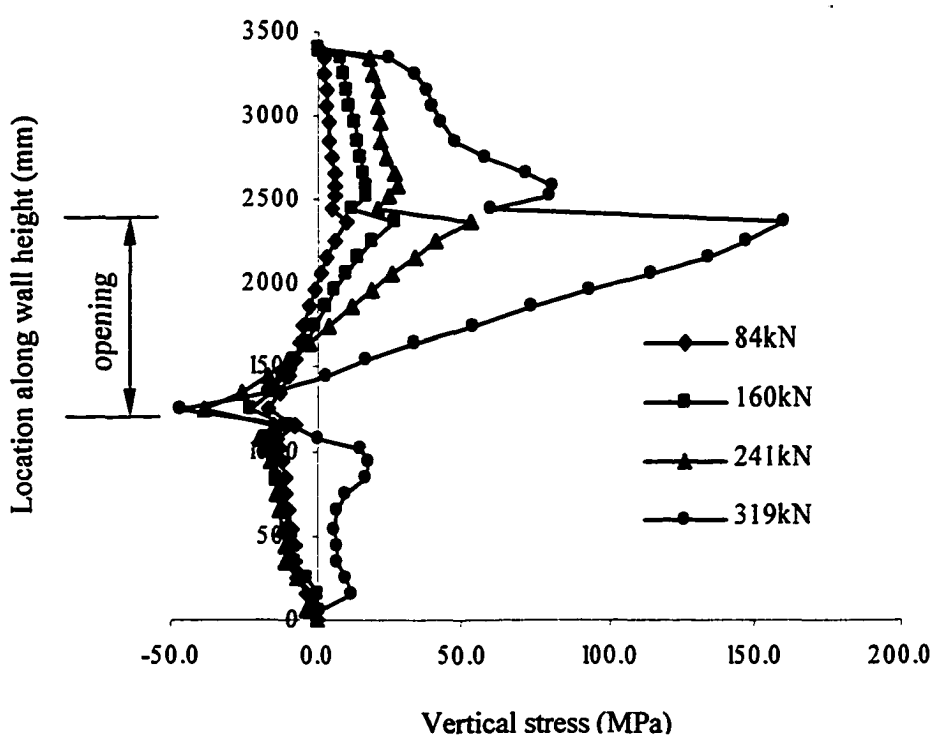

Figure 4-59 V3 Stress Distribution of Vertical CFRP for W4

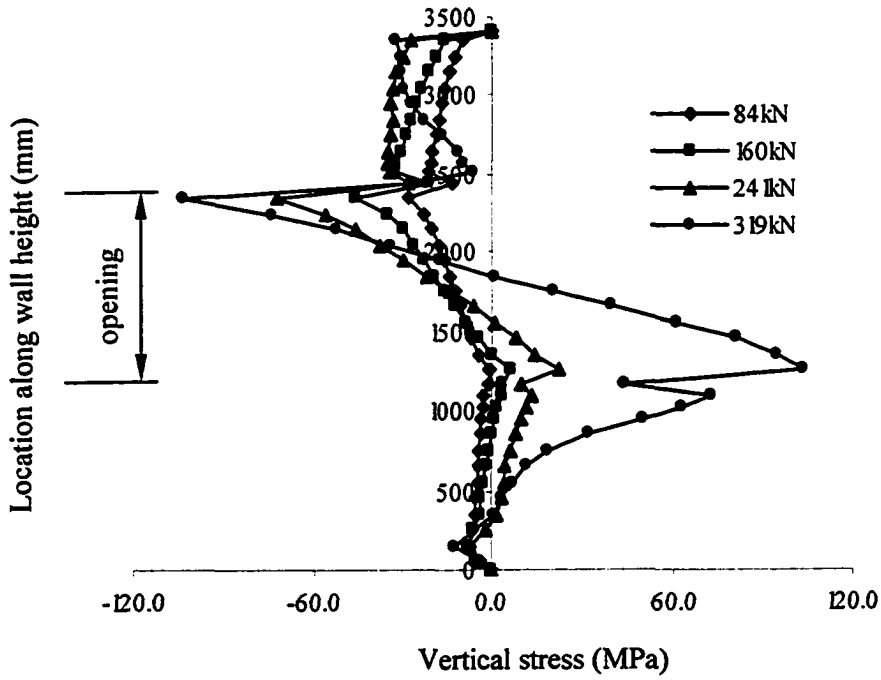

Figure 4-60 V4 Stress Distribution of Vertical CFRP for W4

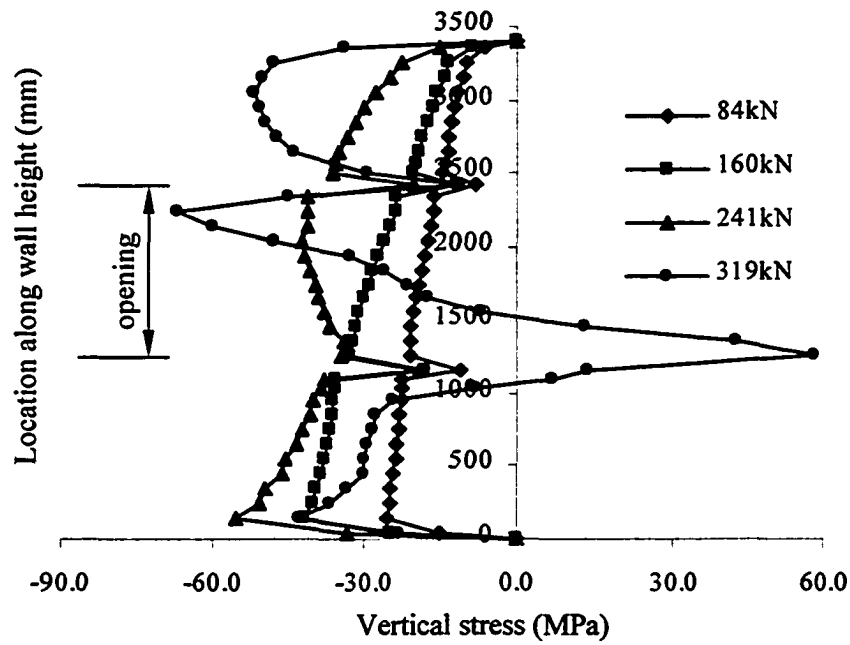

Figure 4-61 V6 Stress Distribution of Vertical CFRP for W4

5. SUMMARY, CONCLUSIONS AND RECOMMENDATIONS

5.1 Summary

Masonry shear walls with window and door openings are common lateral force resisting elements in building structures. However because of the introduction of openings, the flexural and shear stiffness as well as the strength of walls are decreased and therefore the response characteristics to lateral loads are altered. As a result, masonry shear walls perforated by openings are prone to be damaged during earthquakes. To seek the appropriate and effective strengthening schemes for masonry shear walls with openings strengthened with CFRP sheets is the primary research objective of the investigation conducted in this research program. The numerical simulation corresponding to the experimental program is conducted to achieve the research objective.

Four full-scale partially grouted reinforced concrete masonry walls were tested under the combination of constant axial load and monotonic lateral load, which represent the gravity load and seismic or wind load, respectively. The specimens included one control wall and three other walls reinforced with CFRP sheets. The arrangement of CFRP sheets on the three walls differed in width and amount. The test results revealed that substantial increase has been found in both lateral shear capacity and ductility due to the strengthening with CFRP sheets on the masonry shear walls with openings although different increase extent resulted from different strengthening schemes of CFRP sheets.

Numerical models using finite element program ABAQUS have been established to simulate the corresponding masonry specimens and provide a theoretical insight into the structural behaviour and failure mechanism for both the masonry walls and the CFRP sheets under the combination of constant axial load and monotonically increased lateral load. The experimental results derived from the test data are used to verify the modeling results. Discussion and comparisons are conducted based on the test results and numerical outputs. The difference between them is accounted for on the basis of rational analysis.

5.2 Conclusions from Numerical Analysis

A comparison between the output of the numerical models and the experimental results showed that it is possible to predict the lateral load-displacement, the strain and stress distribution at the critical elements, and the strain and stress distribution of CFRP sheets along the fibre directions using macro-modeling that assumes the masonry composite as an isotropic homogeneous continuum and neglects the interface between the masonry units and mortar joints. From a qualitative point of view relatively good agreement is found because the same trend is observed in both sets of diagrams.

Based on the numerical analysis conducted in the above chapters, some conclusions can be drawn. Firstly, it is evident that the lateral load capacity and ductility can be significantly increased by strengthening with the CFRP sheets. This is also found in the experimental results.

Secondly, the increase extent in both lateral load capacity and ductility depends on the width and amount of CFRP sheets. The wider the CFRP sheets, the higher the lateral load capacity and the larger the ductility of the masonry shear walls. In addition, the more the CFRP sheets, the higher the lateral load capacity and the larger the ductility of the masonry shear walls. Comparing the effect of width and amount, the former plays a more effective role on the capacity increasing for masonry shear walls. While for ductility increasing, the effect of CFRP amount is more pronounced. The same conclusions can also be drawn form the experimental analysis.

Thirdly, analyzing the strain values for the control wall and the walls with CFRP sheets at the same areas under the same load level, it is found that CFRP can dramatically decrease strain in masonry elements because it provides definite constraint for these elements.

Finally, the distribution of strain and stress has been changed because of the existence of CFRP sheets. That implies the response characteristics and failure

mechanism of masonry shear walls under in-plane loading are altered due to CFRP sheets.

However there are still three major problems needed to be pointed out for the future study. From the comparison of the lateral load verse displacement curves between the simulation output and test results, it is shown that the stiffness in the models is much larger than those in the test results. There are a number of possible reasons accounted for this problem.

Firstly, it can be accounted for by the boundary conditions at the bottom of the specimen. In the numerical models, the boundary conditions at the bottom of the walls were modeled as pinned or spring-connected; while in the actual experimental program, the wall was connected to the steel plate, which was directly under the wall, by welded dowels and the plate was bolted to the stiff steel beam, which was directly under the steel plate and just situated on the strong floor without any connection between the beam and the floor. Thus the boundary conditions in the experiment were not totally pinned or spring-connected. In addition, from the test data derived from the LVDT mounted to the bottom of the wall it was also showed that there was some sliding along the horizontal direction during the loading process. This sliding led to a decrease of stiffness of the specimen when subjected to in-plane loadings.

Secondly, the homogenous continuum macro-modeling was used for masonry material in terms of average strains and stresses, neglecting the existence of mortar joints which act as planes of weakness. As a matter of fact, the stiffness of mortar joints differs greatly from that of the masonry units.

Thirdly, the stiffness of the mortar joints differs between bed joints, which are reliable and head joints, which are less reliable.

The use of LINK connections of MPC rather than the modeling of debonding process between the masonry walls and CFRP sheets would also lead to the higher stiffness of the numerical models because the LINK constraints offer a pinned rigid link

between two nodes to keep the distance between the two nodes constant; while it is impossible to take place under the experimental situation.

Aside from modeling the debonding process, it appears that part of the effect of CFRP sheets is to modify the tension stiffening response of the masonry blocks over a region around the sheets path. Although some assumptions were made in this aspect during the numerical analysis, more fundamental research needs to be done in this area.

In addition, compressive strains were noted in the CFRP sheets in both the test and the numerical analysis. What is not evident is whether CFRP sheet stiffness is also involved in the response in compression. The demec measurements taken in the test were not available for comparison at the time this work was carried out. But they should be compared at a later time.

5.3 Recommendations for Future Research

Based on the numerical analysis, some recommendations are proposed for future research. This research is only related to the specimens subjected to monotonic lateral load. However, during earthquake or wind the lateral loading is cyclic. Thus, the research for partially-grouted masonry shear walls with openings under cyclic lateral loading is proposed to be conducted.

In order to obtain more accurate data to be used in the constitutive modeling, tension tests for the masonry prisms reinforced with CFRP sheets need to be conducted. Three dimensional (3D) models need to be established which can model the interaction and contact conditions between masonry and CFRP sheets, as well as the debonding process before and after failure occurs. The models conducted in this thesis could model neither the change of interaction between masonry and CFRP sheets nor debonding process because plane stress elements were employed. In addition, material tests on the epoxy used to bond the CFRP sheets to the masonry walls need to be carried out to determine the bond behavour under loading.

Furthermore, further research to study the effect of opening size and location on load carrying capacity, ductility as well as strength of partially-grouted reinforced masonry shear walls with openings is recommended to be conducted in the future.

REFERENCES

ABAQUS/Explicit User's Manual (2002), Version 6.3, Hibbitt, Karlsson & Sorensen, Inc., Pawtucket, RI.

ABAQUS 1998: Getting Started with ABAQUS/Explicit, Hibbitt, Karlsson & Sorensen, Inc., Pawtucket, RI.

Albert, Michael L., J.J. Roger Cheng and Alaa E. Elwi (1998) "Rehabilitation of Unreinforced Masonry Walls with Externally Applied Fibre Reinforced Polymers", Structural Engineering Report No. 226, University of Alberta.

Atkinson, R.H., and M.I. Hammons (1993) "Tension Stiffening Behaviour of Reinforced Masonry", Proceedings of the Sixth North American Masonry Conference, Philadelphia, Pennsylvania, June 6-9, pp. 1053-1063.

Bathe, K.J. (1996) "Finite Element Procedures", Prentice Hall.

Belarbi, Abdeldjelil, Pedro F. Silva and Tong Li (2003) "An Experimental Evaluation of In-Plane URM Walls Strengthened with FRP Composites", Proceedings of the Ninth American Masonry Conference, Clemson, South Carolina, June 1-4, pp. 1101-1112.

Chen, S.J., P.A. Hidalgo, R.L. Mayes, R.W. Clough, and H.D. McNiven (1978) "Cyclic Loading Tests of Masonry Single Piers, Volume 2 - Height to Width Ratio of 1", Report No. UCB/EERC-78/28, Earthquake Engineering Research Centre, University of California, Berkeley, California, December 1978.

Dhanasekar, M., A. W. Page, P.W. Kleeman (1984) "A Finite Element Model for the In-Plane Behaviour of Brick Masonry", Proc. 9th Australasian Conference on Mechanisms of Structures, pp.262-267.

Drysdale, Robert G., Ahmad A. Hamid, and Arthur C. Heidebrecht (1979) "Tensile Strength of Concrete Masonry", Journal of the Structural Division, July 1979, pp. 1261-1276.

El-Shafie, Hany, Ahmad Hamid, Samir Okba, and El-Sayed Naser (1996) "Masonry Shear Walls with Openings: State-of-the Art Report", Proceedings of the Seventh North American Masonry Conference, University of Notre Dame, South Bend, Indiana, June 2-5, pp. 638-653.

Elshafie, Hany, Ahmad A.Hamid and Elsayed Nasr (1999) "Post-Cracking Stiffness of Reinforced Masonry Shear Walls with Openings", Proceedings of the 8th North American Masonry Conference, Austin, June 6-9.

Fam, Amir, Daniel Musiker, Mervyn Kowalsky and Sami Rizkalla (2002) "In-Plane Testing of Damaged Masonry Wall Repaired with FRP", Advanced Composites Letters, Vol. 11, No. 6.

Ghanem, Gouda M. (1992) "Behavioural Characteristics of Partially Reinforced Loadbearing Masonry Wall Structures", Ph.D. Thesis, Helwan University, Cairo, Egypt.

Ghanem, Gouda M., Amr E. Salama, Shreif Abu Elmagd, Ahmad A. Hamid (1993) "Effect of Axial Compression on the Behaviour of Partially Reinforced Masonry Shear Walls", Proceedings of the Sixth North American Masonry Conference, Philadelphia, Pennsylvania, June 6-9, pp. 1145-1157.

Glanville, John I., Michael A. Hatzinikolas, and Hamza A. Ben-Omran (1996) "Engineered Masonry Design – Limit States Design", Winston House, Winnipeg.

Hamilton III, H. R., A. Holberg, J. Caspersen, and C.W. Dolan (1999) "Strengthening Concrete Masonry with Fibre Reinforced Polymers", Fourth International Symposium on

Fibre Reinforced Polymer Reinforcement for Reinforced Concrete Structures, SP-188, ACI International, pp. 1103-1115.

Haroun, Medhat A., Ayman S. Mosallam, and Khaled H. Allam (2003) "In-Plane Shear Behaviour of Masonry Walls Strengthened By FRP Laminates", The Second International Workshop on Structural Composites for Infrastructure Applications, Cairo, Egypt, Dec.17-18.

Hegemier, G.A., R.O. Nunn, and S.K. Arya (1978) "Behaviour of Concrete Masonry under Biaxial Stresses", Proceedings of North American Masonry Conference, University of Colorado, Boulder, Colorado , August 14-16, pp. 1-1~1-28.

Hilleborg, A., M. Modeer, and P.E. Petersson (1976) "Analysis of Crack Formation and Crack Growth in Concrete by Means of Fracture Mechanics and Finite Elements," Cement and Concrete Research, Vol.6, pp.773-782.

Kamel, Ayman Mohamed Samir (2003) "Experimental and Numarical Analysis of FRP Sheets Bonded to Concrete", Ph.D. Thesis, University of Alberta

Khattab, Magdy M., Robert G. Drysdale (1993) "The Effect of Reinforcement on the Shear Response of Grouted Concrete Masonry", Proceedings of the Sixth North American Masonry Conference, Philadelphia, Pennsylvania, June 6-9, pp. 1121-1132.

Kuzik, Marc D., Alaa E. Elwi and, J.J. Roger Cheng (1999) "Cyclic Behaviour of Masonry Walls with GFRP", Structural Engineering Report No. 228, University of Alberta.

Lee, J., and G.L. Fenves (1998) "Plastic-Damage Model for Cyclic Loading of Concrete Structures", Journal of Engineering Mechanics, Vol. 124, No. 8, pp. 892-900.

Leiva, Gilberto and Richard E. Klingner (1993) " Behaviour and Design of Multi-Story Masonry Walls under In-Plane Seismic loading" Proceedings of the Sixth North American Masonry Conference, Philadelphia, Pennsylvania, June 6-9, pp. 1171-1181.

Lotfi, H.R., P.B. Shing (1994) "Interface Model Applied to Fracture of Masonry Structures", Journal of Structural Engineering, ASCE, Vol.120, No.1, pp.63-80.

Lourenço, Paulo B. (1996) "Computational Strategies for Masonry Structures", Delft University Press.

Lourenço, Paulo B. and Jan G. Rots (1997) "Multisurface Interface Model for Analysis of Masonry Structures", Journal of Engineering Mechanics, July 1997, ASCE, pp. 660-668.

Lourenço, Paulo B., Jan G. Rots, and Johan Blaauwendraad (1998) "Continuum Model for Masonry: Parameter Estimation and Validation", Journal of Structural Engineering, June 1998, ASCE, pp. 642-652.

Lubliner, J., J. Oliver, S. Oller, and E. Onate (1989) "A Plastic-Damage Model for Concrete", International Journal of Solids and structures, Vol. 25, pp. 299-329.

Miao, Honglan (2004) "CFRP Sheet Application to Masonry Shear Walls with Openings", University of Alberta.

Pietruszczak, S., R. Ushaksaraei (2003) "Description of Inelastic Behaviour of Structural Masonry", International Journal of Solids and Structures, Vol. 40, pp. 4003-4019.

Rosenhaupt, S., Y. Sokal (1965) "Masonry Walls on Continuous Beams", J. Structural Division, ASCE, Vol. 91, No ST1, pp.155-171.

Saw, C.B. (1974) "Linear Elastic Finite Element Analysis of Masonry Walls on Beams", Building Science, Vol.9, pp.299-307.

Schultz, Arturo E. (1994) "NIST Research Program on the Seismic Resistance of Partially-Grouted Masonry Shear Walls", NISTIR 5481, Building and Fire Research Laboratory, National Institute of Standards and Technology, Gaithersburg, MD 20899, June 1994.

Scrivener, J.C. (1986) "Summary of Findings of Cyclic Shear Tests on Masonry Piers", U.S. – Japan Coordinated Program for Masonry Building Research , Atkinson-Noland & Associates, Boulder, Colorado, June 1986.

Shing, P.B., J.L. Noland, E. Klamerus, and H. Spaeh (1989) "Inelastic Behaviour of Concrete Masonry Shear Walls", Journal of Structural Engineering, ASCE, Vol. 115, No. 9, September 1989, pp. 2204-2225.

Shing, P. Benson and Li Cao (1997) "Analysis of Partially Grouted Masonry Shear Walls", NIST GCR 97-710, Building and Fire Research Laboratory, Gaithersburg, Maryland 20899, March 1997.

Tumialan, Gustavo, Antonio Morbin, Antonio Nanni, and Claudio Modena (2001) " Shear Strengthening of Masonry Walls with FRP Composites", COMPOSITES 2001 Convention and Trade Show, Composites Fabricators Association, Tampa, FL, October 3-6, 6 pp. CD-ROM.

Tzamtzis, A.D., P.G. Asteris (2003a) "Finite Element Analysis of Masonry Structures: Part I – Review of Previous Work", Proceedings of the Ninth American Masonry Conference, Clemson, South Carolina, June 1-4, pp. 101-111.

Tzamtzis, A.D., P.G. Asteris (2003b) "Finite Element Analysis of Masonry Structures: Part II - Proposed 3-D Nonlinear Microscopic Model", Proceedings of the Ninth American Masonry Conference, Clemson, South Carolina, June 1-4, pp. 146-155.

Ushaksaraei, R. and S. Pietruszczak (2002) "Failure Criterion for Structural Masonry

based on Critical Plane Approach", Journal of Engineering Mechanics, July 2002, pp. 769-778.

Vermeltfoort, A.Th., Th.M.J. Raijmakers and H.J.M. Janssen (1993) " Shear Tests on Masonry Walls", Proceedings of the Sixth North American Masonry Conference, Philadelphia, Pennsylvania, June 6-9, pp. 1171-1181.

Wolde-Tinsae, Amde M., R.H. Atkinson and Ahmad A. Hamid (1993) " State-of-the-Art Modulus of Elasticity of Masonry", Proceedings of the Sixth North American Masonry Conference, Philadelphia, Pennsylvania, June 6-9, pp. 1209-1220.

Woodward, Kyle, Frank Rankin (1985) "Shear Resistance of Unreinforced Hollow Concrete Block Masonry Walls", Proceedings of the Third North American Masonry Conference, Arlington, Texas, June 3-5, pp. 38-1~38-15.

Zhao, Tong, Jian Xie and Haoju Li (2003) " Strengthening of Cracked Concrete Block Masonry Walls Using Continuous Carbon Fiber Sheet", Proceedings of the Ninth American Masonry Conference, Clemson, South Carolina, June 1-4, pp. 156-167.